EVERGREEN, SEMI-EVERGREEN, AND DECIDUOUS WOODY PLANTS IN A SEMI-ARID SAVANNA: PHOTOSYSTEM ENERGY DYNAMICS AND NEAR-CANOPY REMOTE SENSING WITH CCI/PRI

A Thesis

by

HARRISON DONALD RAUB

Submitted to the Office of Graduate and Professional Studies of
Texas A&M University
in partial fulfillment of the requirements for the degree of

MASTER OF SCIENCE

Chair of Committee,	Jason B. West
Committee Members,	Kevin McInnes
	Nithya Rajan
Head of Department,	Kirk Winemiller

December 2020

Major Subject: Ecosystem Science and Management

ABSTRACT

Woody encroachers have transformed the Southern Great Plains across its semi-arid regions. Little is known how these encroachers—particularly the drought tolerant *Juniperus*—may be vulnerable to hotter temperatures and water limitations in future climate projections and how that will affect their light utilization for photosynthesis and dissipation of excess energy. Additionally, photosynthetic changes in drylands are not adequately captured with remote sensing partly due to use of greenness indices in the presence of evergreens. Responses among three co-occurring encroachers to seasonal water-limitations were compared using photosynthetic rates, energy partitioning of absorbed light, and sustained energy dissipation, while the recently created Chlorophyll Carotenoid Index (CCI) was tested to track the photosynthetic phenology of trees varying in leaf persistence.

Declining stem water potential (-5 MPa) during the summer dry period elicited strong photochemical stress in *J. ashei*. The actual quantum yield for PSII decreased to 4%, regulatory light-induced energy dissipation increased to 84%, while the maximal quantum yield of PSII in a dark-adapted condition (F_V/F_M) declined to 75% from sustained dissipation. Photochemical stress was less severe in the drought avoiders with neither decreasing in F_V/F_M, while regulatory light-induced dissipation increased to 43% in *Prosopis glandulosa* and *Quercus fusiformis* remained near ~50%. Consequently, water stress elicited stronger photochemical stress in *J. ashei* relative to the other two drought avoiders.

Canopy CCI was the only index to track the slow-adjusting chlorophyll/carotenoid and F_V/F_M across the deciduous (Chl:Car $R^2 = 0.88$, $p < 0.02$, F_V/F_M $R_{rmc}^2 = 0.54$, $p < 0.001$) to evergreen species (Chl:Car $R^2 = 0.44$, $p < 0.07$, F_V/F_M $R^2 = 0.74$, $p < 0.0006$) plus foliage density ($R^2 = 0.81$, $p < 0.006$) of the deciduous *P. glandulosa*. Consequently, CCI may improve estimates of productivity in drylands with its relationships across species, but future studies at greater spatiotemporal scales are needed. The photochemical reflectance index had stronger relationships with F_V/F_M and Chl:Car than CCI, which may be due to the incomplete knowledge on variation sources in CCI. Dynamic parameters at midday had species-specific moderate relationships or non-significant relationships underscoring the difficulty relating instantaneous measurements to slow-adjusting reflectance signals in drylands.

DEDICATION

Dedicated to my lovely wife, Taylor Raub, who quite simply provided the best support one could ask. Your words of encouragement and thoughtful actions were greatly appreciated on the whole journey.

ACKNOWLEDGEMENTS

I would like to thank my committee chair, Dr. Jason B. West, and my committee members, Dr. Nithya Rajan and Dr. Kevin McInnes, for their extensive guidance and support throughout the course of this research. The feedback, expertise, and logistical support you all provided were immeasurable towards the completion of this work.

Much of my thanks goes to all my friends and colleagues who helped along the way. Without the help of the members of Texas A&M Sonora Research Station staff, this work would not have been completed. Particular thanks goes out to Nick Garza for helping me devise a mobile tree sampling platform that had innumerous failed versions along the way and for helping me learn how to use a workshop. I would like to thank Dr. Doug Tolleson for lending me his ASD FieldSpec and extend thanks to Robert Moen, Ishmael Sanchez, and Miguel Ibarra for their onsite logistical support and physical help that kept this research running on-site. All of you had incredible character and I feel thankful to have worked with you.

I would like to additionally thank the members of the Stable Isotopes for Biosphere Science Laboratory, Dr. Ayumi Hyodo for help in developing and performing the pigment extraction protocol, and Dr. Tom Boutton for use of the facilities and instrumentation. I appreciate the mentoring by Dr. Aline Jaimes-Hernandez, support by Dr. Rachel Adams, and the extensive fieldwork and idea bouncing by Nicole Havrilchak in this process. Special thanks goes to Pedro Leite, Rachel Barnett, and Dillon See for their hard work in the field and the long days.

Finally, I'd like to thank my wife, Taylor Raub, and family—Hope Raub, Slater Raub, Joy Raub, and Forrest Radarian—for all the support they've given me and the words of encouragement. All your patience and love has been greatly appreciated.

CONTRIBUTORS AND FUNDING SOURCES

Contributors

This work was supervised by a thesis committee consisting of my advisor, Dr. Jason B. West, and Dr. Kevin McInnes of the Department of Soil and Crops Sciences and Dr. Nithya Rajan of the Department of Soil and Crops Sciences.

Instrumentation for the project, advising, and reviewing of all chapters was provided by all three committee members. All other work conducted for the thesis was completed by the student independently.

Funding Sources

Graduate study was supported by the Excellence Fellowship from the College of Agriculture and Life Sciences at Texas A&M University, the Sid Kyle Endowment administered by Texas A&M University, and the Harry Wayne Springfield Graduate Assistantship provided by the Department of Ecosystem Science and Management. A travel grant from the Department of Ecosystem Science and Management additionally provided funding to present research virtually at the 2020 Ecological Society of America Conference.

NOMENCLATURE

A_{Net}	Net Photosynthesis
APAR	Absorbed Photosynthetically Active Radiation
CCI	Chlorophyll Carotenoid Index
Chl:Car	Ratio of Chlorophyll to Carotenoid Pigment Pools
DOY	Day of year
E	Transpiration
ε	Light use efficiency constant
EVI	Enhanced Vegetation Index
EVI2	Two-Band Enhanced Vegetation Index
FD	Foliage Density
F_M	Maximal Fluorescence in a Dark-Adapted State
$F_{M'}$	Maximal Fluorescence in a Light-Adapted State
F_o	Minimum Fluorescence in a Dark-Adapted State
FOV	Field of view
fPAR	Fraction of Photosynthetically Active Radiation Absorbed
F_s	Steady-State Fluorescence in a Light-Adapted State
F_V	$F_M - F_o$
$F_{V'}$	$F_{M'} - F_s$
F_V/F_M	Maximum Quantum Yield in a Dark-Adapted State
$F_{V'}/F_{M'}$	Maximum Quantum Yield in a Light-Adapted State

g_s	Stomatal Conductance
NDVI	Normalized Difference Vegetation Index
NPQ	Non-Photochemical Quenching
PRI	Photochemical Reflectance Index
rmc	Repeated Measures Correlation
SAVI	Soil Adjusted Vegetation Index
VPD	Vapor Pressure Deficit
$\phi_{(f,D)}$	Quantum Yield of Constitutive Non-Regulatory NPQ
ϕ_{PSII}	Actual Quantum Yield of PSII in a Light-Adapted State
$\phi^{r}_{(NP)}$	Quantum Yield of Regulatory Light-Induced NPQ
Ψ_{MD}	Midday Stem Water Potential
Ψ_{PD}	Predawn Water Potential

TABLE OF CONTENTS

Page

LIST OF FIGURES

Page

LIST OF TABLES

Page

1. INTRODUCTION

The Southern Great Plains region has experienced the second highest rates of woody encroachment in North America that has shifted landscapes away from grasslands with increasing levels of woody biomass (Barger et al. 2011). Semi-arid regions such as those composing parts of the Southern Great Plains are critical towards driving the interannual variation in atmospheric CO_2 levels based on water availability and temperatures (Poulter et al. 2014, Ahlström et al. 2015) but climatic shifts are likely to increase temperatures and drought severity in the future (Seager et al. 2007, Strzepek et al. 2010, Cook et al. 2015). Such shifts necessitate a better understanding of how woody encroachers of varying functional traits and water status levels may be vulnerable and respond to increased levels of seasonal stressors. However, limited studies have assessed the photosynthetic and energetic consequences of seasonally dry periods and additionally infrequent freezing periods on woody encroachers. Additionally, our ability to remotely capture photosynthetic changes in drylands has been partially limited due to use of greenness vegetation indices that are inadequate for areas where evergreen vegetation is present (Smith et al. 2019) but recent advances in carotenoid-based indices hold promise (Gamon et al. 2016). Greenness values vary little in evergreens due to their relatively stable canopy foliage densities over the season and chlorophyll retention in the winter, but evergreens do experience shifts in carotenoid pigments under stress (Gamon et al. 2016).

Consequently, Chapter 2 will address gaps in our knowledge involving photosynthetic and energetic responses of three major co-occurring woody encroacher

genera in the Southern Great Plains—*Prosopis glandulosa*, *Juniperus ashei*, and *Quercus fusiformis*. Chapter 3 will address recent advancements in remote sensing involving the Chlorophyll Carotenoid Index (CCI) that has been useful in tracking photosynthetic changes in mixed coniferous and deciduous boreal forests but is tested here in this water limited system on woody encroachers of varying leaf lifespans (deciduous, evergreen, and semi-evergreen leaves respectively).

1.1. **References**

Ahlstrom, A., M. R. Raupach, G. Schurgers, B. Smith, A. Arneth, M. Jung, M. Reichstein, J. G. Canadell, P. Friedlingstein, A. K. Jain, E. Kato, B. Poulter, S. Sitch, B. D. Stocker, N. Viovy, Y. P. Wang, A. Wiltshire, S. Zaehle, and N. Zeng. 2015. The dominant role of semi-arid ecosystems in the trend and variability of the land CO2 sink. Science **348**:895–899.

Barger, N. N., S. R. Archer, J. L. Campbell, C. Huang, J. A. Morton, and A. K. Knapp. 2011. Woody plant proliferation in North American drylands: A synthesis of impacts on ecosystem carbon balance. Journal of Geophysical Research: Biogeosciences **116**:1-17.

Cook, B. I., T. R. Ault, and J. E. Smerdon. 2015. Unprecedented 21st century drought risk in the American Southwest and Central Plains. Science Advances **1**:1-7.

Gamon, J. A., K. F. Huemmrich, C. Y. S. Wong, I. Ensminger, S. Garrity, D. Y. Hollinger, A. Noormets, and J. Peñuelas. 2016. A remotely sensed pigment index reveals photosynthetic phenology in evergreen conifers. Proceedings of the National Academy of Sciences **113**:13087–13092.

Poulter, B., D. Frank, P. Ciais, R. B. Myneni, N. Andela, J. Bi, G. Broquet, J. G. Canadell, F. Chevallier, Y. Y. Liu, S. W. Running, S. Sitch, and G. R. van der Werf. 2014. Contribution of semi-arid ecosystems to interannual variability of the global carbon cycle. Nature **509**:600–603.

Seager, R., M. Ting, I. Held, Y. Kushnir, J. Lu, G. Vecchi, H.-P. Huang, N. Harnik, A. Leetmaa, N.-C. Lau, C. Li, J. Velez, and N. Naik. 2007. Model projections of an imminent transition to a more arid climate in Southwestern North America. Science **316**:1181–1184.

Smith, W. K., M. P. Dannenberg, D. Yan, S. Herrmann, M. L. Barnes, G. A. Barron-Gafford, J. A. Biederman, S. Ferrenberg, A. M. Fox, A. Hudson, J. F. Knowles, N. MacBean, D. J. P. Moore, P. L. Nagler, S. C. Reed, W. A. Rutherford, R. L. Scott, X. Wang, and J. Yang. 2019. Remote sensing of dryland ecosystem structure and function: Progress, challenges, and opportunities. Remote Sensing of Environment **233**:1-23.

Strzepek, K., G. Yohe, J. Neumann, and B. Boehlert. 2010. Characterizing changes in drought risk for the United States from climate change. Environmental Research Letters **5**:1-9.

2. PHOTOINHIBITION AND PHOTOPROTECTIVE ENERGY DISSIPATION ACROSS MAJOR NORTH AMERICAN CO-OCCURRING WOODY ENCROACHERS

2.1. **Introduction**

Drylands of North America have experienced substantial shifts in vegetation over the last two centuries leading to higher fractions of woody plants on tens of millions of hectares of land (Van Auken 2009). This woody encroachment is a globally occurring phenomena due to fire suppression and overgrazing (Van Auken 2009, Stevens et al. 2017) which has led to increases in aboveground biomass in these systems (Barger et al. 2011). These dryland regions are defined as arid and semi-arid climates where potential evapotranspiration exceeds precipitation. Semi-arid regions of the Southern Great Plains have been particularly affected over the past century by having the second highest rates of encroachment in North America based on multi-decadal studies (Barger et al. 2011). These woody encroachers face a changing climate globally where regular droughts and "hotter droughts" are projected to become more frequent, intense, and lengthen over the 21st century (Dai 2013, Trenberth et al.2013, Allen et al. 2015). Semi-arid regions of the Southern Great Plains are particularly expected to see increased aridity (Seager et al. 2018) and drought severity (Seager et al. 2007, Strzepek et al. 2010, Cook et al. 2015).

Photosynthetic activity of semi-arid vegetation drives the interannual variation in atmospheric CO_2 due to their varying climatic conditions involving temperature and precipitation (Poulter et al. 2014, Ahlström et al. 2015). Climatic shifts in these regions

will have considerable impacts on photosynthetic uptake such as the increased variability of productivity predicted in the Southern Great Plains by the end of the century (Klemm et al. 2020). Climatic effects on woody plants will be of considerable concern due to their varying susceptibility to water stress and mortality during strong drought events (Fensham et al. 2009, Choat et al. 2012, Moore et al. 2016) coupled with their recent expansion. With water deficits and temperatures likely to increase in the future, we need a better understanding of how co-occurring encroaching species in the semi-arid regions of the Southern Great Plains will photosynthetically and energetically respond to seasonal stressors (temperature extremes and drought) that are expected to strengthen in the future.

Many of the encroaching trees in North America have adopted differing but effective traits for these water-limited landscapes such as varying rooting depths, leaf lifespans (evergreen to deciduous), leaf architectures (needle versus broadleaf; Barger et al. 2011), hydraulic strategies, and degrees of stomatal control (Johnson et al. 2018[a]). Combinations of these traits lead to varying levels of leaf water status during periods of seasonal water stress. Drought tolerators are capable of experiencing lower water potentials due to resistance to embolism, and drought avoiders maintain steady water status (Wei et al. 2019) by minimizing transpirational water loss or maximizing water uptake with extensive deep roots (Abobatta 2019).

One such drought tolerator is juniper (*Junperus* spp.) (Willson et al. 2008), an evergreen genus found on shallow rocky soil or steep slopes with limited water access (Van Auken and Smeins 2008), while mesquite (*Prosopis* spp.) are deciduous trees

considered to be drought avoiders due to their extensive deep and lateral rooting strategies in deeper soils allowing access to lower water sources (Lombardini and Rossi 2019, Wilson et al. 2001). Both *Juniperus* and *Prosopis* are among the four greatest woody encroacher genera in western North America (Barger et al. 2011) but differ in both leaf traits and water status. Oak (*Quercus* spp.) is an additional encroacher that is prevalent in more locally scattered areas (Van Auken 2009). All three genera have species (*J. ashei*, *P. glandulosa*, *Q. fusiformis*) in the Southern Great Plains that co-occur on the Edwards Plateau in west-Central Texas. This allows for a unique opportunity to study photosynthetic and energy dissipating responses in some of the most prevalent North American woody encroacher genera.

Droughts elicit protective mechanisms by reducing leaf-level stomatal conductance to prevent transpirational water loss and maintain water status, but it also reduces photosynthetic capacity (Yan et al. 2016). Closing stomata can cause excess absorbed energy to rise to damaging levels making quick energy dissipation vital for maintaining leaf functionality (Schymanski et al. 2013). Absorbed light by the photosystems in chlorophyll can be dynamically quenched in three ways: 1) photochemical quenching (photosynthesis), 2) fluorescence of excited chlorophyll electrons, and 3) heat release of excess energy through non-photochemical quenching (NPQ; Maxwell and Johnson 2000). NPQ is of particular interest due its photoprotective role in dissipating excess energy over seconds to hours (Maxwell and Johnson 2000, Lazár 2015, Ruban 2016, Murchie and Ruban 2020). With only three fates for absorbed light energy, more energy allocated to photosynthesis reduces heat dissipation, while less

light utilization for photosynthesis requires greater energy dissipation via NPQ (Maxwell and Johnson 2000, Lazár 2015).

If photochemical quenching capabilities are surpassed under stressful conditions, plants may employ both dynamic and sustained forms of energy dissipation (NPQ) in order to protect leaves from photodamage of PSII reaction centers (Malnoë 2018, Verhoeven et al. 2018). Photodamage is caused by reactive oxidants formed from an inability to dissipate excess energy, while photoprotective mechanisms safely quench energy and produce antioxidants (Demmig-Adams and Adams 2018, Malnoë 2018). As dynamic stressors like excessive light, temperature, and evaporative demand increase over the day, the fraction of light used in photochemical quenching (quantum yield of PSII) decreases from predawn maximal levels to midday due to closing reaction centers while photosynthetic uptake increases to light saturated levels (Demmig-Adams and Adams 1996, Murchie and Lawson 2013). Stomatal closure is additionally sensitive to increasing Vapor Pressure Deficit (VPD) levels occurring at midday (Turner et al. 1984), which can decrease intercellular CO_2 concentrations and lower quantum yields of PSII (Kalaji et al. 2017). Consequently, dynamic energy dissipation increases diurnally by the regulatory light-induced NPQ ($\phi^{r}_{(NP)}$). This is a photoprotective mechanism activated by pH changes created from proton accumulation in the thylakoid lumen in response to excess light absorption (Demmig-Adams and Adams 1996, Hendrickson et al. 2004). The pH gradient induces changes in the xanthophyll cycle pigments, a pool of three carotenoid pigments that shift relative accumulations based on excess light (Müller et al. 2001, Hendrickson et al. 2004). The xanthophyll pigments zeanzanthin and

antheraxanthin accumulate at midday and serve to quickly quench excess energy under changing dynamic stressors before relaxing overnight with greater relative pools of violaxanthin (Demmig-Adams and Adams 1996).

Over longer periods of stress, sustained NPQ becomes necessary which causes sustained photoinhibition of the maximum quantum yield of photosystem II (Verhoeven 2014, Verhoeven et al. 2018). Photoinhibition refers to the decreased ability to fix CO_2 relative to non-stressful conditions and can result from either photoprotective or photodamaging mechanisms (Malnoë 2018). Photoinhibition can occur diurnally with dynamic stressors (Liu and Guan 2016) or over seasonal periods due to sustained stressors like low temperatures or water limitations (Fernández-Marín et al. 2017). While the xanthophyll cycle and maximal quantum yields of PSII can recover overnight from diurnal stressors, sustained stressors lead to retention of the zeanzanthin and anetheraxanthin pigments overnight (Demmig-Adams and Adams 1996). This retention in the energy dissipating state reduces the maximal quantum yields by photosystem II that recovers overnight (Fernández-Marín et al. 2017, Verhoeven 2014, Verhoeven et al. 2018) which can reduce photosynthetic uptake substantially under light-limiting periods such as dawn and under light-saturating conditions at midday in more severe cases (Adams et al. 2008, Murchie and Ruban 2020). Additional carotenoid pigments have been found to dissipate excess energy by increasing in concentration during droughts, low temperatures, and chilling to quench excited chlorophyll and singlet oxygen molecules (Esteban et al. 2015, Fernández-Marín et al. 2017).

There is a paucity of studies evaluating the impacts of seasonal stressors on both photosynthetic and energy dissipating responses among major co-occurring North American woody encroachers—particularly in the semi-arid regions of the Southern Great Plains that have received the second highest rates of woody encroachment (Barger et al. 2011). Most studies on photoinhibitory and dynamic energy responses to water limitations for co-occurring woody species have focused on tropical savannas (Franco et al. 2007) and Mediterranean chaparral dryland vegetation (Martínez-Ferri et al. 2000, Werner et al. 2002, Ain-Lhout et al. 2004, Baquedano and Castillo 2007, Fernández-Marín et al. 2017). Studies of diurnal photoinhibition in several woody encroachers (*Prosopis* sp. and *Larrea* sp.) of the North American southwest have been conducted (Liu and Guan 2016), while seasonal photoinhibition in *Juniperus* in the Nebraska sandhills have occurred (Msanne et al. 2017). Only one study has evaluated photoinhibitory responses to water limitations in two major woody encroachers (*Pinus* spp. and *Juniperus* spp.), but it was restricted to controlled water limitations on potted saplings in a greenhouse experiment (Bihmidine et al. 2010). A comparison of seasonal photoinhibiting responses and energy partitioning of light at midday among the most prevalent co-occurring woody encroachers in North America or the Southern Great Plains does not appear to have been done—particularly without field studies involving matured trees with representative rooting behaviors. This gap in understanding is particularly concerning considering the diversity of functional strategies that North American encroachers possess (Barger et al. 2011), which may induce differing photosynthetic responses among major encroachers under future drought regimes.

Comparisons of the rooting distributions of the three co-occurring woody encroachers on the Edwards Plateau lead to differential soil moisture access. Ashe juniper (*Juniperus ashei*) is a drought tolerant evergreen that is shallowly rooted on soils as thin as 4 – 6 inches above limestone bedrock on the Edwards Plateau (Hall 1952), but can develop tap roots through fractured limestone as deep as 7 – 9 m (Jackson et al. 1999, McElrone et al. 2004). It is capable of forming numerous lateral roots into inter-canopy space and very dense mats of fibrous roots near soil surfaces (Thurow and Hester 1997). Live oak (*Q. fusiformis*) is a semi-evergreen drought avoider that can vary from shallowly rooted to as deep as 22 m through limestone (Jackson et al. 1999). Honey mesquite (*Prosopis glandulosa*) is a deciduous drought avoider that is traditionally deep-rooted but can establish in some moderate soil depths of 1.5 to 2 m on the Edwards Plateau (Eggemeyer and Schwinning 2009). However, it likely struggles in shallower soils due to inability to send tap roots deeper (Eggemeyer and Schwinning 2009). Lateral roots can be a significant source of water for *P. glandulosa* in xeric sites (Ansley et al. 1998). Consequently, *J. ashei* is restricted to the driest areas of the landscape, *P. glandulosa* can be responsive to water limitations on the Edwards Plateau, and *Q. fusiformis* may access very deep water in the limestone.

Leaf functional traits vary among these co-occurring encroachers that can affect their relative photosynthetic capacities. Leaf lifespans range from ~7 months for the deciduous *P. glandulosa*, to slightly less than a year for the semi-evergreen *Q. fusiformis*, to estimates of upwards of 6 years for evergreen *Juniperus* species (Reich et al. 1999). Leaves fall off in the spring and new buds quickly emerge for *Q. fusiformis*.

Leaves for *Juniperus* sp. are tightly appressed small scales (1- 3 mm) with stomata sunken into the leaf surface that are not usually exposed due to the appression, have poor stomatal control (anisohydric), and stomatal densities range from 500 to 1,000 cm^{-2} on the respective abaxial and adaxial surfaces (Johnsen 1963, Johnson et al. 2018[a]). The biggest leaves among species are produced by *Q. fusiformis*. A closely related species with similar physiology, *Q. virginiana*, has been found to have numerous trichomes on the abaxial sides of leaves to prevent water loss, while stomatal densities on the abaxial side are higher than *Juniperus* sp. and range from 6,000 to 9,000 cm^{-2} (Thyroff et al. 2019). We assume such traits are similar to the closely related *Q. fusiformis* as their ranges slightly overlap. Leaflets for *P. glandulosa* are generally long (10 – 65 mm) and narrow (2.5 – 4 mm), are very thin with less structural support compared to the other species, and have the greatest stomatal densities ranging from 11,400 – 14,100 cm^{-2} on the abaxial and ~20,000 on the adaxial surfaces (Meyer and Morton 1971). The differences in stomatal densities and investment in structural tissues for longer leaf lifespans have likely contributed to the lowest leaf-level photosynthetic levels in *J. ashei* and higher values in *Q. fusiformis* and *P. glandulosa* (Owens 1996, Eggemeyer and Schwinning 2009, Bendevis et al. 2010).

Evidence suggests there are differing photosynthetic and energy dissipating responses among encroachers based on leaf traits and water status strategies in response to environmental stressors. The deeply rooted woody *P. velutina* has shown reduced sensitivities to temperature stress and lack of rainfall by maintaining high gas-exchange rates through better deep-water access relative to shallowly rooted species like

bunchgrasses (Barron-Gafford et al. 2012). The drought tolerant *J. virginiana* in the Nebraska sandhills has experienced mild amounts of photoinhibition in late summer relative to late spring, but greater sustained photoinhibition when temperatures fell below 0° C (Msanne et al. 2017). Viewing water status in the context of Mediterranean species, individuals with low predawn water potential values were most at risk of sustained photoinhibition, while drought avoiders only experienced dynamic NPQ during dry periods (Werner et al. 2002, Ain-Lhout et al. 2004). Drought tolerant species have experienced greater dynamic photoinhibition (i.e. diurnal drops in quantum yield) and increased NPQ at midday relative to drought avoiders during the hot Mediterranean summer (Martínez-Ferri et al. 2000, Baquedano and Castillo 2007). Summer dry periods and high irradiance have yielded higher dynamic photoinhibition in evergreen shrubs, while cold temperatures and dry periods have led to greater sustained photoinhibiton (Baquedano and Castillo 2007).

The objectives here were to broadly assess the photosynthetic and energy dissipating capacities of prevalent co-occurring encroacher genera in the semi-arid Southern Great Plains in response to seasonally dry periods and freezing temperatures. Specifically, we assess how differential access to soil moisture and leaf persistence influences light-utilization for photosynthesis and energy dissipation during seasonal dry periods and freezing events among the woody encroachers. We hope by evaluating the photosynthetic responses that we can help provide basic understandings of how different major encroachers may respond to seasonal environmental stressors. Particularly, we compared responses between the drought tolerant *J. ashei* to the two drought avoiding

species (*P. glandulosa* and *Q. fusiformis*) due to its potential vulnerability associated with its low water status and general restriction to the driest locations on the landscape (Hall 1952). Doing so can provide useful knowledge on how the major encroaching genera in the semi-arid regions of the Southern Great Plains may respond under the drier and hotter climatic conditions predicted by the end of the century.

It was hypothesized that the drought tolerant evergreen *J. ashei* would experience mild sustained photoinhibition and greater dynamic energy dissipation in hot, dry periods with mild sustained photoinhibition during the winter (Martínez-Ferri et al. 2000, Werner et al. 2002, Ain-Lhout et al 2004, Baquedano and Castillo 2007, Msanne et al. 2017). Additionally, it was hypothesized that both drought avoiders, *P. glandulosa* and *Q. fusiformis*, would exhibit minimal increases in sustained energy dissipation and lowered dynamic dissipation during summer dry periods (Martínez-Ferri et al. 2000, Werner et al. 2002, Ain-Lhout et al. 2004, Barron-Gafford et al. 2012), while the semi-evergreen *Q. fusiformis* would exhibit mild sustained photoinhibition over the winter (Baquedano and Castillo 2007).

2.2. **Methods**

2.2.1. Study Site, Tree Selection, and Mobile Sampling Platform

The study was conducted at the Sonora Experimental Research Station (30.25873 N, 100.56799 W) on the karst landscape of the Edwards Plateau in west-central Texas (Fig 2.1). Average temperatures range from 10.5 °C to 26.3 °C with annual rainfall averaging 550 mm (Western Regional Climate Center). The climate is considered semi-arid, and the research site is dominated by Tarrant stony and silty clays on level ground.

The site has experienced numerous historical management plans involving grazing and fire over its 100-year use, so care was taken not to include trees that appeared impacted by these historical factors.

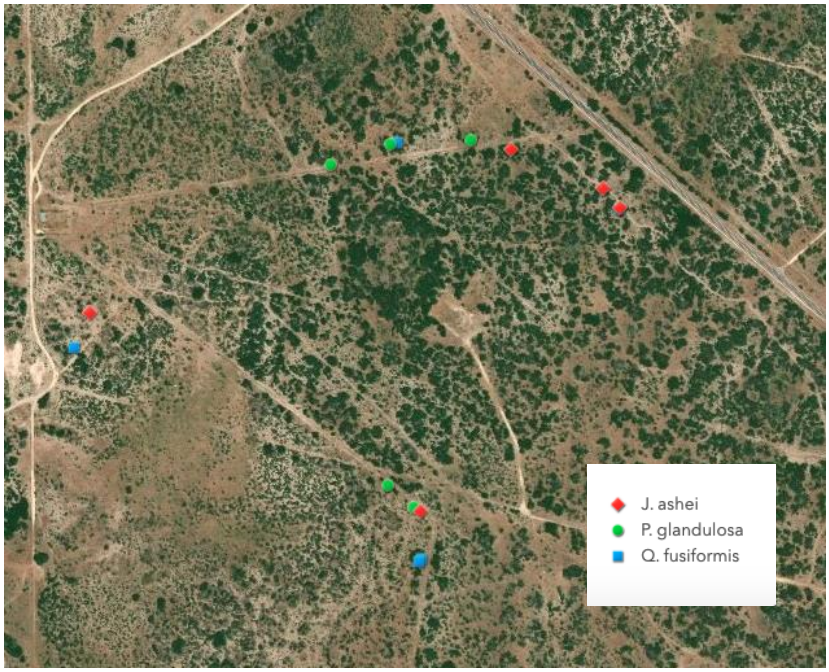

Figure 2.1 Map of study site and selected trees at the Sonora Experimental Research Station in west-central Texas. Red triangles are *Juniperus ashei,* green circles are *P. glandulosa*, and blue squares are *Quercus fusiformis*.

Five individuals from each species (N = 15) were selected based on isolation from other trees located 1 m away, signs of good leaf health, full canopies, placement on level terrain, and road accessibility for a 13 ft mobile sampling ladder located on a trailer (Fig 2.2). Selected trees were within the average tree height classes (~3 – 5 m) for each species (Fortes et al. *unpublished*) ranging from 2.8 - 4.2 m for *P. glandulosa*, 2.8 – 3.8

m for *Q. fusiformis*, and 3 – 4.2 m for *J. ashei*. Half of each species were found on Tarrant Silty Clay, while the remaining halves were found on Tarrant Stony Clay. Individuals from the same species were sampled no further than three trees apart from each other over the course of the day to reduce temporal bias for any species. All measurements were taken over ~3-4 days for each collection period every month from late July 2019 to late April 2020. Vapor pressure deficits were calculated from daily measurements of temperature and relative humidity (EE184, Campbell Scientific, Inc.; Logan, Utah) using the *plantecophys* package (Duursma 2019) in RStudio version 1.3.1056, while daily precipitation was collected with a tipping rain bucket (TB4, Campbell Scientific, Inc.; Logan, Utah).

2.2.2. Soil Depth Survey

Soil depth was recorded by hammering a metal pole until an impenetrable layer was hit similar to prior methodology on the Edwards Plateau (Elkington et al. 2014). Measurements were taken in the four cardinal directions and one meter away from each tree base. A maximum of 70 cm in soil depth was measured with this method and an average soil depth measurement per tree was created from the four sub-samples.

2.2.3. Gas-Exchange Measurements

A portable gas-exchange system (LI-6800, LI-COR Biosciences; Lincoln, Nebraska) was used to measure instantaneous gas-exchange parameters including net carbon assimilation rates (A_{Net}), transpiration rates (E), and stomatal conductance (g_s). Any leaves smaller than the 2 cm^2 gasket were cut and stored in wetted plastic bags for later leaf-area corrections. Projected leaf areas were scanned into ImageJ (U.S. National

Figure 2.2 Mobile tree sampling platform for leaf-level physiology measurements.

Institutes of Health, Bethesda, Maryland) and all gas exchange parameters were corrected on a one-sided leaf area basis. Due to the three-dimensional structure of juniper leaves, *J. ashei* leaflets were debranched and the projected leaf area was multiplied by $\pi/2$ (Cregg 1992).

Environmental parameters were set to 1500 (± 25) μmol m^{-2} s^{-1} for saturating light conditions, ambient temperature and humidity, 415 (± 5) μmol mol^{-1} CO_2, 700 μmol s^{-1} flow, and 10,000 (±10) revolutions per minute for the mixing fan. Oxygen was set to ambient conditions of 21% air composition and the stomatal ratio was assumed to be 0.5. All gas-exchange warm-up tests and sample and reference infrared gas analyzers were matched before measurements began. Matching continued to follow every 30

minutes and between tree samplings. Measurements were taken on two sun exposed leaves per individual tree that were close to horizontal orientations. These fully expanded leaves were located as far apart as could be reached from the ladder and were checked for contact with the chamber head thermocouple. Three logs per leaf were taken when sample CO_2 levels stabilized at average rate changes of ± 0.5 μmol m^{-2} s^{-1} min^{-1} (varying no more than ± 0.1 mmol m^{-2} s^{-1} min^{-1} standard deviations) and when sample H_2O levels stabilized at averages rate changes of ± 0.1 mmol m^{-2} s^{-1} min^{-1} (variation no greater than ± 0.1 mmol m^{-2} s^{-1} min^{-1} standard deviations) over 20 seconds. Individual logs were removed if they fell outside of the designated parameter ranges or had a leak percentage greater than 10%. Negative *E* values between 0 and -0.50 μmol m^{-2} s^{-1} were changed to 1 μmol m^{-2} s^{-1} due to the rates likely falling within the error range between the infrared gas analyzers. Average leaf-level gas exchange values per tree were created by averaging the remaining logs per leaf and then averaging the two leaves per tree.

2.2.4. Fluorescence Measurements and Calculations

Fluorescence measurements were made with a LI-6800 Multiphase Flash Fluorometer (LI-COR Biosciences; Lincoln, Nebraska) on two leaves per tree canopy. Predawn fluorescence measurements were taken to determine the minimal (F_0) and maximum (F_M) fluorescence values of leaves in a dark-adapted state. Once the rate of the demodulated fluorescence signal stabilized to ± 1 min^{-1} (± 1 min^{-1} standard deviation) over 20 seconds, a saturating rectangular flash of 8,000 μmol of photons m^{-2} s^{-1} was applied for 1 s. The first two months accepted stabilization rates of ± 5 min^{-1} due to low dark measuring beam modulation rates. Midday fluorescence measurements were

taken immediately after gas exchange once fluorescence values stabilized under the actinic light conditions of 1,500 μmol m^{-2} s^{-1}. A multiphase saturating flash was conducted in order to ensure the most accurate estimate of the maximal fluorescence in the light-adapted state (F'_M) and steady-state fluorescence (F_S), as traditional saturating rectangular flashes often underestimate F'_M due to rapid turnover in the photosystems (Loriaux et al. 2013). The multiphase flash was composed of light intensity ramping up to 8000 μmol m^{-2} s^{-1}, decreasing in intensity by 25% in phase two, and ramping back up to 8000 μmol m^{-2} s^{-1} in phase three. Each variable of F_0, F_M, F_S, *and* F'_M were processed to remove logs outside the aforementioned parameter limits and values greater than two standard deviations away from the mean. Remaining values were averaged per individual tree.

The maximal quantum yield of PSII photochemistry (F_V/F_M) is a measurement of the fraction of absorbed light that is used in photochemistry if all PSII reaction centers are open under relaxed dark-adapted conditions. It is used as a key indicator of sustained NPQ and photoinhibition (Lazár 2015, Verhoeven et al. 2018) and is calculated by (Maxwell and Johnson 2000):

$$F_V/F_M = (F_M - F_0)/F_M \quad \text{(Eq. 2.1)}$$

Healthy leaves have values near 0.83 (Björkman and Demmig 1987) with values lower than this indicating an increase in photoinhibiting processing (Malnoë 2018). Strong photoinhibition refers to F_V/F_M values below 0.2, moderate photoinhibition between 0.4 – 0.7 (Adams et al. 2008), while sustained energy dissipation is considered present

below 0.8 which we will consider the threshold for mild photoinhibition (Verhoeven et al. 2014).

The actual quantum yield of PSII for a light-adapted state (ϕ_{PSII}) is calculated by:

$$\phi_{PSII} = (F'_M - F_S) / F'_M \quad \text{(Eq. 2.2)}$$

with ϕ indicating the quantum yield and ϕ_{PSII} being indicative of the actual proportion of absorbed light used for photosynthesis during lighted conditions (Lazár et al. 2015). ϕ_{PSII} is a midday depression in actual photosystem yield from its maximal level (F_V/F_M) at predawn (Demmig-Adams et al. 2012) due to closing reaction centers (Maxwell and Johnson 2000) and reductions in maximal quantum yield of PSII under lighted conditions (Lazár 2015). Non-photochemical quenching (NPQ) reflects thermal dissipation of excess energy and is calculated by:

$$NPQ = (F_M - F'_M) / F'_M \quad \text{(Eq. 2.3)}$$

where NPQ helps minimize excited singlet chlorophyll from decaying and forming singlet oxygens that are extremely damaging (Müller et al. 2001).

2.2.5. Energy Partitioning

Energy partitioning can be useful for assessing dynamic changes of light-use within and between species by estimating the fractions of absorbed light quenched by the different pathways. While complex energy partitioning strategies have been developed for specific situations, the partitioning equations by Hendrickson et al. (2004) were used due to its simplicity and lack of lengthy measurements (Lazár 2015). The proportions of light energy allocated to photochemical pathways (ϕ_{PSII}, described above), quantum yield of constitutive non-regulatory NPQ ($\phi_{f,D}$), and quantum yield of regulatory light-induced

NPQ (ϕ^{r}_{NP}) can be estimated using equations and notations derived from Hendrickson et al. (2004):

$$\phi_{f,D} = \frac{F_S}{F_M} \quad \text{(Eq. 2.4)}$$

$$\phi^{r}_{NP} = \frac{F_S}{F'_M} - \frac{F_S}{F_M} \quad \text{(Eq. 2.5)}$$

where $\phi_{f,D}$ represents the heat loss of both florescence (*f)* and constitutive (*D*) processes and $^{r}_{NP}$ stands for regulatory light-induced NPQ.

The quantum yield of regulatory light-induced NPQ (ϕ^{r}_{NP}) is associated with dynamic quenching mediated by the xanthophyll cycle throughout the day, while the quantum yield of constitutive non-regulatory NPQ ($\phi_{f,D}$) is a contribution of both non-regulatory thermal dissipation processes and regulatory sustained NPQ (Hendrickson et al. 2004, Lazár 2015). While sustained energy dissipation contributes to ($\phi_{f,D}$), F_V/F_M is used more frequently to assess changes (Lazár 2015, Verhoeven et al. 2018). Sustained NPQ persists in the dark (Verhoeven et al. 2018) and is caused by a protein reconfiguration that retains the xanthophyll cycle in a dissipating state without the presence of a light-induced thylakoid pH gradient (Verhoeven 2014).

2.2.6. Pigment Analyses

Pigment analyses were used to test for changing chlorophyll and carotenoid contents due to environmental stressors. Beads of dry silica gel were used to store two sunlit leaf tissue subsamples per tree up to three weeks in a light free environment at room temperature in order to prevent pigment degradation (Esteban et al. 2009). Silica gel performs well at preserving most pigments when liquid nitrogen or lyophilization are

unavailable, but a relaxation of the de-epoxidation state (i.e. increase in relative pools of violaxanthin) for the daily xanthophyll cycle and some phaeophytinization of chlorophyll can occur (Esteban et al. 2009).

Equal masses of both tree's leaf subsamples were homogenized together by freezing the leaf material with liquid nitrogen and grinding the material with a mortar and pestle. Though desiccated tissues are recommended to be extracted with a water-diluted (95-98%) organic solvent for pigment analysis with spectrophotometry (Fernández-Marín et al. 2018), equations specific to low resolution spectrophotometers (Genesys 10 UV Scanning; Thermo Electron Scientific Instrument Corporation, Madison, WI, USA) necessitated extractions with 100% methanol (HPLC grade) under dim lighting before centrifuging (Wellburn 1994). A methanol blank was measured before each sample. Equations for calculating chlorophyll a (C_a), chlorophyll b (C_b), and total carotenoids (C_{x+c}) from Wellburn (1994) were used as follows:

$$C_a = 15.65A_{666} - 7.34A_{653} \quad \text{(Eq. 2.6)}$$

$$C_b = 27.05A_{653} - 11.21A_{666} \quad \text{(Eq. 2.7)}$$

$$C_{x+c} = (1000A_{470} - 2.86C_a - 129.2C_b)/221 \quad \text{(Eq. 2.8)}$$

where A stands for the absorbance value taken at a particular wavelength. Samples were diluted or concentrated as needed for maximum absorbances to fall within the linear range (0.3 to 0.85 absorbance) of the machine (Fernández-Marín et al. 2018). Readings below 0.010 absorbance at 750 nm indicated the sample had been insufficiently centrifuged to prevent plant material interference (Lichtenthaler 1987). All calculations for chlorophyll content and carotenoid content were calculated on a molar dry weight

basis (μmol pigments g^{-1} dry leaf) using molar masses from Sims and Gamon (2002). Total chlorophyll was divided by total carotenoid content to give a ratio (Chl:Car) that reflects relative seasonal shifts in light-harvesting to dissipating capacities. Samples for all parameters outside of two standard deviations of the species' monthly average were removed.

Due to limitations with this technique, individual xanthophyll cycle pigments could not be resolved to assess seasonal shifts within the xanthophyll cycle nor changes in the xanthophyll pigment pool size. Consequently, changes in photoprotective behavior were largely assessed by changing pigment pool sizes of chlorophyll, carotenoids, and Chl:Car as these values change based on environmental stressors (Esteban et al. 2015, Fernández-Marín et al. 2017).

2.2.7. Water Potential Measurements

Predawn water potential measurements were made to indicate the soil-water availability of the tree. Midday measurements were used to indicate the midday water status of the tree and were measured by placing plastic bags over the leaves to bring them into equilibrium with the stem (Turner 1988) for a minimum of 15 minutes in order to stop transpirational water loss. After excising the leaves, the bagged leaf was placed into a pressure chamber (Edaphic Scientific, Model 1000; Moorabbin, VIC, AUS) to record the pressure when water first appeared at the cut end. Two leaves were excised for both predawn and midday measurements which were averaged together for that time period. Sub-samples greater than two standard deviations from the mean for the species were removed.

2.2.8. Statistical Analyses

Mixed model analyses were employed for each physiological response variable for pigments, gas-exchange, and fluorescence in RStudio version 1.3.1056 in the *nlme* package (Pinheiro et al. 2020). Monthly samples were treated as one traditional growing season cohort for analysis. Full models began with fixed effects including day of year (DOY), a quadratic day of year effect, species, and interactions of species with both DOY terms. Each DOY effect was mean centered to reduce multicollinearity issues. Physiological response variables were transformed as necessary by square root, the natural log, its inverse, or quadratically to achieve homogeneity and normality of residuals. Within group residual errors were allowed to vary among species each month with weighted variance arguments (Pinherio and Bates 2000), while the repeated measures on each tree necessitated random intercepts for each tree, while random slopes for both DOY terms were added sequentially (Gałecki and Burykowski 2013). Final model selection was conducted using Akaike's Information Criterion (AIC) and the maximum likelihood ratio test among models differing in random and fixed effects structures (Gałecki and Burykowski 2013). Homogeneity of variance and normality was checked visually using standardized residuals. Post-hoc analyses were conducted to determine significant differences among species with the *emmeans* package (Singmann et al. 2020) using the Bonferroni procedure. Within text results report the post-hoc Bonferroni procedures as t-values while referencing the table for the mixed-effects model output.

2.3. Results

2.3.1. Climatic Conditions – High Evaporative Demand, Water Stress, and Freezing Periods

Summer temperatures averaged 30 °C, while winter months reached average lows of 10 °C (Fig 2.3). Three sampling periods over the winter had multiple nights below freezing in the week leading up to the measurements. Average lows leading up to sampling for those three periods reached 0.90 °C in November, 1.38 °C in January, and 0.72 °C in February. Maximum vapor pressure deficits increased from late July to a peak above 5 kPa in late August indicating the highest evaporative demands (Fig 2.3). One large rain event of 36 mm occurred over the three-month period between late June to the start of October (Fig 2.3). This occurred during the middle of the second sampling period. Precipitation became more frequent from October through late November. The total precipitation of 121 mm that fell during the summer and autumn months (July – Nov) was 57% below the average of 281 mm for these months from 1902 to 2018 (Western Regional Climate Center). Cumulative rainfall for winter months (Dec-Feb) was comparable to historic average values (Western Regional Climate Center), but little rainfall (~18 mm) did occur between late November and mid-January. March and April had four times greater rainfall than historic averages (Western Regional Climate Center) with the largest events reaching values of 56, 140, and 47 mm, while average temperatures began to rise over 20 °C (Fig 2.3).

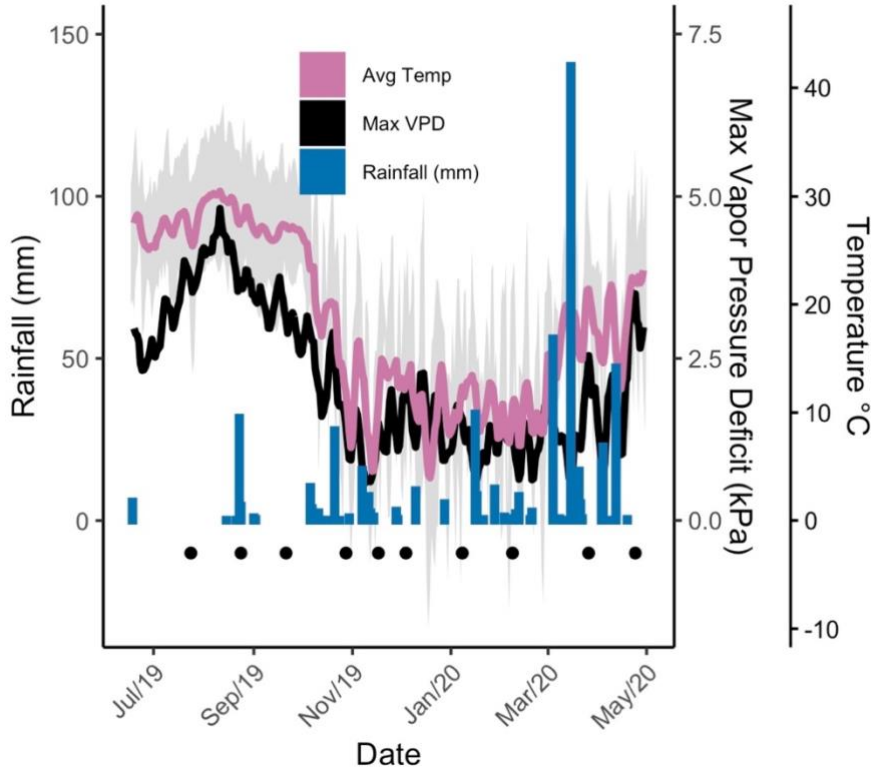

Figure 2.3 Climatic conditions at the Sonora Research Station in Central Texas from June 2019 to May 2020. Total daily rainfall is shown in blue. Five day rolling averages for average air temperature (°C) and max vapor pressure deficit (kPa) are show in pink and black respectively. Minimum and maximum daily air temperatures are shown in grey shading, while sampling dates are shown with black dots.

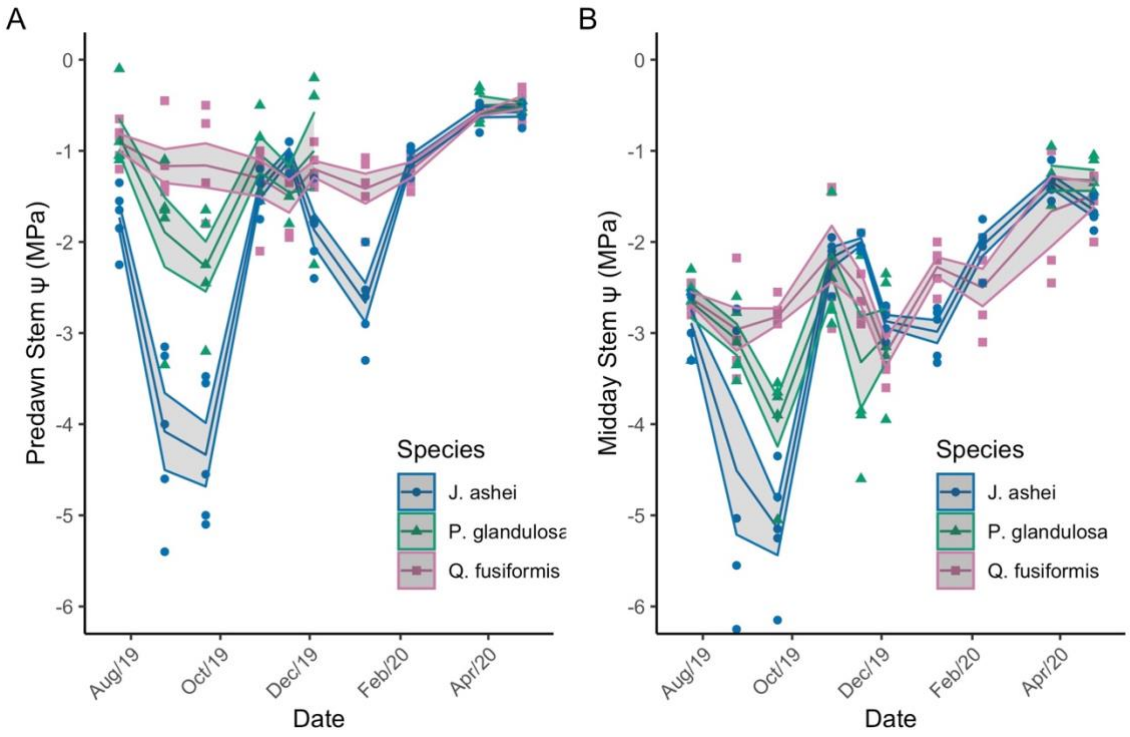

Figure 2.4 Predawn (A) and midday (B) water potentials (MPa) for *J. ashei* (blue circles), *P. glandulosa* (green triangles), and *Q. fusiformis* (pink squares). Shaded areas represent the standard error for each species every month.

Rising vapor pressure deficits and minimal precipitation in late summer led to low soil water availability. This was indicated by declining predawn stem water potentials. The drought tolerant *J. ashei* experienced significantly lower predawn values ($t_{(12)} > 3.90$, $p < 0.006$, Fig 2.4A, Table 2.1) than the other two species. July began with predawn values of -1.7 MPa for *J. ashei* and ~ -1 MPa for the two drought avoiders, *P. glandulosa* and *Q. fusiformis*. Species significantly interacted with quadratic time effects ($F_{(2,117)} = 11.6$, $p < 0.0001$, Table 2.1) with both *P. glandulosa* and *J. ashei* declining to average lows of -2.27 and -4.34 MPa respectively by mid-September (Fig 2.4A). Both

Prosopis and *Juniperus* responded quickly to rain events in the autumn months by increasing predawn values to ~-1 MPa. *Q. fusiformis* had little variation with water availability with consistent predawn values near -1.2 MPa from July to February before increasing to -0.47 MPa in the spring. While *P. glandulosa* experienced dips in predawn values during dry periods, its overall predawn values were not significantly different than the drought avoiding *Q. fusiformis* ($t_{(12)} = -2.10$, $p = 0.17$).

Increasing water deficits during late summer led to increased water limitations for all trees as exhibited by low midday stem water potentials (Fig 2.4B). Juniperus ashei reached the lowest levels of all species during late summer at -5.14 MPa, followed by P. glandulosa at -3.97 MPa, and Q. fusiformis at -2.82 MPa (Fig 2.4B). Midday water potentials for species significantly interacted with time ($F_{(2,117)} = 11.0$, $p < 0.0001$, Table 2.1) and quadratic time effects ($F_{(2,117)} = 9.4$, $p < 0.0002$, Table 2.1) with values rebounding during the cooler winter and water abundant spring months. One dry period during December sampling did see midday values decline to ~-3 MPa for all species. Seasonally, *P. glandulosa* midday water potential values were significantly lower than *Q. fusiformis* ($t_{(12)} = -4.03$, $p < 0.005$) and *J. ashei* ($t_{(12)} = 4.695$, $p < 0.002$) due to the evergreen trees retaining leaves during the more water-abundant winter months.

2.3.2. Soil Depth

Average soil depth was not found to significantly differ among species ($F_{(2,12)} = 0.455$, $p > 0.645$) though maximum soil depths for some *P. glandulosa* individuals were underestimated due to sampling restrictions with the metal pole to 70 cm in depth.

Table 2.1 Mixed model output for stem water potential and gas-exchange variables

Predictor	Ψ_{PD}[a]		Ψ_{MD}[b]		A_{Net}		E[a]		g_s[a]	
	F-value	df(n,d)	F-value	df(n,d)	F-value	df(n,d)	F-value	df(n,d)	F-value	df(n,d)
Intercept	**2,047.7*** **	1, 117	**2,073*** **	1, 117	**271.2*** **	1, 116	**580.11*** **	1, 116	**522.8*** **	1, 119
Species	**6.9***	2, 12	1.8	2, 12	**83.8*** **	2, 12	**27.93*** **	2, 12	**30.7*** **	2, 12
DOY	**9****	1, 117	**72.9*** **	1, 117	0.2	1, 116	**17.09*** **	1, 116	**11.7*** **	1, 119
DOY^2	**11.8*** **	1, 117	**12*** **	1, 117	**5.3***	1, 116	**34.42*** **	1, 116	NA	NA
Species*DOY	0.6	2, 117	**11*** **	2, 117	2.7	2, 116	2.54	2, 116	**3.1***	2, 119
Species*DOY^2	**11.6*** **	2, 117	**9.4*** **	2, 117	**7.5*** **	2, 116	**3.27***	2, 116	NA	NA

* P-values less than or equal to 0.05 (*), 0.01 (**), or 0.001 (***) respectively. Shown in bold.
Unused predictors in final model selection are indicated by NA.
(**a**) Square root or (**b**) inverse transformations of the response variable to achieve normality.

Average soil depth for *P. glandulosa* was slightly lower (48 cm) than the other species, but it ranged from 27 to greater than 70 cm making differences non-significant. Average soil depths for *J. ashei* and *Q. fusiformis* were 41 cm (28 – 66 cm) and 40 cm (31 – 44 cm) respectively.

2.3.3. Seasonal Gas-Exchange and Pigment Trends

Species interacted with both time ($F_{(2,116)} = 2.68$, $p < 0.07$, Table 2.1) and quadratic time effects ($F_{(2,116)} = 7.52$, $p < 0.0008$, Table 2.1) in photosynthesis, with the drought avoiding *P. glandulosa* and *Q. fusiformis* declining over the summer to fall period, while *J. ashei* increased. *P. glandulosa* exhibited the highest A_{Net} rates of all species at 21 μmol m^{-2} s^{-1} in the peak growing season before declining ~48% during the dry period starting in August and leveling off (Fig 2.5B). October to November saw a 61% drop in A_{Net} to 5 μmol m^{-2} s^{-1} as leaves entered the last weeks of their lifespan with leaf-drop occurring Nov-Dec, temperatures cooled, and daylight decreased. Initial spring leaves had net photosynthetic losses before increasing in April for *P. glandulosa* showing its rates were generally higher during growing season months.

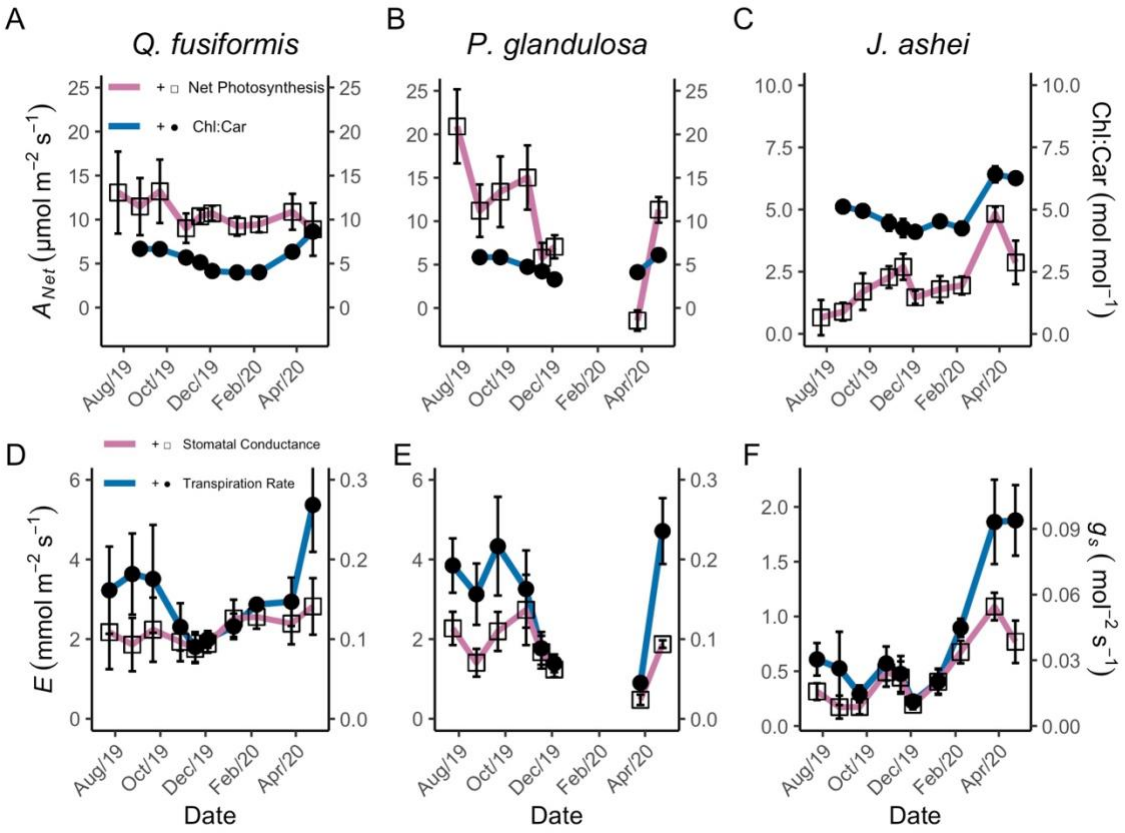

Figure 2.5 Seasonal changes in leaf-level gas exchange and leaf pigment concentrations. Net photosynthetic changes (open squares/pink line) and average chlorophyll:carotenoid ratios (black dotes/blue line) taken for each month for all three woody species (A,B,C). Seasonal transpiration (black dots/blue line) and stomatal conductance (open squares/pink line) rates are depicted in D,E,F. Standard error bars are shown for all measurements. Note: Dual y-axis scales were adjusted to compare trends between two variables at once. The scales for *J. ashei* are smaller than those for *Q. fusiformis* or *P. glandulosa*.

Q. fusiformis exhibited little variation in A_{Net} with values near 13 μmol m^{-2} s^{-1} in the summer months and dropping to 10 μmol m^{-2} s^{-1} for the remainder of the study (Fig 2.5A). These rates for *Q. fusiformis* were significantly higher over the sampling campaign than the other two species ($t_{(12)} > 2.81$, $p < 0.05$). A_{Net} did not show substantial

variation prior to or after the new leaf flush occurring for *Q. fusiformis* trees between March and April. *J. ashei* experienced the lowest A_{Net} values of all species ($t_{(12)} < -3.46$, $p < 0.01$) near 2 μmol m^{-2} s^{-1} throughout the study (Fig 2.5C). Mid-summer lows for *J. ashei* were 0.66 μmol m^{-2} s^{-1} until autumn rains pushed values up to 2.7 μmol m^{-2} s^{-1}. Values of A_{Net} for *J. ashei* declined during the December dry period and through the coldest winter months before peaking in March at 4.83 μmol m^{-2} s^{-1}.

Table 2.2 Mixed model output for leaf pigments.

Predictor	*Total Chl* (μmol g^{-1})		*Total Car* (μmol g^{-1})		*Chl:Car*[a] (mol mol^{-1})	
	F-value	df(n,d)	F-value	df(n,d)	F-value	df(n,d)
Intercept	**1,137*** **	1, 104	**2,174.3*** **	1, 101	**11,427.7*** **	1, 101
Species	**96.7*** **	2, 12	**167.7*** **	2, 12	**7.9** **	2, 12
DOY	NA	NA	0.2	1, 101	**5.2***	1, 101
DOY^2	0.5	1, 104	**101.5*** **	1, 101	**200.2*** **	1, 101
Species*DOY	NA	NA	0.3	2, 101	**6.3** **	2, 101
Species*DOY^2	**5.2** **	2, 104	**18.2*** **	2, 101	**11*** **	2, 101

* P-values less than or equal to 0.05 (*), 0.01 (**), or 0.001 (***) respectively. Shown in bold. Unused predictors in final model selection are indicated by NA.
(a) Logarithmic transformation of the response variable to achieve normality.

Species significantly interacted with the quadratic time effect for total chlorophyll ($F_{(2,104)} = 5.22$, $p < 0.007$, Table 2.2) and total carotenoids ($F_{(2,101)} = 18.21$, $p < 0.0001$, Table 2.2) showing declines in chlorophyll content for *P. glandulosa* and increases in total carotenoid content for all three species beginning October through winter. Total chlorophyll decreased from ~4 to ~2.8 μmol g^{-1} from summer to December

before peaking at 4.75 μmol g^{-1} in April for *P. glandulosa*. Total chlorophyll content was found to be significantly lower in the evergreen *J. ashei* compared to the semi-evergreen and deciduous species ($t_{(12)} < -9.50$, $p < 0.0001$) with values fluctuating slightly near 1.5 μmol g^{-1} compared to values of ~3-4 for *Q. fusiformis*. Conversely, *J. ashei* also experienced significantly lower carotenoid contents with values near 0.3 μmol g^{-1} ($t_{(12)} < -12.0$, $p < 0.0001$), while *P. glandulosa* had significantly higher carotenoid values near 0.75 than the other two species ($t_{(12)} > 3.5$, $p < 0.02$). Carotenoid contents increased from ~0.5 μmol g^{-1} in summer to ~0.85 μmol g^{-1} peak over winter before declining to ~0.3 in the spring for *Q. fusiformis*, while *P. glandulosa* increased from ~0.65 μmol g^{-1} in August to ~0.85 μmol g^{-1} in December. *J. ashei* experienced shifts from 0.25 μmol g^{-1} to 0.4 μmol g^{-1} from summer to winter in total carotenoid contents.

Chlorophyll to carotenoid ratios followed similar patterns across all three species with species significantly interacting with both time ($F_{(2,101)} = 6.33$, $p < 0.003$) and quadratic time effects ($F_{(2,101)} = 11.05$, $p < 0.0001$; Table 2.2, Fig 2.5). Summer values declined to winter lows before reaching their peaks in spring. Summer values of Chl:Car in August were 20% and 23% lower than spring highs for *J. ashei* and *Q. fusiformis* respectively, while *P. glandulosa* had similar values. *Q. fusiformis* had the significantly highest Chl:Car ratio ($t_{(12)} > 3.93$, $p < 0.006$) with 6.56 mol mol^{-1} in August and peaked in April at 8.63 mol mol^{-1} (Fig 2.5A). Both *P. glandulosa* and *J. ashei* started with lower Chl:Car ratios in August. The last sampling in December before leaf-off showed that *P. glandulosa* declined to the lowest Chl:Car ratio of all species at 3.30 mol mol^{-1}. The evergreen *Juniperus ashei* and semi-evergreen *Q. fusiformis* declined to winter lows near

4 mol mol^{-1} in winter (Fig 2.5A & 2.5C). Peak Chl:Car ratio for *J. ashei* was 6.42 mol mol^{-1} during the period of greatest water accumulation in March, while *P. glandulosa* was trending upward in April at 6.1 mol mol^{-1}. Seasonal means for Chl:Car in *J. ashei* were substantially larger than *P. glandulosa* ($t_{(12)} = 2.71$, $p < 0.06$) which had several samplings occur near the two ends of the mesquite leaf lifespans.

Transpiration rates (*E*) for all species interacted with time ($F_{(2,116)} = 2.54$, $p < 0.08$) and quadratic time effects ($F_{(2,116)} = 3.27$, $p < 0.04$, Table 2.1) showing declines from summer to winter before peaking in late spring (Fig 2.5 D,E,F). Transpiration ($t_{(12)} > 4.42$, $p < 0.003$) and stomatal conductance ($t_{(12)} = 5.03$, $p < 0.0009$) rates were significantly higher in *Q. fusiformis* and *P. glandulosa* than the drought-tolerant evergreen *J. ashei.* High transpiration rates for *Q. fusiformis* occurred during the warmest months with the highest VPD levels and reached a high of 5.4 mmol m^{-2} s^{-1} during April (Fig 2.5D). Stomatal conductance values for *Q. fusiformis* varied little over the course of the season at ~0.1 mol $^{-2}$ s^{-1}—similar to the low variability in predawn water potentials. Transpiration and stomatal conductance were tightly coupled within each species for *P. glandulosa* and *J. ashei* (Fig 2.5 E&F). A 23% decline in transpiration from 3.9 mmol m^{-1} s^{-1} occurred July to August for *P. glandulosa* during water deficits, while *J. ashei* saw gradual declines from 0.6 mmol m^{-1} s^{-1} to 0.30 mmol m^{-1} s^{-1} through September. The coupled transpiration and stomatal conductance rates for *J. ashei* reached peak values in the water abundant March with the greatest values at 1.9 mmol m^{-1} s^{-1} and 0.55 mol $^{-2}$ s^{-1} respectively.

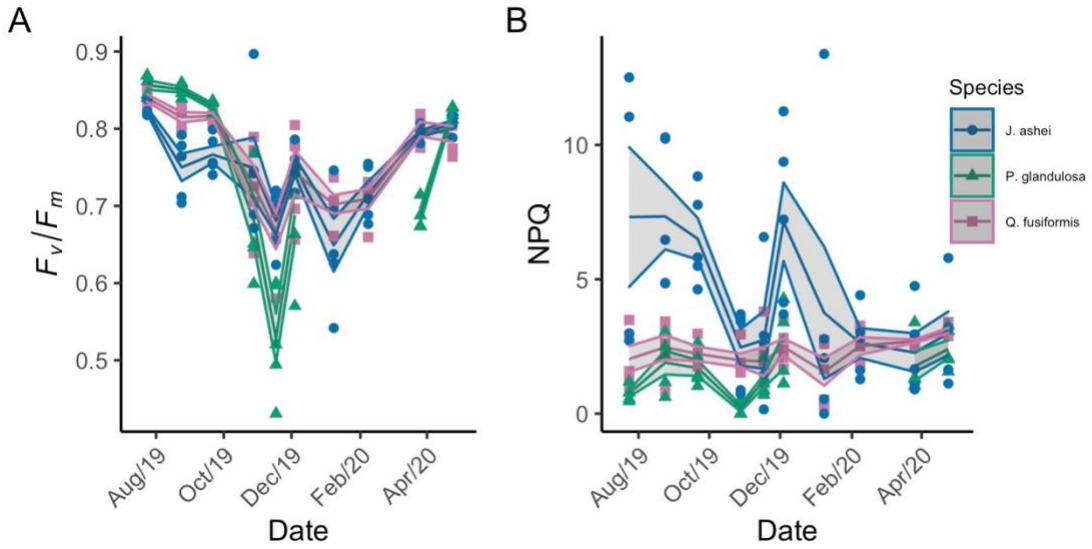

Figure 2.6 Seasonal changes in (A) maximal quantum efficiency of PSII photochemistry (*FV/FM*) and (B) non-photochemical quenching (NPQ). *J. ashei, P. glandulosa,* and *Q. fusiformis* are shown by blue circles, green triangles, and pink squares respectively. Shaded areas represent the standard error for each species every month.

2.3.4. Seasonal Fluorescence Trends

Values for *FV/FM* among species were significantly impacted by quadratic time interactions ($F_{(2,119)} = 12.68$, $p < 0.0001$, Fig 2.6A, Table 2.3). Mild amounts of sustained NPQ and photoinhibition of photosystem II occurred during water limitations for the drought tolerant *J. ashei* in late summer, while freezing temperatures negatively affected all three species later in the growing season. *J. ashei* experienced the lowest values in *FV/FM* across species during the water deficits with values declining from 0.82 in July to 0.75 in late summer (Fig 2.6A).

Table 2.3 Mixed model output for fluorescence variables.

Predictor	F_V/F_M		NPQ		ϕ_{PSII}[a]		$\phi_{f,D}$[b]		ϕ'_{NP}[c]	
	F-value	df(n,d)	F-value	df(n,d)	F-value	df(n,d)	F-value	df(n,d)	F-value	df(n,d)
Intercept	**92,692.2*** **	1, 119	**469.6*** **	1, 121	**2,828.5*** **	1, 116	**1,756.7*** **	1, 120	**696.8*** **	1, 115
Species	**10.0** **	2, 12	**18.3*** **	2, 12	**21.2*** **	2, 12	**12.4** **	2, 12	**27.1*** **	2, 12
DOY	**18.3*** **	1, 119	NA	NA	**6.1***	1, 116	NA	NA	NA	NA
DOY^2	**245.2*** **	1, 119	NA	NA	**79.1*** **	1, 116	**18.5*** **	1, 120	1.9	1, 115
Species*DOY	NA	NA	NA	NA	0.7	2, 116	NA	NA	NA	NA
Species*DOY^2	**12.7*** **	2, 119	NA	NA	**16.3*** **	2, 116	NA	NA	**7.1** **	2, 115

* P-values less than or equal to 0.05 (*), 0.01 (**), or 0.001 (***) respectively. Shown in bold.
Unused predictors in final model selection are indicated by NA.
(a) Square root, **(b)** logarithmic, or (**c)** quadratic transformations of the response variable to achieve normality.

The drought avoiding *P. glandulosa* and *Q. fusiformis* maintained F_V/F_M values above 0.80 during the summer dry period, only showing signs of photoinhibition when freezing nights started appearing in October (Fig 2.6A). One night below freezing during October sampling saw F_V/F_M values for *P. glandulosa* decline from 0.83 to 0.68. The evergreen *J. ashei* and semi-evergreen *Q. fusiformis* maintained values below 0.75 during the winter months, showing the greatest photoinhibitory drops when multiple freezing nights led up to sampling during November, January, and February. Deciduous leaves of *P. glandulosa* only experienced one month of multiple freezing nights in November which led to its greatest sustained NPQ and lowest F_V/F_M values of 0.53. With low values at the end and start of the leaf life cycle, *P. glandulosa* experienced significantly lower F_V/F_M values than *Q. fusiformis* ($t_{(12)} = -3.48$, $p < 0.01$) and substantially lower values than *J. ashei* ($t_{(12)} = -2.47$, $p < 0.09$). *J. ashei* had its lowest F_V/F_M values of 0.65 occur during the slightly water limited but freezing January.

NPQ was highest across species in *J. ashei* ($t_{(12)} > 4.26$, $p < 0.004$, Fig 2.6B, Table 2.3) which peaked at 7.34 during the dry summer months before declining with

cooling temperatures, spiking only once again during the dry period in December (Fig 2.6B). For *P. glandulosa*, NPQ increased to 1.90 during the driest summer months, before declining during the freezing month in October to a low of 0.2 (Fig 2.6B). As leaves began to drop from November to December, *P. glandulosa* experienced increases in NPQ as gas-exchange rates declined to lows. *Q. fusiformis* experienced NPQ values near ~2 with little variation over the sampling period—matching the patterns experienced in predawn stem water potential and stomatal conductance values. All species had similar NPQ values during the spring months.

2.3.5. Energy Partition Analysis

The quantum yield of regulatory light-induced NPQ ($\phi^{r}_{(NP)}$) matched NPQ patterns across species, often increasing when NPQ increased. Values were significantly affected by species and quadratic time interactions ($F_{(2,115)} = 7.10$, $p < 0.0012$, Table 2.3). During periods of low transpiration rates in dry months, $\phi^{r}_{(NP)}$ increased for *J. ashei* and *P. glandulosa* (Fig 2.7C). Across species, *J. ashei* had the highest proportion of absorbed light returned by dynamic energy dissipation ($\phi^{r}_{(NP)}$; $t_{(12)} > 5.21$, $p < 0.0007$) and lowest proportion used by the photosystems (ϕ_{PSII}, $t_{(12)} < -3.91$, $p < 0.006$, Fig 2.7 A&C). In non-stressed conditions, ~50% of absorbed light for *J. ashei* was dissipated by $\phi^{r}_{(NP)}$, increasing to an 84% maximum during water stressed periods and low transpiration. Declines for midday ϕ_{PSII} in *J. ashei* reached lows of 4% photochemical light utilization during the late summer months before gradually increasing to a high of 26% in the spring (Fig 2.7A). *P. glandulosa* utilized the highest amounts of absorbed light towards photochemical pathways with midday ϕ_{PSII} reaching 42% in July with lows

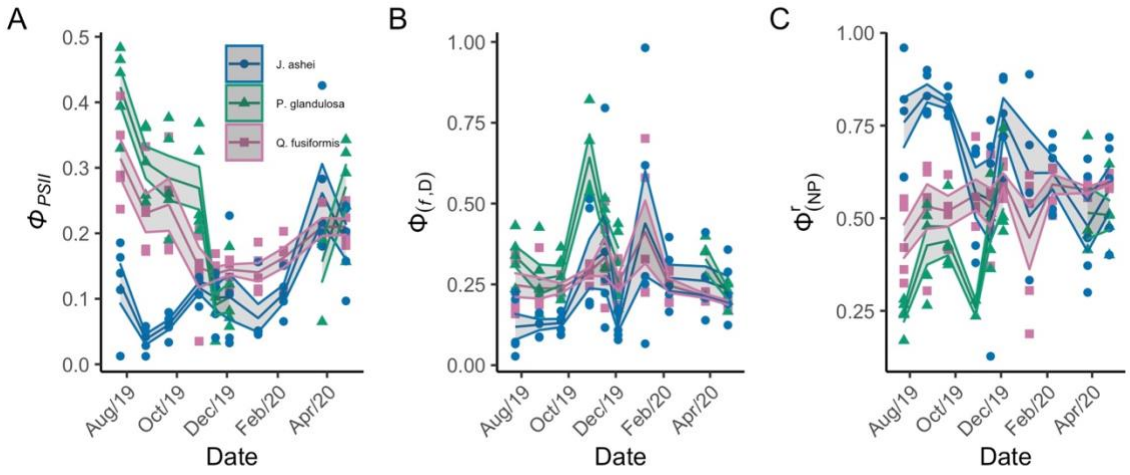

Figure 2.7 Energy partitioning analysis. (A) Actual quantum yield of PSII in a light-adapted state (ϕ_{PSII}) indicates the proportion of light used for photosynthesis. (B) Quantum yields for constitutive non-regulated NPQ ($\phi_{f,D}$) and regulated light induced NPQ ($\phi^{r}_{(NP)}$) represents the proportion of absorbed light returned by NPQ occurring at all times and light responsive dynamic NPQ respectively. *J. ashei, P. glandulosa,* and *Q. fusiformis* are shown by blue circles, green triangles, and pink squares respectively. Shaded areas represent the standard error for each species every month.

in late November near 10% (Fig 2.7A). The lowest relative values of $\phi^{r}_{(NP)}$ experienced across species was *P. glandulosa*, which was never greater than 43% before leaf senescence starting to occur in October.

Similar to its NPQ trends, the semi-evergreen *Q. fusiformis* showed dynamic $\phi^{r}_{(NP)}$ values in between the other species, consistently dissipating ~50% of absorbed light though on average was not significantly different from *P. glandulosa* ($t_{(12)}$ = -2.09, p = 0.18, Fig 2.7A). Quantum yields for constitutive non-regulated NPQ ($\phi_{f,D}$) for *Q. fusiformis* saw slight increases during the winter months (Fig 2.7B). The semi-evergreen leaves experienced moderate ϕ_{PSII} values among species at 31% in July before declining

to lows near 15% over the winter. These initial declines in ϕ_{PSII} yielded marginally greater $\phi^{r}_{(NP)}$ and $\phi_{f,D}$ values for the rest of the sampling period.

The quantum yields of constitutive non-regulated NPQ ($\phi_{f,D}$) and regulatory light-induced NPQ ($\phi^{r}_{(NP)}$) showed inverse patterns to each other across species. Higher $\phi^{r}_{(NP)}$ values in *J. ashei* yielded lower $\phi_{f,D}$ values and vice versa for *P. glandulosa* (Fig 2.7 B&C). As $\phi^{r}_{(NP)}$ increased in dry periods, $\phi_{f,D}$ decreased in *P. glanduosa* and *J. ashei*. $\phi_{f,D}$ only increased during periods of higher transpiration rates relative to the month before and freezing temperatures. Species did not significantly interact with time for $\phi_{f,D}$ (Table 2.3), but *J. ashei* did experience the significantly lowest relative values ($t_{(12)} < -3.09$, $p < 0.03$) , while *P. glandulosa* experienced the greatest ($t_{(12)} > 3.78$, $p < 0.008$). Increases in $\phi_{f,D}$ occurred during the one-night freezing sampled in October for *P. glandulosa* reaching a value of 64% constitutive energy dissipation. Increases in $\phi_{f,D}$ for *J. ashei* occurred after experiencing multiple freezing nights during November and January at a maximum of 44%.

2.4. **Discussion**

The spread of woody encroachers with varying functional traits through the semi-arid regions of the Southern Great Plains is pervasive (Van Auken 2009, Barger et al. 2011). However, little is known how these woody species will photosynthetically and energetically respond to warming temperatures and dry periods predicted to increase in the future (Seager et al. 2007, Strzepek et al. 2010, Cook et al. 2015). Particularly little is known how the drought tolerant *Juniperus* sp. associated with driest parts of the

landscape (shallow rocky soils and steep hillsides) will compare to the drought avoiding *Prosopis* and *Quercus* species. Evaluating responses to seasonal stress among the three co-occurring encroachers that vary in soil water access and leaf persistence in the semi-arid regions of Southern Great Plains should improve our understandings of their potential vulnerabilities to these climatic shifts. Specifically, we assessed how seasonal dry periods and freezing events influenced light-utilization for photosynthesis and energy dissipation among the woody encroachers. In particular, we evaluated responses to water limitations during the hot, dry period of late summer which is projected to increase in severity in the future which could have the greatest impact on the drought tolerant *Juniperus*.

Water availability over this study was particularly limited which allowed for strong comparisons between the woody encroachers in their energy use and photosynthetic capabilities under drier conditions. Rains over the summer and autumn were 57% below average (Western Regional Climate Center) leading to low Ψ_{PD} values. These leaf water potentials were lower (Bendevis et al. 2010, Elkington et al. 2014) or as low to past seasonal studies (Eggemeyer and Schwinning 2009, Johnson et al. 2017[a], Johnson et al. 2017[b]). These greater water limitations caused >50% lower stomatal conductance values for *J. ashei* and *Q. fusiformis*, and average to lower transpiration rates across species compared to past studies (Owens and Schreiber 1992, Eggemeyer and Schwinning 2009, Bendevis et al. 2010).

Relative differences in water status among species were explained by their known rooting behaviors and expected water access but were sometimes inconsistent

with their recorded soil depths. The deepest roots found to absorb water within large cavities of the limestone of the Edwards Plateau has been the drought avoiding *Q. fusiformis* (Jackson et al. 1999, McElrone et al. 2004) which likely aided its relatively stable and high water status recorded here. However, its 40 cm of soil depth was not found to significantly differ from *J. ashei* (41 cm) and the slightly deeper *P. glandulosa* (> 48 cm). Considering the ability of *Q. fusiformis* to penetrate through limestone cracks to deep depths in the karst landscape and ability to uptake water in those layers (Jackson et al. 1999, McElrone et al. 2004), the observed soil sampling depth recorded here may not be the most useful for assessing water access among all species. Indeed, the sampling method for soil depth is susceptible to hitting rocks in the soil matrix (Elkington et al. 2014) and is constrained in deeper soils where *P. glandulosa* was found.

Recorded soil depths in *P. glandulosa* and *J. ashei* were more consistent with expected rooting depths and water access that helped explain their relative responses in water status during dry periods. Generally, *Prosopis* sp. are deeply rooted allowing for deeper water access (Lombardini and Rossi 2019, Wilson et al. 2001), but they can establish in soils depths of 1.5 to 2.5 m on the Edwards Plateau which is deep for the area but relatively shallow for *P. glandulosa* (Eggmeyer and Schwinning 2009). This is consistent with soil depth recorded here indicating that *P. glandulosa* occupied slightly deeper soils (> 48 cm) than the other two species but was not significantly different likely due to the conservative limits of the sampling technique beyond 70 cm. Eggmeyer and Schwinning (2009) note that *P. glandulosa* establishment at these relatively shallow sites can make it as responsive to water limitations as *J. ashei*—blurring its general

distinction as a drought avoider. This responsiveness to water limitations is exhibited in these results where both *P. glandulosa* and *J. ashei* experienced lowered water status during the late summer dry period, though *J. ashei* did appear restricted to the shallowest depths in this study with the lowest recorded water status (Hall 1952, Thurow and Hester 1997). Deeper soils have been suggested to hold greater water storage for this system and species at the same depths (Elkington et al. 2014), which may have benefited *P. glandulosa* with better water access and relatively higher water status in the slightly deeper soils than *J. ashei*.

Together, $\phi^{r}_{(NP)}$ represents dynamic energy dissipation via the xanthophyll cycle and ϕ_{PSII} the photochemical quenching at midday (Hendrickson et al. 2004, Lazár 2015). $\phi^{r}_{(NP)}$ was found to drive overall NPQ dissipation trends within and between species, which is consistent with NPQ being largely driven by light-regulated dissipation processes (Ruban 2016, Marchie and Ruban 2020). Results here suggest that water status and known leaf functional traits played important roles in determining midday ϕ_{PSII} and dynamic $\phi^{r}_{(NP)}$ dissipation needs among the co-occurring encroachers in response to dry and cold periods.

Species with declining water status during dry periods experienced greater decreases in ϕ_{PSII} and increases in $\phi^{r}_{(NP)}$ responses—thus indicating a reduced photochemical capacity during water limitations on hot, dry days. The drought tolerant *J. ashei* and drought avoider *P. glandulosa* experienced their lowest Ψ_{MD} and water access (Ψ_{PD}) during dry periods in late summer. These drops in Ψ_{PD} and Ψ_{MD} coupled with high VPD and temperatures in late summer produced lowered g_s at midday (Turner et al.

1984), which increased photoprotective heat release from $\phi^{r}_{(NP)}$ during dry periods. Closed stomata can decrease ϕ_{PSII} due to decreased intercellular CO_2 levels (Kalaji et al. 2017), which likely increased their dynamic $\phi^{r}_{(NP)}$ energy dissipation. Consequently, the increased water stress coupled with high VPD at midday contributed to declines in light-saturated photosynthetic rates for both species over this period. The drought tolerant *J. ashei* experienced the greatest reductions in photochemical yields at midday (4% for the ϕ_{PSII}) with the highest dynamic energy dissipation (84% for the $\phi^{r}_{(NP)}$) indicating that the *Juniperus* species was the most photochemically stressed encroacher under light-saturating conditions during the hot, dry period in late summer.

Conversely, the drought avoiding *Q. fusiformis* experienced smaller changes in Ψ_{PD}, Ψ_{MD}, and g_s during late-summer (July-Sept) coupled with smaller fluctuating dynamic energy $\phi^{r}_{(NP)}$ dissipation needs in response to dry periods. Photosynthetic rates did not vary considerably over this period though ϕ_{PSII} did decline slightly with a slight increase in $\phi^{r}_{(NP)}$ from July to August before both stabilized through September. This indicates that the fraction of absorbed light used in photosynthesis may have decreased slightly under the hotter drier temperatures, but that fraction of absorbed light for photochemical quenching was sufficient to create similar light-saturated photosynthetic rates to those in the less evaporatively demanding July. Though some dynamic energy dissipation increased slightly, the light-saturated photosynthetic rates were largely unaffected in the drought avoiding *Q. fusiformis* during the late summer dry period as a result.

In addition to the greater dynamic energy dissipation by $\phi^{r}_{(NP)}$, the drought tolerant *J. ashei* suffered from mild amounts of sustained energy dissipation and photoinhibition of the maximal quantum yield of PSII (F_V/F_M) due to water limitations in late summer. This was indicated by *J. ashei* experiencing the greatest declines in F_V/F_M across species during the water deficits with values declining from 0.82 in July to 0.75 in late summer (Fig 2.6A). While ϕ_{PSII} constrains photosynthetic activity at midday and is influenced by the maximal quantum yield of PSII under lighted conditions ($F_{V'}/F_{M'}$), $F_{V'}/F_{M'}$ decreases from the dark-adapted maximal value (F_V/F_M) that recovers overnight. Consequently, reductions in F_V/F_M reduces the quantum yields under light-limited conditions to begin the day which can substantially constrain A_{Net} during low light periods (Adams et al. 2008, Murchie and Ruban 2020). Consequently, lack of recovery in the predawn maximal quantum yields would show greater constraints on photosynthetic activity for *Juniperus* over the course of a day than *Q. fusiformis* or *P. glandulosa*. Diurnal studies are further needed to confirm this. The two drought avoiders with shorter leaf lifespans did not experience sustained photoinhibition under drier conditions.

Generally, ranges of non-stressed values of F_V/F_M across similar functional types tend to be 0.83 to 0.85 (Björkman and Demmig 1993), which are similar to the highest values for *J. ashei* that were 0.81 or greater during July and April. These higher values are consistent with non-stressed values found for related drought tolerant species *J. phoenicea* (Werner et al. 2002, Ain-Lhout 2004) and *J. virginiana* (Msanne et al. 2017) indicating that *J. ashei* was relatively unstressed under high water availability and

warmer temperatures. Sustained energy dissipation is often considered present when plants are stressed and F_V/F_M falls below 0.80 (Verhoeven 2014). These declines in F_V/F_M for *J. ashei* during late summer were comparable to *J. virginiana* dips in the cooler Nebraska sandhills during late summer (Msanne et al. 2017). Hot and dry Mediterranean climates have shown *J. phoenicea* dropping to minimums of 0.62 in summer (Werner et al. 2002). The magnitude of sustained NPQ and consequential drop in F_V/F_M can depend on the species, length of acclimation, and extent of the stressor (freezing temperatures or lowered leaf water content) on the leaf tissue (Verhoeven et al. 2018). Consequently, the seasonal dry period created mild amounts of sustained energy dissipation and photoinhibition for the most water limited encroacher in *Juniperus*. These declines in maximal quantum yields would likely lead to depressed photosynthetic activity throughout the day for *Juniperus* (Adams et al. 2008, Murchie and Ruban 2020) during dry periods. The lack of substantial declines in F_V/F_M during the dry period for *P. glandulosa* or *Q. fusiformis* indicate their photosynthetic capacities during light-limited times of the day would be minimally impacted as their photosystems fully recovered overnight. Consequently, water limitations not only decreased midday photochemical capacities (ϕ_{PSII} and light-saturated A_{Net}) for *Juniperus* but maximal capacities for utilizing light (F_V/F_M) was also reduced, which can be additionally impactful during light-limited portions of the day such as the early morning.

Chl:Car ratios were highest in the spring for *J. ashei* and *Q. fusiformis* with relatively lower values during summer (20% and 23% lower respectively) indicating that spring was a period shifted towards maximizing light-harvesting and increasing

photosynthetic levels, while late summer was shifted towards increasing photoprotective energy dissipation (Esteban et al. 2015). It should be noted that *P. glandulosa* did not appear to have differing light-harvesting capacities between spring and summer as Chl:Car values were similar. Despite increased light-harvesting capabilities, impacts on photosynthesis seemed negligible in *Q. fusiformis* which experienced little variation in gas-exchange over the entire sampling period but also had leaf-turnover occurring in March and April that may have affected the photosynthetic capacities in the spring. The shifting pigment pools may have been more important in the drought tolerant *J. ashei* which showed July A_{Net} values were 86% lower than March values while dynamic and sustained energy dissipation occurred over the summer before the onset of cooler temperatures. Therefore, the period of greatest water availability in spring for the drought tolerant *Juniperus* showed the greatest photosynthetic capacities, light-harvesting capabilities with highest Chl:Car ratios, and decreased needs for sustained or dynamic energy dissipation, while the summer showed opposite patterns for all parameters. Thus, the drought tolerant *Juniperus* required greater photoprotective and reduced photosynthetic capacities during the hot, dry summer with limited water availability relative to the water abundant spring.

The arrival of cold temperatures and rain in October did lead to differing energy uses under light-saturating conditions between the drought tolerant *J. ashei* and the two drought avoiders. ϕ_{PSII} declined to lows in *P. glandulosa* upon cold temperature onset as leaves neared the end of their lifespans and gas-exchange rates dropped. These reductions in gas-exchange rates are expected due to chlorophyll content drops as

temperatures cool and daylight decreases in autumn (Rosenthal and Camm 1997) which is consistent with the concurrent chlorophyll and Chl:Car declines recorded here for *P. glandulosa*. *Q. fusiformis* also experienced declines in ϕ_{PSII} and A_{Net} with cold temperature onset in October due to increases in constitutive non-regulated ($\phi_{f,D}$) dissipation—indicating some increased contributions of sustained energy dissipation (Lazár 2015). *J. ashei* responded positively to the onset of colder months through early spring (November – March) by increasing ϕ_{PSII} and A_{Net} values and reducing $\phi^{r}_{(NP)}$. One exception was December where low predawn water availability produced low gas-exchange rates that caused a spike in $\phi^{r}_{(NP)}$. Consequently, cooler temperatures brought declines in light-saturated photosynthetic activity for *P. glandulosa* and *Q. fusiformis* but increases for *Juniperus.*

The cooler temperatures and greater water availability from late fall through early spring likely allowed for higher ϕ_{PSII} and midday A_{Net} rates for *J. ashei*, while *P. glandulosa* and *Q. fusiformis* had higher rates in the summer. These temporally separated peaks for *J. ashei* and *Q. fusiformis* are similar to patterns recorded by Owens (1996) and Bendevis et al. (2010) in these systems. The slightly higher midday A_{Net} and ϕ_{PSII} found here and in the prior studies (Owens 1996, Bendevis et al. 2010) may indicate this period provides preferable conditions for midday net photosynthetic uptake for *J. ashei* due to less severe temperature, water status, and VPD constraints at midday. Additionally, the lowered daylight hours in winter would need to be considered in terms of total leaf carbon uptake over the day. Some evidence of photosynthetic increases in

other conifer species (*Pinus halpensis*) has been recorded in the similarly cool but infrequently freezing winters of Mediterranean systems (Werner et al. 2002).

While only the drought tolerant *J. ashei* experienced mild photoinhibition and sustained energy dissipation under dry periods, all species were negatively impacted by the onset of freezing conditions—though dry periods compounded freezing effects in *J. ashei*. Neither drought avoiding species (*Q. fusiformis* and *P. gladulosa*) experienced substantial drops in F_V/F_M until the freezing nights started in October. Cold temperatures also marked the beginning of leaf senescence for *P. glandulosa* as leaves began to abscise from mid-October until complete leaf-off in mid-December (pers. obs.). Photoinhibition and sustained NPQ were particularly large during the one freezing night in October and multiple freezing nights in November leading to a low of 0.53 for *P. glandulosa*. Shifts away from photosynthetic capacities in *P. glandulosa* was driven by decreasing chlorophyll content with smaller increases in photoprotective carotenoid contents in late fall. Consequently, pigments shifted towards photoprotection as illustrated in the lowered Chl:Car ratios. In order to avoid the stressors of colder temperatures, winter deciduous species often senesce in autumn (Verhoeven et al. 2018). Otherwise, freezing temperatures can put similar desiccation stress on leaf cells as drought (Verhoeven et al. 2018) by forming ice in the intercellular spaces that draws water from surrounding cells (Verhoeven 2014). Low temperature tolerant plants can help maintain functioning by accumulating sugars in the cells and utilizing membrane stabilizing reactions to prevent loss of water (Verhoeven et al. 2018, Ouellet and Charron 2013). As a winter deciduous species that is low temperature averse, freezing

temperatures likely required the greater sustained energy dissipation over this period for *P. glandulosa*.

The semi-evergreen leaves of *Q. fusiformis* also showed increased sustained energy dissipation under colder temperatures, but these increases were milder and similar to *J. ashei*. Overwintering evergreen leaves can increase their carotenoid content with 20 to >100% more xanthophyll or lutein pigments compared to summer values to improve energy dissipating capabilities while maintaining chlorophyll content for photosynthesis (Verhoeven 2014). This is consistent with the total carotenoid content increases and steady chlorophyll levels exhibited by both *J. ashei* and *Q. fusiformis* over the winter. Consequently, such shifts towards increased photoprotection in the overwintering species is shown in the decreasing Chl:Car ratios over winter. Meta-analyses show this is a prevalent trend in species experiencing low temperature or drought stress (Esteban et al. 2015, Fernández-Marín et al. 2017). As both freezing and dry periods can cause desiccating effects (Verhoeven et al. 2018), the combined effects likely caused greater sustained energy dissipation in *J. ashei* during the dry and freezing sampling period in January.

Relative differences in ϕ_{PSII} and A_{Net} between species was consistent with the known leaf functional traits associated with each encroacher which directly affected their dynamic $\phi^{r}_{(NP)}$ dissipation needs. Longer leaf lifespans generally emphasize greater structural support to maintain low gas-exchange rates over longer periods of time, while shorter lived leaves emphasize maximizing photosynthetic rates (Reich and Walters 1992, Wright et al. 2004). The results of this study align with that concept showing

greater ϕ_{PSII} and A_{Net} at midday during summer in the shorter-lived *P. glandulosa* leaves and greater photoprotective $\phi^{r}_{(NP)}$ at midday in the longer-lived *J. ashei* leaves. The highest ϕ_{PSII} (42% maximum) and A_{Net} coupled with the lowest $\phi^{r}_{(NP)}$ (25 – 43%) needs in the summer months for *P. glandulosa* was likely aided by its much greater stomatal densities than the other two species and its lack of investment in strong structural leaf tissue for long leaf longevity (Meyer and Morton 1971). Decreased transpiration at the end of the leaf-life for *P. glandulosa* in Nov-Dec likely caused $\phi^{r}_{(NP)}$ to climb upwards of 50% as chlorophyll content and gas-exchange capabilities decreased (Rosenthal and Camm 1997). A closely related species to *Q. fusiformis* has recorded moderately high stomatal densities and desiccating preventative trichomes (Thyroff et al. 2019) that we assume *Q. fusiformis* similarly featured and allowed it to obtain the moderately high photosynthetic capacities exhibited here. The low stomatal densities and greater investments in durable scale like appressed leaves likely yielded the lowest photosynthetic capacities (ϕ_{PSII} of 4 – 26%) and highest dynamic dissipation via $\phi^{r}_{(NP)}$ (48 – 84%) among encroachers for *J. ashei* (Johnsen 1963). Additionally, low g_s reduces intercellular CO_2 which decreases ϕ_{PSII} (Kalaji et al. 2017). This should necessitate greater dynamic dissipation by $\phi^{r}_{(NP}$ for those with lower conductance values like *J. ashei*.

2.5. **Conclusions**

We found that the drought tolerant *Juniperus* is likely to exhibit greater photochemical stress during periods of water limitations compared to co-occurring *Prosopis* or *Quercus* species due to its reductions in photosystem II capacities at midday

(4% low of ϕ_{PSII}) and recovery overnight (F_V/F_M decline to 75%). This is supportive of our initial hypotheses of greater rates of dynamic and sustained energy dissipation in *J. ashei* during dry periods similar to other *Juniperus* species (Martínez-Ferri et al. 2000, Werner et al. 2002, Ain-Lhout et al. 2004,) over the two drought avoiders. Conversely, neither of the drought avoiders (*P. glandulosa* nor *Q. fusiformis*) increased their sustained photoinhibition of F_V/F_M during seasonal water limitations—though *P. glandulosa* did experience reductions in light-saturated A_{Net} due to declining Ψ_{MD} and g_s under the high VPD and low Ψ_{PD}. Light-saturated A_{Net} for the drought avoiding *Q. fusiformis* was largely unaffected during the dry period due to its stable water status. The photochemical stress for *J. ashei* observed at midday and recovery overnight during periods of water limitations may cause *Juniperus* sp. to be more negatively impacted by the increasing drought severity predicted through the 21st century compared to co-occurring *Prosopis* and *Quercus* species in drier regions of the Southern Great Plains. More controlled studies on the effects of water limitations covering the full growing season and diurnal comparisons among the co-occurring species are necessary to support these conclusions.

All woody encroachers increased sustained energy dissipation with the arrival of freezing temperatures at night as hypothesized, but the midday photosynthetic responses to the cooler temperatures and increased water availability over winter varied among the encroachers. While A_{Net} can be expected to be reduced in the light-limiting conditions around dawn due to increased photoinhibition of F_V/F_M from freezing nights (Adams et al. 2008, Verhoeven et al. 2018, Murchie and Ruban 2020), F_V/F_M declines were greatest

in the winter deciduous *P. glandulosa* and mild for *J. ashei* and *Q. fusiformis*. Dry periods during freezing conditions were additionally stressful for the F_V/F_M of *J. ashei* but not *Q. fusiformis*. While the infrequent freezing temperatures may decline F_V/F_M mildly across species, the cooler midday temperatures and increased water availability from late fall to early spring may yield higher midday photosynthetic capacities for *J. ashei* (Owens 1996, Bendevis et al. 2010) though more studies should be pursued to ascertain this. If supported, it is unclear how changing water availability and growing season lengths from warming temperatures coupled with shortened daylight hours could impact midday photosynthetic performance of *J. ashei* during the winter.

This study furthered our understanding of the photosynthetic and energetic responses of major co-occurring woody encroachers in the semi-arid Southern Great Plains that vary in water status and leaf functional traits. This is particularly important considering their differing tolerances to water limitations and drought mortality (highest in the drought tolerant *J. ashei* on the Edwards Plateau) among species (Moore et al. 2016), the heavy woody encroachment rates of these genera in the Southern Great Plains (Barger et al. 2011), and the important role that semi-arid regions play in atmospheric CO_2 levels (Poulter et al. 2014, Ahlstrom et al. 2015). Such knowledge furthers our understanding of how the different woody encroachers of these heavily transformed landscapes in the Southern Great Plains are likely to respond under more variable and stronger climatic conditions predicted in the future (Seager et al. 2007, Strzepek et al. 2010, Cook et al. 2015)—with *Juniperus* likely to the most severely impacted during dry periods. Studies of more woody species and degrees of environmental stressors are

further needed to assess the variable responses among encroachers geographically, diurnally, and within genera.

2.6. **References**

Abobatta, W. F. 2019. Drought adaptive mechanisms of plants – a review. Advances in Agriculture and Environmental Science **2**:42–45.

Adams, W. W., C. R. Zarter, K. E. Mueh, V. Amiard, and B. Demmig-Adams. 2008. Energy dissipation and photoinhibition: a continuum of photoprotection. In Demmig-Adams, B., W. W. Adams, and A. K. Matoo (Ed.), Photoprotection, photoinhibition, gene regulation, and environment, Springer, Dordrecht, Netherlands. 49-64.

Ahlstrom, A., M. R. Raupach, G. Schurgers, B. Smith, A. Arneth, M. Jung, M. Reichstein, J. G. Canadell, P. Friedlingstein, A. K. Jain, E. Kato, B. Poulter, S. Sitch, B. D. Stocker, N. Viovy, Y. P. Wang, A. Wiltshire, S. Zaehle, and N. Zeng. 2015. The dominant role of semi-arid ecosystems in the trend and variability of the land CO2 sink. Science **348**:895–899.

Ain-Lhout, F., M. C. D. Barradas, M. Zunzunegui, H. Rodríguez, F. G. Novo, and M. A. Vargas. 2004. Seasonal differences in photochemical efficiency and chlorophyll and carotenoid contents in six Mediterranean shrub species under field conditions. Photosynthetica **42**:399–407.

Allen, C. D., D. D. Breshears, and N. G. McDowell. 2015. On underestimation of global vulnerability to tree mortality and forest die-off from hotter drought in the Anthropocene. Ecosphere **6**:1-55.

Ansley, R.J., Trevino, B.A., & Jacoby, P.W. 1998. Intraspecific competition in honey mesquite: Leaf and whole plant responses. Journal of Range Management **51:**345-352.

Baquedano, F. J., and F. J. Castillo. 2007. Drought tolerance in the Mediterranean species *Quercus coccifera*, *Quercus ilex*, *Pinus halepensis*, and *Juniperus phoenicea*. Photosynthetica **45**:229-238.

Barger, N. N., S. R. Archer, J. L. Campbell, C. Huang, J. A. Morton, and A. K. Knapp. 2011. Woody plant proliferation in North American drylands: A synthesis of impacts on ecosystem carbon balance. Journal of Geophysical Research: Biogeosciences **116**:1-17.

Barron-Gafford, G. A., R. L. Scott, G. D. Jenerette, E. P. Hamerlynck, and T. E. Huxman. 2012. Temperature and precipitation controls over leaf- and ecosystem-level CO2 flux along a woody plant encroachment gradient. Global Change Biology **18**:1389–1400.

Bendevis, M. A., M. K. Owens, J. L. Heilman, K. J. McInnes. 2010. Carbon exchange and water loss from two evergreen trees in a semiarid woodland. Ecohydrology **3**:107–115.

Bihmidine, S., N. M. Bryan, K. R. Payne, M. R. Parde, J. A. Okalebo, S. E. Cooperstein, and T. Awada. 2010. Photosynthetic performance of invasive *Pinus ponderosa* and *Juniperus virginiana* seedlings under gradual soil water depletion. Plant Biology **12**:668–675.

Björkman, O., and B. Demmig. 1987. Photon yield of O2 evolution and chlorophyll fluorescence characteristics at 77 K among vascular plants of diverse origins. Planta **170**:489–504.

Choat, B., S. Jansen, T. J. Brodribb, H. Cochard, S. Delzon, R. Bhaskar, S. J. Bucci, T. S. Feild, S. M. Gleason, U. G. Hacke, A. L. Jacobsen, F. Lens, H. Maherali, J. Martínez-Vilalta, S. Mayr, M. Mencuccini, P. J. Mitchell, A. Nardini, J. Pittermann, R. B. Pratt, J. S. Sperry, M. Westoby, I. J. Wright, and A. E. Zanne. 2012. Global convergence in the vulnerability of forests to drought. Nature **491**:752–755.

Cook, B. I., T. R. Ault, and J. E. Smerdon. 2015. Unprecedented 21st century drought risk in the American Southwest and Central Plains. Science Advances **1**:1-7.

Cregg, B. M. (1992). Leaf area estimation of mature foliage of *Juniperus*. Forest Science **8:**61-67.

Dai, A. 2013. Increasing drought under global warming in observations and models. Nature Climate Change **3**:52–58.

Demmig-Adams, B., and W. W. Adams. 1996. The role of xanthophyll cycle carotenoids in the protection of photosynthesis. Trends in Plant Science **1**:21-26.

Demmig-Adams, B., C. M. Cohu, O. Muller, and W. W. Adams. 2012. Modulation of photosynthetic energy conversion efficiency in nature: from seconds to seasons. Photosynthesis Research **113**:75–88.

Demmig-Adams, B., and W. W. Adams. 2018. An integrative approach to photoinhibition and photoprotection of photosynthesis. Environmental and Experimental Botany **154**:1–3.

Duursma, R. 2019. *plantecophys*. R package version 1.4-4, https://www.rdocumentation.org/packages/plantecophys.

Eggemeyer, K. D., and S. Schwinning. 2009. Biogeography of woody encroachment: Why is mesquite excluded from shallow soils? Ecohydrology **2**:81–87.

Elkington, R. J., K. T. Rebel, J. L. Heilman, M. E. Litvak, S. C. Dekker, and G. W. Moore. 2014. Species-specific water use by woody plants on the Edwards Plateau, Texas. Ecohydrology **7**:278–290.

Esteban, R., L. Balaguer, E. Manrique, R. Rubio de Casas, R. Ochoa, I. Fleck, M. Pintó-Marijuan, I. Casals, D. Morales, M. S. Jiménez, R. Lorenzo, U. Artetxe, J. M. Becerril, and J. I. García-Plazaola. 2009. Alternative methods for sampling and preservation of photosynthetic pigments and tocopherols in plant material from remote locations. Photosynthesis Research **101**:77–88.

Esteban, R., O. Barrutia, U. Artetxe, B. Fernández-Marín, A. Hernández, and J. I. García-Plazaola. 2015. Internal and external factors affecting photosynthetic pigment composition in plants: A meta-analytical approach. New Phytologist **206**:268–280.

Fensham, R. J., R. J. Fairfax, and D. P. Ward. 2009. Drought-induced tree death in savanna. Global Change Biology **15**:380–387.

Fernández-Marín, B., A. Hernández, J. I. Garcia-Plazaola, R. Esteban, F. Míguez, U. Artetxe, and M. T. Gómez-Sagasti. 2017. Photoprotective strategies of Mediterranean plants in relation to morphological traits and natural environmental pressure: A meta-analytical approach. Frontiers in Plant Science **8**:1-16.

Fernández-Marín B., J.I. García-Plazaola, A. Hernández, and R. Esteban. 2018. Plant photosynthetic pigments: Methods and tricks for correct quantification and identification. In Sánchez-Moreiras A., Reigosa M. (Eds.) Advances in Plant Ecophysiology Techniques. Springer, Cham. 29-51.

Franco, A. C., S. Matsubara, and B. Orthen. 2007. Photoinhibition, carotenoid composition and the co-regulation of photochemical and non-photochemical quenching in neotropical savanna trees. Tree Physiology **27**:717–725.

Gałecki, A., and T. Burzykowski. 2013. Linear mixed-effects models using R. Springer, New York, NY.

Hall, M. T. 1952. Variation and hybridization in *Juniperus*. Annals of the Missouri Botanical Garden **39**:1–64.

Hendrickson, L., R. T. Furbank, and W. S. Chow. 2004. A simple alternative approach to assessing the fate of absorbed light energy using chlorophyll fluorescence. Photosynthesis Research **82**:73–81.

Jackson, R. B., L. A. Moore, W. A. Hoffmann, W. T. Pockman, and C. R. Linder. 1999. Ecosystem rooting depth determined with caves and DNA. Proceedings of the National Academy of Sciences **96**:11387–11392.

Johnsen, T. N., Jr. 1963. Anatomy of scalelike leaves of Arizona junipers. Botanical Gazette **124**:220-224.

Johnson, D. M., Z. C. Berry, K. V. Baker, D. D. Smith, K. A. McCulloh, and J.-C. Domec. 2018a. Leaf hydraulic parameters are more plastic in species that experience a wider range of leaf water potentials. Functional Ecology **32**:894–903.

Johnson, D. M., J.-C. Domec, Z. Carter Berry, A. M. Schwantes, K. A. McCulloh, D. R. Woodruff, H. Wayne Polley, R. Wortemann, J. J. Swenson, D. Scott Mackay, N. G. McDowell, and R. B. Jackson. 2018b. Co-occurring woody species have diverse hydraulic strategies and mortality rates during an extreme drought: Belowground hydraulic failure during drought. Plant, Cell & Environment **41**:576–588.

Kalaji, H. M., G. Schansker, M. Brestic, F. Bussotti, A. Calatayud, L. Ferroni, V. Goltsev, L. Guidi, A. Jajoo, P. Li, P. Losciale, V. K. Mishra, A. N. Misra, S. G. Nebauer, S. Pancaldi, C. Penella, M. Pollastrini, K. Suresh, E. Tambussi, M. Yanniccari, M. Zivcak, M. D. Cetner, I. A. Samborska, A. Stirbet, K. Olsovska, K. Kunderlikova, H. Shelonzek, S. Rusinowski, and W. Bąba. 2017. Frequently asked questions about chlorophyll fluorescence, the sequel. Photosynthesis Research **132**:13–66.

Klemm, T., D. D. Briske, and M. C. Reeves. 2020. Vulnerability of rangeland beef cattle production to climate-induced NPP fluctuations in the US Great Plains. Global Change Biology **26**:4841–4853.

Lazár, D. 2015. Parameters of photosynthetic energy partitioning. Journal of Plant Physiology **175**:131–147.

Lichtenthaler, H.K. 1987. Chlorophyll and carotenoids: Pigments of biosynthetic compounds. Methods in Enzymology **148**:350-382.

Liu, N., and L. Guan. 2012. Linkages between woody plant proliferation dynamics and plant physiological traits in southwestern North America. Journal of Plant Ecology **5**:407–416.

Lombardini, L., and L. Rossi. 2019. Ecophysiology of plants in dry environments. In P. D'Odorico, A. Porporato, and C. Wilkinson Runyan (Ed.), Dryland Ecohydrology. Springer International Publishing, Switzerland. 71-100.

Loriaux, S. D., T. J. Avenson, J. M. Welles, D. K. Mcdermitt, R. D. Eckles, B. Riensche, and B. Genty. 2013. Closing in on maximum yield of chlorophyll fluorescence using a single multiphase flash of sub-saturating intensity. Plant, Cell & Environment **36**:1755–1770.

Malnoë, A. 2018. Photoinhibition or photoprotection of photosynthesis? Update on the (newly termed) sustained quenching component qH. Environmental and Experimental Botany **154**:123–133.

Martínez-Ferri, E., L. Balaguer, F. Valladares, J. M. Chico, and E. Manrique. 2000. Energy dissipation in drought-avoiding and drought-tolerant tree species at midday during the Mediterranean summer. Tree Physiology **20**:131–138.

Maxwell, K., and G. N. Johnson. 2000. Chlorophyll fluorescence—a practical guide. Journal of Experimental Botany **51**:659–668.

McElrone, A. J., W. T. Pockman, J. Martinez-Vilalta, and R. B. Jackson. 2004. Variation in xylem structure and function in stems and roots of trees to 20 m depth. New Phytologist **163**:507–517.

Meyer, R.E. and Morton, H.L. 1971. Morphology and Anatomy of Honey Mesquite. Agricultural Research Service, USDA Technical Bulletin No **1423**:1-185.

Moore, G. W., C. B. Edgar, J. G. Vogel, R. A. Washington-Allen, R. G. March, and R. Zehnder. 2016. Tree mortality from an exceptional drought spanning mesic to semiarid ecoregions. Ecological Applications **26**:602–611.

Msanne, J., T. Awada, N. M. Bryan, W. Schacht, R. Drijber, Y. Li, X. Zhou, J. Okalebo, D. Wedin, J. Brandle, and J. Hiller. 2017. Ecophysiological responses of native invasive woody *Juniperus virginiana* L. to resource availability and stand characteristics in the semiarid grasslands of the Nebraska Sandhills. Photosynthetica **55**:219–230.

Müller, P., X.-P. Li, and K. K. Niyogi. 2001. Non-photochemical quenching. A response to excess light energy. Plant Physiology **125**:1558–1566.

Murchie, E. H., and T. Lawson. 2013. Chlorophyll fluorescence analysis: A guide to good practice and understanding some new applications. Journal of Experimental Botany **64**:3983–3998.

Murchie, E. H., and A. V. Ruban. 2020. Dynamic non-photochemical quenching in plants: From molecular mechanism to productivity. The Plant Journal **101**:885–896.

Ouellet, F., and J.-B. Charron. 2013. Cold acclimation and freezing tolerance in plants. eLS John Wiley & Sons, Ltd, Chichester, UK, 1-10.

Owens, M. K., and M.C. Schreiber. 1992. Seasonal gas exchange characteristics of two evergreen trees in a semiarid environment. Photosynthetica **26:**389-398.

Owens, M. K. 1996. The role of leaf and canopy-level gas exchange in the replacement of *Quercus virginiana* (Fagaceae) by *Juniperus ashei* (Cupressaceae) in semiarid savannas. American Journal of Botany **83**:617–623.

Pinheiro, J. C. and Bates, D. M. 2000. Mixed-effects models in S and S-PLUS, Springer, New York.

Pinheiro J, Bates D, DebRoy S, Sarkar D, R Core Team. 2020. *nlme: Linear and Nonlinear Mixed Effects Models*. R package version 3.1-148, https://CRAN.R-project.org/package=nlme.

Poulter, B., D. Frank, P. Ciais, R. B. Myneni, N. Andela, J. Bi, G. Broquet, J. G. Canadell, F. Chevallier, Y. Y. Liu, S. W. Running, S. Sitch, and G. R. van der Werf. 2014. Contribution of semi-arid ecosystems to interannual variability of the global carbon cycle. Nature **509**:600–603.

Reich, P. B., M. B. Walters, and D. S. Ellsworth. 1992. Leaf life-span in relation to leaf, plant, and stand characteristics among diverse ecosystems. Ecological Monographs **62**:365–392.

Reich, P. B., D. S. Ellsworth, M. B. Walters, J. M. Vose, C. Gresham, T. C. Volin, and W. D. Bowman. 1999. Generality of leaf trait relationships: A test across six biomes. Ecology **80**:1955-1969.

Rosenthal, S. I., and Camm, E.L. 1997. Photosynthetic decline and pigment loss during autumn foliar senescence in western larch (*Larix occidentalis).* Tree Physiology **17**:767-775.

Ruban, A. V. 2016. Nonphotochemical chlorophyll fluorescence quenching: Mechanism and effectiveness in protecting plants from photodamage. Plant Physiology **170:**1903–1916.

Schymanski, S. J., D. Or, and M. Zwieniecki. 2013. Stomatal control and leaf thermal and hydraulic capacitances under rapid environmental fluctuations. PLoS ONE **8**:1-16.

Seager, R., M. Ting, I. Held, Y. Kushnir, J. Lu, G. Vecchi, H.-P. Huang, N. Harnik, A. Leetmaa, N.-C. Lau, C. Li, J. Velez, and N. Naik. 2007. Model projections of an imminent transition to a more arid climate in Southwestern North America. Science **316**:1181–1184.

Seager, R., J. Feldman, N. Lis, M. Ting, A. P. Williams, J. Nakamura, H. Liu, and N. Henderson. 2018. Whither the 100th meridian? The once and future physical and human geography of America's arid–humid divide. Part II: The meridian moves East. Earth Interactions **22**:1–24.

Sims, D. A., and J. A. Gamon. 2002. Relationships between leaf pigment content and spectral reflectance across a wide range of species, leaf structures and developmental stages. Remote Sensing of Environment **81**:337–354.

Singmann, H, Hervé, M, Love, J., & Buerkner, P. 2020. *emmeans: Estimated marginal means AKA least square means*. R package version 1.5, https://cran.r-project.org/web/packages/emmeans/index.html.

Stevens, N., C. E. R. Lehmann, B. P. Murphy, and G. Durigan. 2017. Savanna woody encroachment is widespread across three continents. Global Change Biology **23**:235–244.

Strzepek, K., G. Yohe, J. Neumann, and B. Boehlert. 2010. Characterizing changes in drought risk for the United States from climate change. Environmental Research Letters **5**:1-9.

Thurow, T.L., and J. W. Hester. 1997. Ch. 4 Holistic perspective, rangeland hydrology and wildlife considerations in juniper management: How an increase or reduction in juniper cover alters rangeland hydrology. Texas Agricultural Experiment Station Technical Report 97-1 (Proceedings of 1997 Juniper Symposium), Taylor CA (ed.) Texas A&M University Research and Extension Center: Sonora, TX; 9–22.

Thyroff, E. C., O. T. Burney, M. V. Mickelbart, and D. F. Jacobs. 2019. Unraveling shade tolerance and plasticity of semi-evergreen oaks: Insights from maritime forest live oak restoration. Frontiers in Plant Science **10**:1-11.

Trenberth, K. E., A. Dai, G. van der Schrier, P. D. Jones, J. Barichivich, K. R. Briffa, and J. Sheffield. 2014. Global warming and changes in drought. Nature Climate Change **4**:17–22.

Turner, N. C., E.D. Schulze, and T. Gollan. 1984. The responses of stomata and leaf gas exchange to vapour pressure deficits and soil water content. Oecologia **63**:338-342.

Turner, N. C. 1988. Measurement of plant water status by the pressure chamber technique. Irrigation Science **9**:289–308.

Van Auken, O.W. and F. Smeins. 2008. Western North American *Juniperus* communities: Patterns and causes of distribution and abundance. In Van Auken, O.W. (Ed.), Western North American *Juniperus* communities: A dynamic vegetation type. Springer, New York. 3 -18.

Van Auken, O. W. 2009. Causes and consequences of woody plant encroachment into western North American grasslands. Journal of Environmental Management **90**:2931–2942.

Verhoeven, A. 2014. Sustained energy dissipation in winter evergreens. New Phytologist **201**:57–65.

Verhoeven, A., J. I. García-Plazaola, and B. Fernández-Marín. 2018. Shared mechanisms of photoprotection in photosynthetic organisms tolerant to desiccation or to low temperature. Environmental and Experimental Botany **154**:66–79.

Wei, L., C. Xu, S. Jansen, H. Zhou, B. O. Christoffersen, W. T. Pockman, R. S. Middleton, J. D. Marshall, and N. G. McDowell. 2019. A heuristic classification of woody plants based on contrasting shade and drought strategies. Tree Physiology **39**:767–781.

Wellburn, A.R. 1994. The spectral determinations of chlorophylls *a* and b, as well as total carotenoids, using various solvents with spectrophotometers of different resolutions. Journal of Plant Physiology **144**:307-313.

Werner, C., O. Correia, and W. Beyschlag. 2002. Characteristic patterns of chronic and dynamic photoinhibition of different functional groups in a Mediterranean ecosystem. Functional Plant Biology **29**:999-1011.

Western Regional Climate Center (WRCC). 2020. Sonora, TX: Total of precipitation (inches). https://wrcc.dri.edu/cgi-bin/cliMAIN.pl?tx8449.

Willson, C. J., P. S. Manos, and R. B. Jackson. 2008. Hydraulic traits are influenced by phylogenetic history in the drought-resistant, invasive genus *Juniperus* (Cupressaceae). American Journal of Botany **95**:299–314.

Wilson, T. B., R. H. Webb, and T. L. Thompson. 2001. Mechanisms of range expansion and removal of mesquite in desert grasslands of the Southwestern United States. U.S. Department of Agriculture, Forest Service, Rocky Mountain Research Station, Ft. Collins, CO, 1-28.

Wright, I. J., P. B. Reich, M. Westoby, D. D. Ackerly, Z. Baruch, F. Bongers, J. Cavender-Bares, T. Chapin, J. H. C. Cornelissen, M. Diemer, J. Flexas, E. Garnier, P. K. Groom, J. Gulias, K. Hikosaka, B. B. Lamont, T. Lee, W. Lee, C. Lusk, J. J. Midgley, M.-L. Navas, Ü. Niinemets, J. Oleksyn, N. Osada, H. Poorter, P. Poot, L. Prior, V. I. Pyankov, C. Roumet, S. C. Thomas, M. G. Tjoelker, E. J. Veneklaas, and R. Villar. 2004. The worldwide leaf economics spectrum. Nature **428**:821–827.

Yan, W., Y. Zhong, and Z. Shangguan. 2016. A meta-analysis of leaf gas exchange and water status responses to drought. Scientific Reports **6**:1–9.

3. CHLOROPHYLL CAROTENOID INDEX (CCI) TRACKS SLOW-ADJUSTING PARAMETERS OF PHOTOSYNTHETIC PHENOLOGY IN THREE WOODY ENCROACHERS ON A SEMI-ARID SAVANNA

3.1. **Introduction**

Drylands cover 40% of the earth's surface (Reynolds et al. 2007) and drive the interannual variation in atmospheric CO_2 levels with their photosynthetic responses to varying temperature and precipitation events (Poulter et al. 2014, Ahlström et al. 2015). These systems constitute semi-arid and arid climates where potential evapotranspiration is greater than annual precipitation making photosynthetic activity in these regions water limited. Drylands can vary from carbon sources to sinks due to their sensitivity to water availability, high temperatures, and stress from vapor pressure deficits (VPD) during the growing season (Biederman et al. 2017, Roby et al. 2020). Midday photosynthetic values are often depressed during hot dry periods compared to water abundant periods (Scott et al. 2009). Though less studied in drylands, lower temperatures can be additionally stressful for photosystems of overwintering species—resulting in both dry periods and chilling capable of producing sustained photoinhibitory (i.e. decreased capacity to absorb CO_2) responses under light limited conditions (Baquedano and Castillo 2007, Verhoeven et al. 2018. Raub Ch. 2). While drylands play a large role globally, our ability to accurately track photosynthetic phenology using remote sensing products has been limited (Biederman et al. 2017).

Remote sensing in dryland environments often suffers due to the heterogenous landscape and greenness vegetation indices are less useful when evergreen vegetation is present (Smith et al. 2019). Greenness indices like the Normalized Difference Vegetation Index (NDVI) have historically been used as an assessment of photosynthesis due to their ability to track reflectance signals from changing chlorophyll content (i.e. the light harvesting capacity of the photosystems) and canopy leaf area over the course of a season (Running et al. 2004, Esteban et al. 2015, Xue & Su 2017). Chlorophyll content can decline under high temperatures (Fernández-Marín et al. 2017), drought, and chilling (Esteban et al. 2015) in addition to changes during leaf development and senescence. However, these greenness indices struggle with evergreens (Stylinski et al. 2002, Gamon et al. 2016, Springer et al. 2017, Wong et al. 2019) which see little variation in greenness and canopy changes seasonally (Gamon et al. 1995, Smith et al. 2019). This can be problematic as woody plants of varying leaf lifespans (Barger et al. 2011) have globally encroached on dryland ecosystems (Van Auken 2009, Stevens et al. 2017), which has contributed to evergreen landscapes.

Emerging carotenoid-based vegetation indices have been more successful at tracking evergreen seasonal photosynthetic rates than traditional greenness indices (Stylinski et al. 2002, Gamon et al. 2016, Springer et al. 2017, Wong et al. 2019). These carotenoid pigment pools play photoprotective roles by dissipating excess energy and accumulate in concentration under prolonged stressors of drought, chilling, and low temperatures (Esteban et al. 2015). Over diurnal periods, a subsidiary group of carotenoids called the xanthophylls quickly dissipates excess energy and reduces

photochemical light use (Demmig-Adams et al. 1996). The photochemical reflectance index (PRI) was first developed to narrowly track diurnal changes in the xanthophyll cycle (Gamon et al. 1992) but has been related to the seasonal changing ratio of chlorophyll to carotenoids in evergreens (Wong and Gamon 2015) and deciduous plants (Sims and Gamon 2002). This is important as shifting pigment pool sizes (Stylinski et al. 2002)—particularly the changing ratio of Chl:Car—has been related to photosynthetic changes in evergreens (Gamon et al. 2016). Consequently, PRI has been found to strongly track photosynthetic rates of uptake in evergreen vegetation (Zhang et al. 2016, Zhang et al. 2017, Wong et al. 2019) and moderately strong in deciduous trees (Springer et al. 2017).

In the light-use efficiency model developed by Monteith (1972), photosynthesis is the product of the absorbed photosynthetically active radiation (*APAR*) and the light use efficiency constant (ε), which is the efficiency of the plant in converting the absorbed light into absorbed carbon. *APAR* is derived from the product of the photosynthetically active radiation (*PAR*) and the fraction of the photosynthetically active radiation (*fPAR*) actually absorbed for photosynthesis. PRI has been strongly linked to ε across many scales and systems (Zhang et al. 2016), while greenness indices like the normalized difference vegetation index (NDVI) have been linked to *fPAR* as it measures changes in the chlorophyll content and/or general structural changes in the canopy (Running et al. 2004, Xue & Su 2017).

While PRI and NDVI are hypothesized to form complementary information on Monteith's (1972) photosynthesis model, the recently developed chlorophyll carotenoid

index (CCI) has been hypothesized to be more directly related to photosynthetic activity across species than either PRI or NDVI alone (Gamon et al. 2016, Springer et al. 2017, Wong et al. 2020). While PRI had bands narrowly centered to track the xanthophyll cycle originally, CCI was created with bands centered more on total chlorophyll and carotenoid pools (Gamon et al. 2016). By doing so, CCI appears capable of tracking both canopy structural changes for deciduous trees like NDVI, while tracking the changes in carotenoid and chlorophyll pools for all leaf lifespans similar to PRI (Springer et al. 2017, Wong et al. 2020). However, weak relationships between CCI and midday photosynthetic rates and strong relationships with photosystem status (including the maximal quantum yield of PSII in a dark-adapted state (F_v/F_m) and the quantum yield of PSII (ϕ_{PSII})) have also been recorded (D'Odorico et al. 2020, Fréchette et al. 2020). F_v/F_m represents sustained photoinhibition and decreased photosynthetic capacity under light-limited to light-saturated conditions in severe cases, (Adams et al. 2008, Murchie and Ruban 2020) while ϕ_{PSII} is the actual proportion of light being used for photosynthesis under lighted conditions respectively (Maxwell and Johnson 2000). Just as sustained stressors lead to decreasing chlorophyll and increased carotenoid contents (Esteban et al. 2015, Fernández-Marín et al. 2017), sustained low temperatures and desiccation can lead to decreased maximal quantum yield of PSII photochemistry (Verhoeven 2014, Verhoeven et al. 2018), while ϕ_{PSII} decreases dynamically with midday stressors of light, temperature, and VPD (Demmig-Adams and Adams 1996, Murchie and Lawson 2013).

Despite the potential of CCI in tracking both deciduous and evergreen photosynthetic phenology, studies have been limited to boreal species and common garden seedlings (Gamon et al. 2016, Springer et al. 2017, Wong et al. 2019, D'Odorico et al. 2020, Fréchette et al. 2020, Wong et al. 2020). Improved relationships between CCI with leaf and ecosystem photosynthesis (Gamon et al. 2016, Springer et al. 2017, Wong et al. 2020) has not always consistently performed better across species than PRI (Wong et al. 2019, Fréchette et al. 2020). Little in the way of validation has been performed on species under differing climatic conditions or individuals in a natural field setting—except for Wong et al. (2020)—in tracking photosynthetic phenology. These photosynthetic patterns include the relationship of CCI to photosynthetic uptake and photosystem stress metrics associated with F_V/F_M or ϕ_{PSII}. Particularly, little is known how well CCI tracks photosynthetic behavior of species experiencing low water availability, hot temperatures, and higher VPD during the summer in addition to cold periods in the winter. Understanding if CCI can similarly track photosynthetic behaviors across dryland species of varying leaf lifespans and where water is additionally constraining could prove critical towards improving remote sensing capabilities in dryland systems.

Here, CCI and PRI were compared with several greenness indices in tracking photosynthetic behaviors of three woody encroachers varying in leaf life-spans in a semi-arid savanna. Seasonal water limitations were an added stressor here that studies of boreal species did not explicitly experience. Additionally, we assessed how the vegetation indices tracked photosystem stress in the plant as manifested by changing

Chl:Car pools and decreased capacity for photosystem light use (F_V/F_M and ϕ_{PSII}). It was hypothesized that CCI would have the strongest relationships with all photosynthetic parameters across species, while PRI would be slightly weaker.

3.2. **Methods**

3.2.1. Study Site, Species, and Physiological Variables

This study was conducted in tandem with Raub (Ch. 2, 2020) and detailed descriptions of the site, physiological measurements, and their results should be referenced there. A brief overview of key information is provided here.

Three woody encroacher species were selected for study at the Sonora Experimental Research Station (30.266 N, 100.566 W). The site is a semi-arid savanna in west-central Texas with average rainfall of 550 mm (Western Regional Climate Center). Species selected included one evergreen (*Juniperus ashei*), one semi-evergreen whose leaves fall off and bud anew within weeks in the spring (*Quercus fusiformis*), and one deciduous species (*Prosopis glandulosa*). Water status strategies range from drought tolerant (tolerates low water potentials) in *J. ashei* to drought avoiders (experience smaller variability in water potential values) in *Q. fusiformis* and *P. glandulosa*. Five individuals from each species (N = 15) were selected with full canopies and within the average height range (~3 – 5 m) of the species (Fortes et al., *unpublished*). The study occurred from late July 2019 to April 2020 at monthly intervals.

Physiological variables selected included gas-exchange, fluorescence, and pigment parameters and were reported in detail in Raub (Ch. 2, 2020). Gas-exchange parameters included leaf-level net photosynthesis under light saturating conditions (A_{Net}),

leaf transpiration (E), and stomatal conductance (g_s). Fluorescence variables selected included the maximal quantum efficiency of PSII photochemistry (F_V/F_M; a measurement of photoinhibition and sustained energy dissipation), the actual quantum yield of PSII under light-adapted conditions (ϕ_{PSII}; the actual fraction of light being used for photosynthesis under lighted conditions), and non-photochemical quenching (NPQ; midday energy dissipation often driven by the xanthophyll cycle). Decreased F_V/F_M can indicate a decreased capacity for A_{Net} in light limited conditions and in more severe cases a decrease in light-saturated conditions as well (Adams et al. 2008, Murchie and Ruban 2020) due to sustained energy dissipation (Verhoeven et al. 2018). Decreased ϕ_{PSII} is a lowered photochemical capacity to use light in photosystem II (Maxwell and Johnson 2000). The Chl:Car ratio was determined spectrophotometrically using equations from Wellburn (1994).

3.2.2. Foliage Density

Foliage density was measured to track individual canopy changes in leaf abundance. It required one-time measurements of each tree's canopy dimensions and monthly Leaf Area Index (LAI) measurements—the amount of leaf area over one area of ground. LAI measurements were taken with a LAI-2000 Plant Canopy Analyzer (LI-COR Biosciences, Lincoln, NE, USA) under dawn or dusk conditions in the four cardinal directions of an isolated tree. This method utilized the gap fraction method to calculate LAI which is a ratio of under canopy light divided by the above canopy light (Weiss et al. 2004). Above canopy light conditions were taken in open areas in the savanna (radius ~3.5 times average tree heights) in the same cardinal direction as the

below canopy measurement. Measurements of below canopy light conditions were taken with a 270° FOV restrictor at the trunk of the tree above the lowest branches and facing out towards the edge of its canopy. Transmittance of radiation was calculated at five angles (7°, 23°, 38°, 53°, 68°) to calculate LAI, but the 68° ring was removed in post-processing FV-2000 software due to the small canopy sizes.

3.2.3. Leaf-Level Reflectance Measurements

Two sub-samples of sunlit leaves from each tree canopy were taken within ± 2.5 h of solar noon, stored in cold plastic bags within a cooler, and optically sampled within ~4 h of collection within a lab setting. Leaf-level reflectance measurements were performed with a FieldSpec 4 Standard-Resolution spectroradiometer (Analytical Spectral Devices Inc., Boulder, CO, USA) with a sampling bandwidth of 1.4 nm for 350 to 1000 nm and 1.1 nm for 1,001 to 2,500 nm. After warming up for 30 minutes, sampling integration time was optimized and a white reference measurement (Spectralon; Labsphere Inc., North Sutton, NH, USA) taken before the start of sampling and re-done every few samples.

Three readings on the adaxial (top) side of the leaf were taken at three different positions with a plant probe leaf-clip. The leaves of *Q. fusiformis* covered the field of view (FOV) of the plant probe but the other two species did not. For *P. glandulosa,* leaves were arranged in a mat with no overlapping regions, taped together at the ends and sampled at three different locations over the leaf mat. Leaflets from *J. ashei* were debranched and placed in a mat over the leaf clip's FOV that minimized gaps and overlapping leaves similar to needle mats used in other studies (Lehmann et al. 2015,

Shiklomanov et al. 2016, Čepl et al. 2019, Serbin et al. 2019). Three scans were taken on *J. ashei* mats in one location, slight adjustments to needle positionings were made, and the process repeated twice more for a total of nine logs. The nine logs per leaf were averaged together for an average leaf reflectance curve. Measurement values of the two sub-samples per tree were then averaged together to produce an individual tree reflectance curve before vegetation indices were calculated.

3.2.4. Canopy Reflectance Measurements

A tree sampling platform for sampling spectral responses of individual tree canopies was constructed using a 12 ft ladder, trailer, and a metal boom arm (Fig 3.1) that was originally designed for use with a tripod system on crops (Da Ros Carvalho 2019). The ladder was positioned on a side of a tree that was opposite the sun, as close to the edge of the canopy as possible, and minimized shading over sunlit leaves (Fig 3.1). Canopy spectral data for individual trees were collected with a field spectroradiometer (SS-110; Apogee Instruments Inc., Logan, UT, USA) with a scanning range from 340 to 820 nm (measurement interval of 1 nm and a wavelength resolution of 3 nm full width half maximum) and a 25° FOV restrictor. All measurements were made under sunny conditions (zero to minimal cloud cover) within $\pm$ 2.5 hours of solar noon. The sensor and boom arm were leveled with two height-adjustable work stands on the ground ~30 cm above a white reference panel (Spectralon; Labsphere Inc., North Sutton, NH, USA). The integration time was optimized with the panel before taking dark and white reference measurements and setting to reflectance mode. The spectroradiometer boom arm was then attached to a platform on top of the ladder that allowed for the boom to be

adjusted in all three planes using bubble levels located near the sensor and on the boom arm.

Figure 3.1 Spectral sampling for the canopy of *Juniperus ashei.*

Once attached, the spectroradiometer was swung out over the tree canopy using a rope and a minimum of nine reflectance measurements were taken over sunlit leaves. Care was taken to complete this task within 10 minutes from the white reference measurement. It has been found this produces a 1% error within one hour of solar noon

and up to 6% error over 10 minutes within 3 hours of solar noon in other spectroradiometers (Goetz 2012). Due to variability in tree heights, the measurement varied between 1 and 2 m above the tree canopy that sampled a conical area between 0.1 and 0.62 m^2 to capture the geometric features of the canopy vegetation (Pfitzner et al. 2011). Trees with small canopy areas had little sweeping occur to ensure that sampling captured primarily the spectral signals of the tree canopy. It is likely that small amounts of background influence from the soil, understory plants, and trailer were recorded in the spectral signal though every attempt was used to minimize the signals by sampling directly over the tree canopy itself. Measurements suspected of self-shading or sampling within large tree canopy gaps were removed in post-processing by visual observation of the reflectance curves. Remaining reflectance curves for each tree were averaged together. It should be noted that canopy measurements began two months later in September than leaf-level spectral measurements which began in July.

3.2.5. Calculating the Vegetation Indices

Vegetation indices were calculated using reflectance (R) values at particular wavelengths. Greenness indices included NDVI (Rouse et al. 1974), the soil-adjusted vegetation index (SAVI), and the enhanced vegetation index (EVI). While NDVI has been used to track greenness and canopy FD changes, it is highly susceptible to influences from shadows, soil brightness and color, and atmospheric changes (Running et al. 2004; Xue & Su 2017). The Soil Adjusted Vegetation Index (SAVI) reduces the impact from soil color and brightness by adding a soil conditioning index (L)—often equal to 0.5—to the NDVI equation (Huete 1988). The Enhanced Vegetation Index

(EVI) was developed to reduce effects from both soil and atmospheric effects on NDVI by introducing the blue band and coefficients for soil and the atmosphere to reduce aerosol effects (Liu and Huete 1995). Indices were calculated in Table 3.1, showing the original authors followed by later authors whose equations were used in this study.

Table 3.1 Equations for vegetation indices. Sources are listed on the right. R_x is the reflectance at *x* nm wavelength.

$CCI = \frac{R_{532}-R_{630}}{R_{532}+R_{630}}$	(Gamon et al. 2016, Springer et al. 2017)
$PRI = \frac{R_{532}-R_{570}}{R_{532}+R_{570}}$	(Gamon et al. 1992, Springer et al. 2017)
$NDVI = \frac{R_{800}-R_{630}}{R_{800}+R_{630}}$	(Rouse et al. 1974, Springer et al. 2017)
$SAVI = \frac{(R_{800}-R_{630})(1+0.5)}{(R_{800}+R_{630}+0.5)}$	(Huete 1988)
$EVI = 2.5 * \frac{R_{800}-R_{670}}{R_{800}+6*R_{670}-7.5*R_{400}+1}$	(Liu and Huete 1995; Zarco-Tejada et al. 2013)

3.2.6. Statistical Analyses

Physiological parameters and spectral indices were averaged by species every month before undergoing a Pearson's correlation to determine the strength of the relationship between index and parameter. Repeated measures correlations (rmc) were also applied due to its greater statistical power involving all original data points (i.e. non-averaged), while providing information on the strength of the average intra-tree

relationships between indices and physiological parameters (Bakdash and Marusich 2017). A rmc coefficient valuing -1 to 1 was obtained using the *rmcorr* package (Bakdash and Marusich 2017) using common assumptions for regular linear models. To relax distributional assumptions involving normality, a more robust bootstrapped version of the correlation coefficient was also determined by resampling from the original data 100 times with replacement. A distribution of resulting rmc coefficients were created from which the median repeated measures correlation coefficient was selected.

Bootstrapped versions of the coefficients of determination differed little from the original repeated measures coefficients of determination that assumed normality (Tables A-1, A-2, A-3). In comparison to values obtained by Pearson's correlations, the rmc yielded the same conclusions but generally showed weaker relationships between physiological parameters and vegetation indices. The improved power from using all the individual observations for each month in the rmc did improve *P. glandulosa* canopy relationships as only five months were available for analysis. January and February were leaf off periods and March was removed due to leaves that had just budded and were not physiologically similar to adult leaves. Consequently, the improved power from all the observations for each month did improve *P. glandulosa* canopy relationship significance and are noted where necessary along with the bootstrapped R^2 in parentheses. Results for the rmc are included in Appendix A.

Foliage density changes across time and species were assessed using a linear mixed effects model in RStudio version 1.3.1056 in the *nlme* package (Pinheiro et al. 2020). Monthly foliage density values were treated as coming from the same growing

season cohort. Model selection began with full fixed effects, before adding random intercepts for trees and slopes across time to account for the repeated nature of the measurements, then reducing the number of fixed effects. Model selection was determined by use of the Akaike's Information Criterion (AIC) and the maximum likelihood ratio test (Gałecki and Burykowski 2013), which settled on a final model including a quadratic day of year interaction with species and a linear day of year term while allowing for random intercepts across individual trees. Residuals were allowed to vary by species and month with weighted variance arguments (Pinherio and Bates 2000), while both day of year terms were mean-centered. A Bonferroni post-hoc analysis was conducted using the *emmeans* package (Singmann et al. 2020) to determine differences among species.

3.3. **Results**

3.3.1. Physiological Seasonal Trends

A brief description of physiological patterns and environmental conditions will be provided here (Figure 3.2) but the data has been drawn from Raub (Ch. 2 2020) and discussed in greater detail there. Generally, rain was 57% below average in the summer through fall months, average over the winter, and four times greater in the spring months (Western Regional Climate Center). *Q. fusiformis* had fairly stable gas-exchange rates, ϕ_{PSII}, water access (Ψ_{PD}), and high-water status levels (Ψ_{MD}), while *P. glandulosa* and *J. ashei* declined in soil moisture access (Ψ_{PD}), water status (Ψ_{MD}), midday ϕ_{PSII}, and gas-exchange rates during the dry periods. *J. ashei* experienced small declines in F_V/F_M from summer highs during late summer water deficits but remained low during winter near

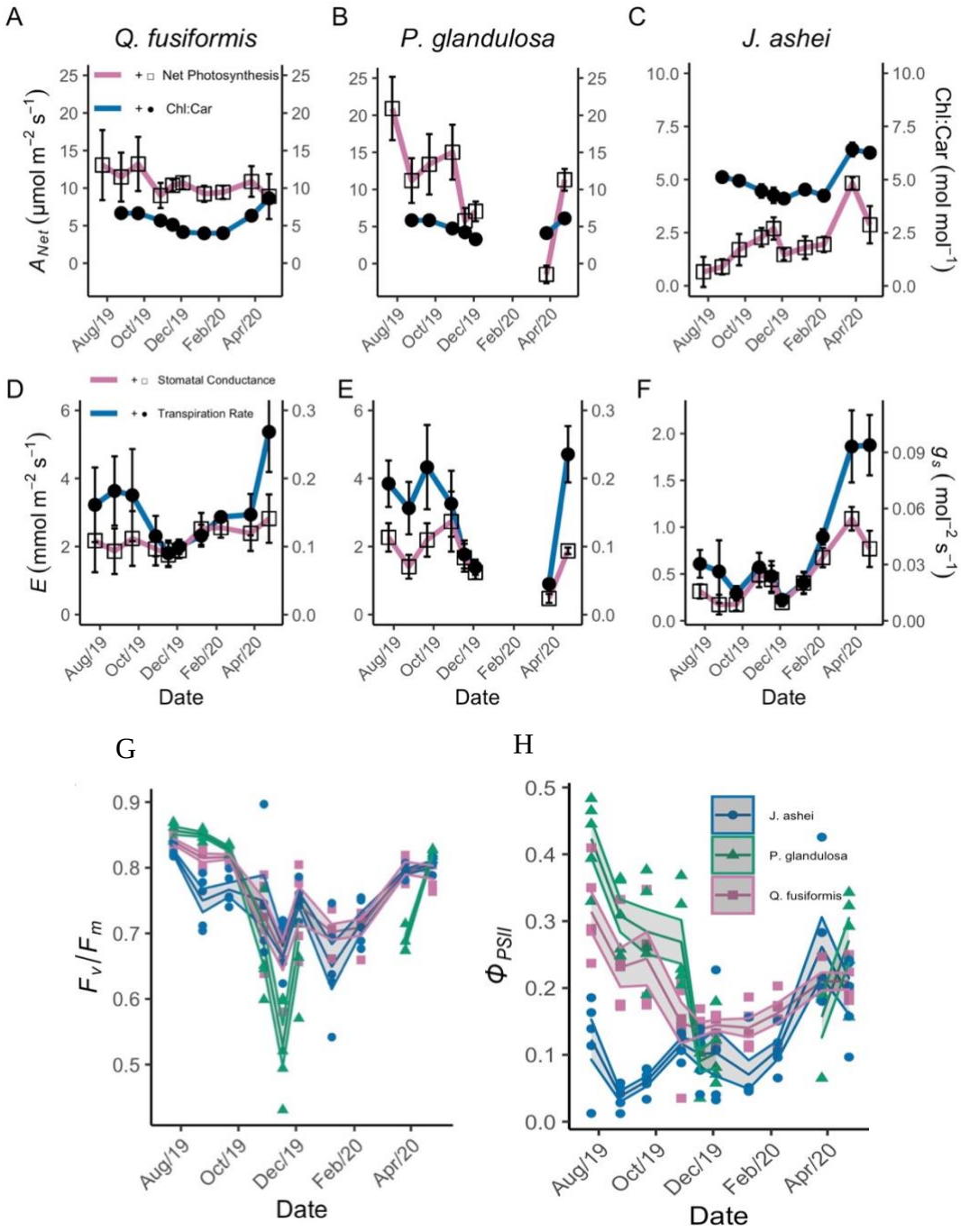

Figure 3.2 Selected physiological parameters reprinted from Raub (Ch. 2 2020). Please refer back to Ch. 2 for in-depth descriptions of each figure. Shaded areas represent the standard error for each species every month.

~0.70 similar to the overwintering *Q. fusiformis* (Fig 3.2). Values of F_V/F_M for *P. glandulosa* and *Q. fusiformis* did not decline during dry periods but had the greatest decreases upon arrival of the first freezing night in mid-October. Photosynthetic rates for *J. ashei* increased from late summer lows through winter to spring peaks, while *P. glandulosa* declined from summer through fall senescence before trending up again in the spring. ϕ_{PSII} often followed similar patterns to A_{Net} across species though it experienced less variability in its trends through the seasons. Transpiration and stomatal conductance were generally lower and NPQ was higher during hot, drier periods for *P. glandulosa* and *J. ashei*. All species experienced similar trends in Chl:Car that decreased from high summer values to low winter values before increasing to highs again in the spring.

3.3.2. Seasonal Trends of Foliage Density and Vegetation Indices

The average reflectance spectra for all three species is shown for April as this was a period of relatively low stress in terms of water availability, recently matured leaves at the beginning of their growth cycle, and abundant sunlight (Fig 3.3). Little variation occurred in the visible spectrum among all species, but *Q. fusiformis* did show the greatest reflectance in the near-infrared region at both scales, followed by *P. glandulosa*, then *J. ashei*.

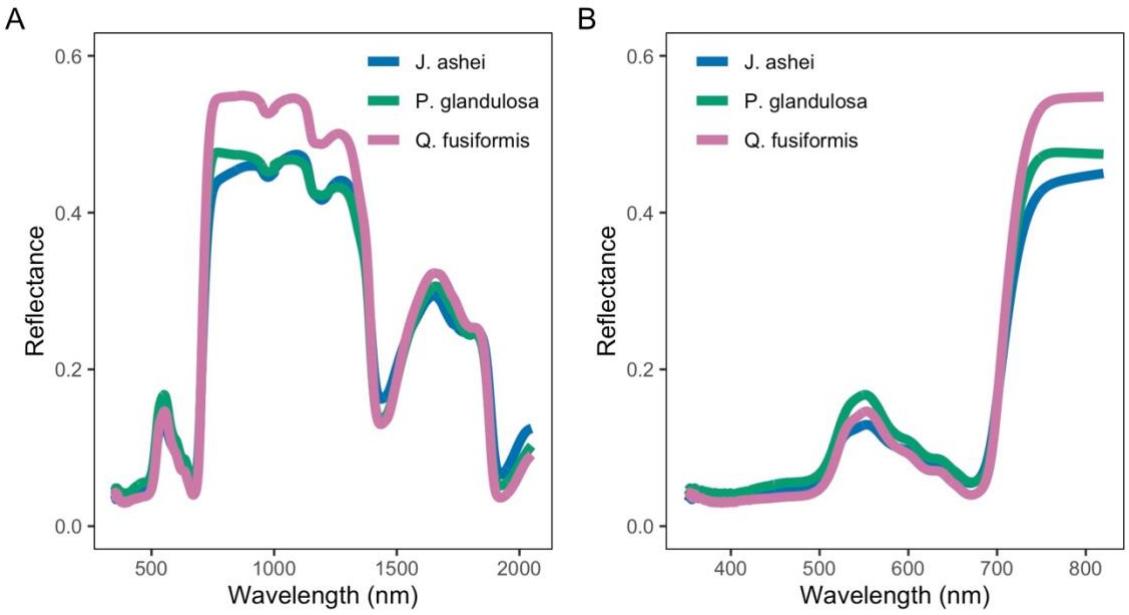

Figure 3.3 Average (A) leaf and (B) canopy spectra for *J. ashei* (blue), *P. glandulosa* (green), and *Q. fusiformis* (pink) on April 24th, 2020. April was chosen for its relatively low stress (high water abundance, sunlight, and matured leaves at the beginning of their life cycle).

Foliage density (FD) was found to have a significant interaction between species and quadratic day of year effect ($F_{(12,115)} = 11.41$, $p < 0.0001$) over the course of the study. FD values for *P. glandulosa* were significantly lower ($t < -5.13$, $p < 0.0007$) than *J. ashei* or *P. glandulosa*, while experiencing the greatest change over time (Fig 3.4). Highs for FD in the deciduous *P. glandulosa* occurred in August and April at ~ 1 m^2 m^{-3}, while falling leaves consistently lowered values across autumn until spring buds emerged in March. The evergreen *J. ashei* experienced minimal variation in FD with values near 1.2 m^2 m^{-3} but showed a slight downwards trend through winter (Fig 3.4).

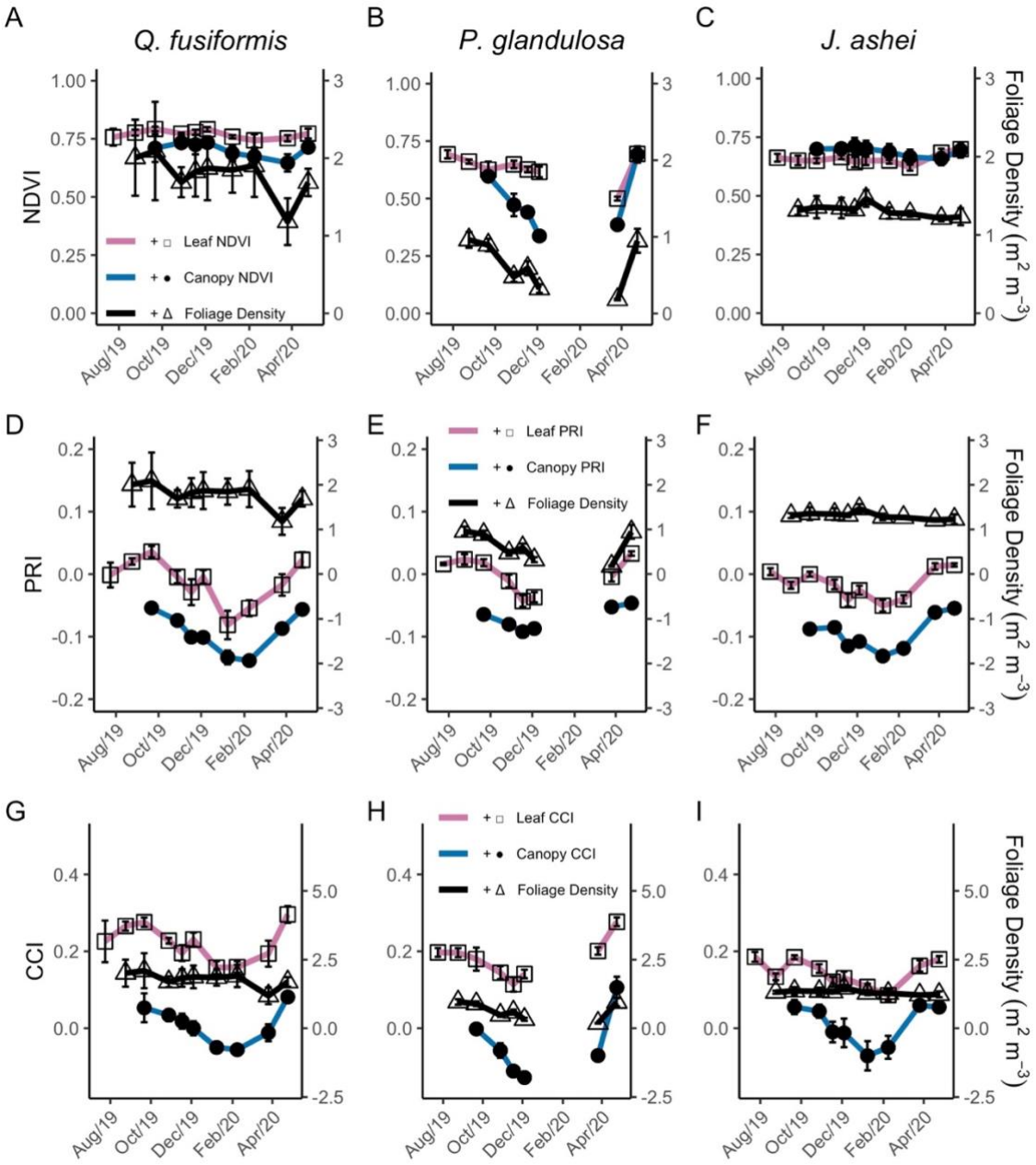

Figure 3.4 Seasonal trends of vegetation indices and foliage density. Leaf (pink/open squares) and canopy (blue/black dots) level vegetation indices: NDVI (A,B,C), PRI (D,E,F), and CCI (G,H,I) shown for all three woody species with standard error bars. Seasonal foliage density is shown on the right axis to compare trends with the indices.

The semi-evergreen *Q. fusiformis* did experience greater variability within months for FD than the other two species likely due to the heterogenous canopy architecture creating large gaps read by the LAI-meter (Fig 3.4). Across seasons, *Q. fusiformis* values were ~2 m^2 m^{-3} with the most noticeable drop in values occurring in March when three of the five trees were transitioning from the 2019 leaf cohort to new leaves.

Seasonal patterns of the vegetation indices did not appear to show clear changes during water deficits in late summer (Aug-Sept) except for leaf-level PRI and CCI for the drought tolerant evergreen *J. ashei* where slight dips occurred (Fig. 3.4 F&I). Leaf-level and canopy NDVI varied little over the course of the season for *J. ashei* similar to its FD values but not leaf level physiological changes (Fig 3.4). Leaf NDVI showed little variation seasonally for the semi-evergreen *Q. fusiformis*, while canopy NDVI did appear to capture leaf turnover in the spring. Canopy NDVI patterns mirrored FD changes, Chl:Car, and most physiological parameters for the deciduous *P. glandulosa*, while leaf NDVI showed slightly weaker seasonal trends.

CCI followed a similar pattern to PRI across species (Fig 3.4), while the other greenness indices (SAVI, EVI, EVI2) followed similar patterns to NDVI (not pictured). Both carotenoid indices at leaf and canopy levels matched patterns for FD, physiological parameters, and Chl:Car changes in *P. glandulosa*. (Fig 3.4). Though FD for *J. ashei* and *Q. fusiformis* varied little over the season, PRI and CCI at both scales clearly declined from summer to winter before increasing in the spring similar to Chl:Car changes in both species. However, PRI and CCI at both scales did not always match photosynthetic patterns. Midday photosynthetic rates (A_{Net}) and ϕ_{PSII} for *J. ashei* actually increased as

cooler temperatures began in October in contrast to declining Chl:Car, PRI, and CCI values at both scales (Fig 3.2C). Similarly, PRI and CCI in *Q. fusiformis* steeply declined to lows during winter months like Chl:Car, but A_{Net} declined only slightly during cold temperature onset and remained fairly stable thereafter (Fig 3.2A). At both leaf and canopy scales, PRI and CCI across species did experience similar patterns to that of F_V/F_M across species which generally declined from summer to winter lows before increasing again. ϕ_{PSII} for *Q. fusiformis* and *P. glandulosa* showed similar patterns to PRI and CCI with declines through late summer and autumn before increasing in the spring.

3.3.3. Relationships Between Vegetation Indices with Chl:Car and Foliage Density

Moderate to strong relationships were found across species for the carotenoid indices and Chl:Car. Relationships between Chl:Car and leaf PRI ($R^2 = 0.89$, $p < 0.005$) and canopy PRI ($R^2 = 0.78$, $p < 0.05$) of the deciduous *P. glandulosa* were stronger than the semi-evergreen *Q. fusiformis* relationships of PRI at leaf ($R^2 = 0.59$, $p < 0.02$) and canopy ($R^2 = 0.75$, $p < 0.006$) levels (Tables 3.2 & 3.3, Fig 3.5). The evergreen *J. ashei* showed similarly strong relationships between Chl:Car and leaf PRI ($R^2 = 0.72$, $p < 0.004$) and canopy PRI ($R^2 = 0.75$, $p < 0.006$; Table 3.4, Fig 3.5)—though interpretation should be cautioned as normality was not achieved in Chl:Car for *J. ashei*. Moderately strong relationships between CCI and Chl:Car was found for the semi-evergreen *Q. fusiformis* (leaf $R^2 = 0.67$, $p < 0.007$; canopy $R^2 = 0.72$, $p < 0.008$) and deciduous *P. glandulosa* (leaf $R^2 = 0.59$, $p < 0.07$, canopy $R^2 = 0.88$, $p < 0.02$), and moderate relationships in the evergreen *J. ashei* (leaf $R^2 = 0.42$, $p < 0.06$, canopy $R^2 = 0.44$, $p <$

0.07; Tables 3.2, 3.3, & 3.4, Fig 3.5). All canopy level greenness indices in *P. glandulosa* had a very strong relationships with Chl:Car ($R^2 > 0.96$, $p < 0.01$).

Relationships across species between Chl:Car and vegetation indices still remained moderate to strongly related using rmc. In the deciduous species (*P. glandulosa*), canopy CCI had a stronger relationship ($R_{rmc}^2 = 0.74$, $p < 0.001$) with Chl:Car than canopy PRI ($R_{rmc}^2 = 0.63$, $p < 0.001$), while all canopy greenness indices were comparably high ($R_{rmc}^2 = 0.69$, $p < 0.001$, Table A-2). Conversely, leaf-level PRI was more strongly related ($R_{rmc}^2 = 0.69$, $p < 0.001$) to Chl:Car than leaf-level CCI ($R_{rmc}^2 = 0.42$, $p < 0.001$, Table A-2). Canopy PRI relationships with Chl:Car in *Q. fusiformis* ($R_{rmc}^2 = 0.55$, $p < 0.001$) and *J. ashei* ($R_{rmc}^2 = 0.59$, $p < 0.001$) were greater than CCI at

Table 3.2 *Quercus fusiformis* coefficients of determination (R^2) from Pearson's correlations of physiological variables with vegetation indices at leaf and canopy levels.

Vegetation Index	A_{Net}	E	g_s	F_V/F_M	ϕ_{PSII}	NPQ	Chl:Car	FD	Ψ_{PD}	Ψ_{MD}
Leaf NDVI	0.08	0.00	0.27	0.01	0.01	0.00	0.06	0.23	0.05	0.22
Canopy NDVI	0.00	0.02	0.32	0.06	0.10	0.04	0.00	0.30	0.16	0.19
Leaf PRI	0.25	0.32	0.04	**0.51***	0.32	0.25	**0.59***	0.02	0.19	0.01
Canopy PRI	0.14	0.32	0.00	**0.51***	0.46	0.17	**0.75****	0.01	0.25	0.07
Leaf CCI	0.10	**0.48***	0.00	**0.42***	0.23	0.25	**0.67****	0.05	0.20	0.00
Canopy CCI	0.04	0.34	0.00	0.26	0.26	0.15	**0.72***	0.00	0.16	0.05
Leaf SAVI	0.01	0.01	0.23	0.01	0.09	0.00	0.05	0.19	0.07	0.14
Canopy SAVI	0.14	0.16	**0.58***	0.04	0.04	0.20	0.03	0.42	0.41	**0.51***
Leaf EVI	0.00	0.20	0.31	0.13	0.25	0.04	0.05	0.20	0.30	0.21
Canopy EVI	0.12	0.18	**0.61***	0.04	0.05	0.20	0.04	0.38	0.40	0.48
Leaf EVI2	0.01	0.01	0.23	0.01	0.10	0.00	0.04	0.20	0.08	0.14
Canopy EVI2	0.16	0.16	**0.57***	0.03	0.03	0.20	0.03	0.42	0.40	**0.51***

* P-values less than or equal to 0.05 (*), 0.01 (**), or 0.001 (***) respectively. Shown in bold.
Original linear relationships before transformations are shown in parentheses.

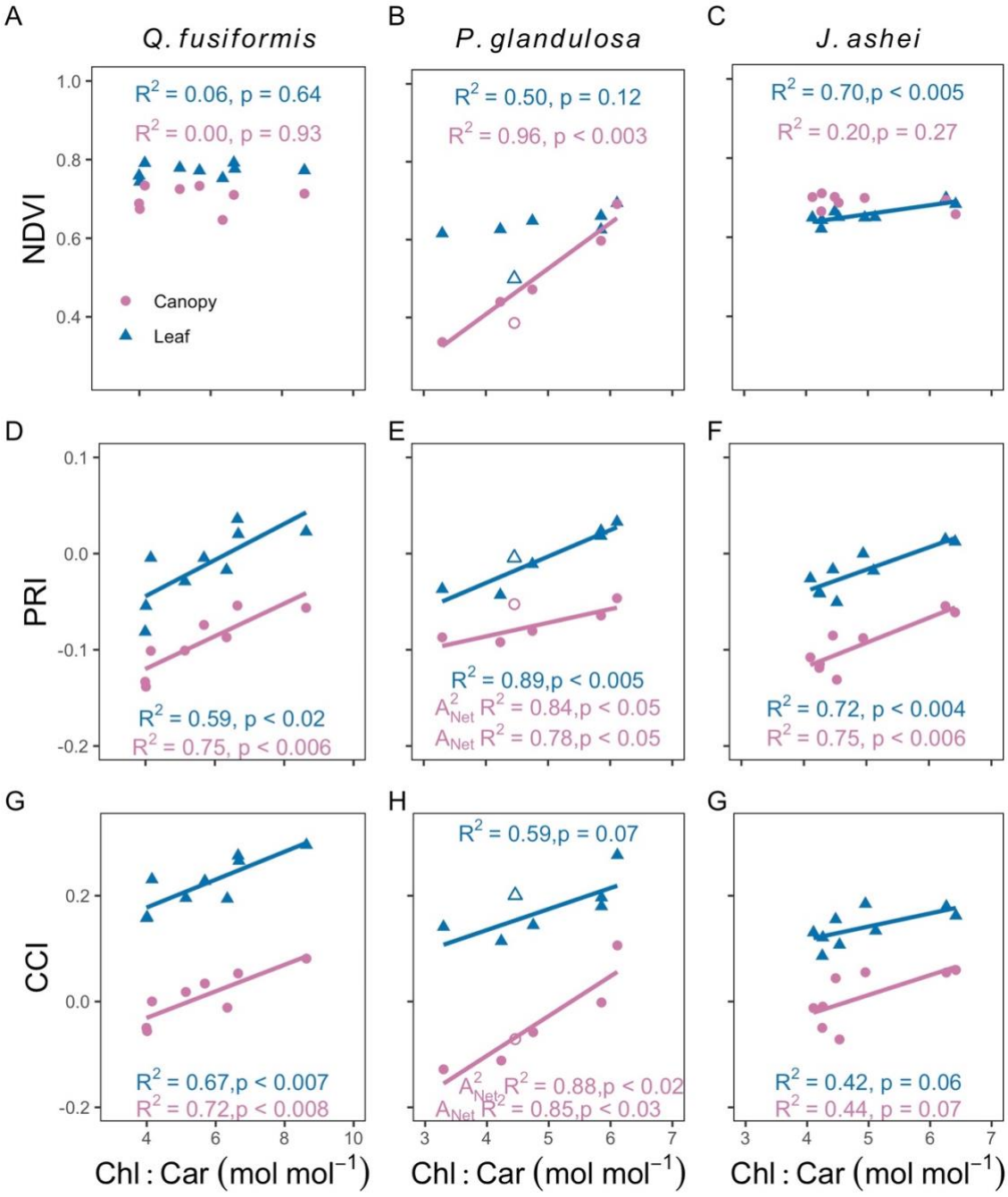

Figure 3.5 Linear relationships between leaf (blue triangles) and canopy (red circles) level NDVI, PRI, and CCI with Chl:Car (mol mol^{-1}). Open symbols for *P. glandulosa* indicate immature leaves in March which were excluded from the final analyses. Original linear relationships are shown in E and H at the canopy level and not the relationships with the quadratic transformed Chl:Car values. The scale for Chl:Car is slightly larger in *Q. fusiformis* than the two other species.

Table 3.3 *Prosopis glandulosa* coefficients of determination (R^2) from Pearson's correlations of physiological variables with vegetation indices at leaf and canopy levels.

Vegetation Index	A_{Net}	E	g_s	F_V/F_M	ϕ_{PSII}	NPQ	Chl:Car	FD	Ψ_{PD}	Ψ_{MD}
Leaf NDVI	0.40	0.45	0.08	0.37	**0.56***	0.00	0.50	0.40	0.27	0.53
Canopy NDVI	0.27	**0.90***	0.15	0.50	0.61	0.05	**0.96****	**0.95*****	0.00	0.16
Leaf PRI	0.35	**0.83****	0.06	**0.83****	**0.77[a] (0.67)****	0.03	**0.89****	**0.78***	0.01	0.11
Canopy PRI	0.26	**0.84***	0.05	**0.78*[b]** (0.75)	0.59	0.20	**0.84[b] (0.78)***	0.19	0.02	0.27
Leaf CCI	0.12	**0.64***	0.00	**0.58***	0.4[a] (0.33)	0.19	0.65[b] (0.59)	0.61[b] (0.55)	0.08	0.40
Canopy CCI	0.27	**0.87***	0.10	0.64[b] (0.6)	0.60	0.11	**0.88[b] (0.85)***	**0.86[b] (0.81)****	0.04	0.33
Leaf SAVI	0.00	0.13	0.01	0.10	0.04	0.09	0.22	0.16	0.20	**0.68***
Canopy SAVI	0.53	**0.94****	0.41	0.48	**0.81***	0.00	**0.97****	**0.88****	0.07	0.03
Leaf EVI	0.00	0.14	0.03	0.01	0.01	0.01	0.10	0.03	0.44	**0.89****
Canopy EVI	0.53	**0.96****	0.37	0.53	**0.82***	0.00	**0.98****	**0.89****	0.05	0.05
Leaf EVI2	0.00	0.10	0.01	0.08	0.02	0.11	0.21	0.15	0.18	**0.65***
Canopy EVI2	0.55	**0.93****	0.42	0.49	**0.82***	0.00	**0.96****	**0.87****	0.08	0.02

* P-values less than or equal to 0.05 (*), 0.01 (**), or 0.001 (***) respectively. Shown in bold.
[a] The physiological variable underwent a natural log transformation to improve linearity.
[b] The physiological variable underwent an exponential (X^2) transformation to improve linearity.
Original linear relationships before transformations are shown in parentheses.

Table 3.4 *Juniperus ashei* coefficients of determination (R^2) from Pearson's correlations of physiological variables with vegetation indices at leaf and canopy levels.

Vegetation Index	A_{Net}	E	g_s	F_V/F_M	ϕ_{PSII}	NPQ	Chl:Car	FD	Ψ_{PD}	Ψ_{MD}
Leaf NDVI	0.24	**0.51***	0.24	0.38	**0.48***	0.03	**0.70****	0.18	0.12	0.12
Canopy NDVI	0.29	0.34	**0.55***	0.04	0.33	0.16	0.20	0.40	0.10	0.14
Leaf PRI	0.09	0.36	0.10	**0.87*****	0.34	0.02	**0.72****	0.09	0.01	0.00
Canopy PRI	0.41	**0.58***	0.31	**0.85****	**0.57***	0.04	**0.75****	0.15	0.10	0.07
Leaf CCI	0.01	0.08	0.00	**0.66****	0.11	0.08	0.42	0.00	0.01	0.03
Canopy CCI	0.26	0.22	0.08	**0.74****	0.28	0.00	0.45	0.02	0.00	0.00
Leaf SAVI	0.01	0.16	0.06	0.24	0.10	0.05	0.21	0.19	0.07	0.04
Canopy SAVI	0.44	**0.68***	**0.77****	0.04	**0.56***	0.31	0.40	**0.63***	0.40	0.46
Leaf EVI	0.03	0.24	0.13	0.27	0.20	0.08	0.25	0.23	0.18	0.12
Canopy EVI	0.37	**0.62***	**0.71****	0.03	0.49	0.28	0.35	**0.61***	0.35	0.41
Leaf EVI2	0.00	0.14	0.05	0.24	0.09	0.04	0.19	0.18	0.06	0.03
Canopy EVI2	0.41	**0.67***	**0.74****	0.04	**0.55***	0.29	0.41	**0.61***	0.38	0.43

* P-values less than or equal to 0.05 (*), 0.01 (**), or 0.001 (***) respectively. Shown in bold.

the same level ($R_{rmc}^2 = 0.30$, $p < 0.001$; $R_{rmc}^2 = 0.31$, $p < 0.001$ respectively; Tables A-1 & A-3). Leaf-level NDVI was also weakly correlated with Chl:Car in *J. ashei* ($R_{rmc}^2 = 0.31$, $p < 0.001$, Table A-3).

At the canopy level, all four greenness indices ($R^2 > 0.87$, $p < 0.01$) and CCI ($R^2 = 0.86$, $p < 0.01$) showed the strongest relationships with changing FD in *P. glandulosa*, while leaf PRI ($R^2 = 0.78$, $p < 0.01$) was also strongly linked (Table 3.3, Fig 3.6). The three greenness indices capable of reducing background soil and atmospheric influence had moderately strong relationships with FD in J. ashei ($R^2 > 0.61$, $p < 0.05$) but the carotenoid indices did not (Table 3.3). No vegetation index was significantly related to FD in *Q. fusiformis*. Moderately strong relationships between all vegetation indices and FD in *P. glandulosa* were still found with rmc though relationships in *Q. fusiformis* and *J. ashei* were either weak or non-significant. Canopy greenness vegetation indices had the strongest relationships with FD ($R^2_{rmc} = 0.69$ to 0.79, $p < 0.001$), while CCI was a close second for *P. glandulosa* ($R^2_{rmc} = 0.65$, $p < 0.001$, Table A-2).

3.3.3.1. Relationships Between Vegetation Indices with Gas-Exchange Parameters, Water-Potential, and Photosystem Status

NPQ, Ψ_{PD}, and A_{Net} were not found to be significantly related to any vegetation index across the three species at leaf or individual canopy scales ($p > 0.05$, Tables 3.1, 3.2, 3.3). Relationships between vegetation indices and A_{Net}, Ψ_{PD}, and NPQ were similarly either weakly correlated or non-significant in rmc (Tables A-1, A-2, and A-3). Relationships were strong between *E* in *P. glandulosa* and all canopy level vegetation indices ($R^2 > 0.84$, $p < 0.05$), leaf-level PRI ($R^2 = 0.83$, $p < 0.01$), and moderate in

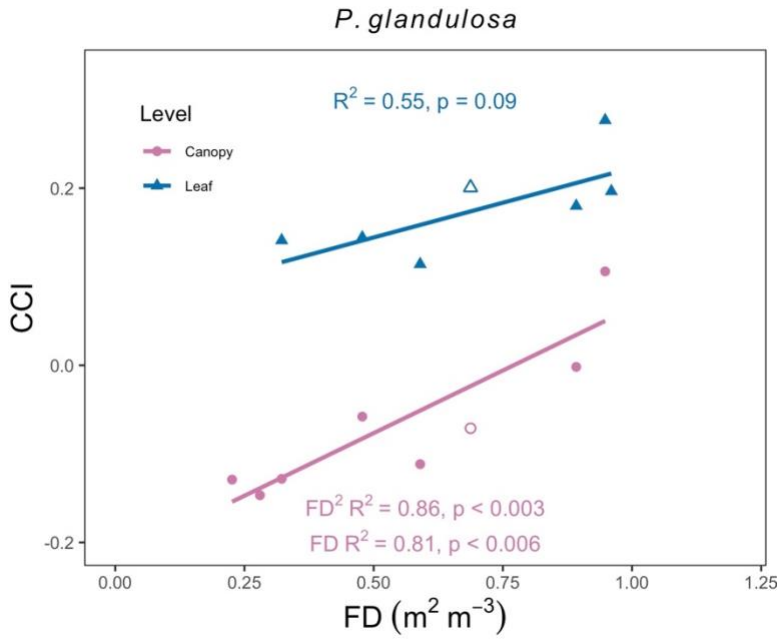

Figure 3.6 Linear relationships between leaf (blue triangles) and canopy (red circles) level CCI with Foliage Density (FD; mol mol^{-1}) in the deciduous *P. glandulosa*. Open symbols for *P. glandulosa* indicate immature leaves in March which were excluded from the final analyses. Original linear relationship is shown at the canopy level and not the relationship with the quadratic transformed FD values.

leaf-level CCI (R^2 = 0.64, $p < 0.05$; Table 3.3). In *Q. fusiformis*, only leaf-level CCI was moderately associated with *E* (R^2 = 0.48, $p < 0.05$; Table 3.2). Canopy level SAVI, EVI, EVI2, and PRI had moderate (negative for the first three and positive for PRI) relationships ($R^2 > 0.58$, $p < 0.05$) with *E* in *J. ashei* in addition to leaf level NDVI (R^2 = 0.51, $p < 0.05$, Table 3). Interpretation of relationships with *J. ashei* should be cautioned as normality was not met in *E.* Stomatal conductance in *Q. fusiformis* had moderate negative relationships with the canopy greenness indices (SAVI, EVI, EVI2) ($R^2 > 0.57$, $p < 0.05$), while g_s in *J. ashei* was negatively related to all canopy greenness indices

(NDVI $R^2 > 0.55$, $p < 0.05$; SAVI, EVI, EVI2 $R^2 > 0.71$, $p < 0.01$). No relationships between stomatal conductance and vegetation indices were found in *P. glandulosa*.

Weakly moderate relationships between *E* and canopy level PRI in the rmc was found for *J. ashei* ($R^2_{rmc} = 0.40$, $p < 0.001$) and *P. glandulosa* ($R^2_{rmc} = 0.49$, $p < 0.001$, Tables 4 & 5). Slightly weaker relationships were found between *E* and canopy level vegetation indices for *P. glandulosa* including the greenness indices ($R^2_{rmc} = 0.38$, $p < 0.001$) and CCI ($R^2_{rmc} = 0.39$, $p < 0.001$, Table 5). Leaf-level relationships between vegetation indices and g_s were generally weaker than the canopy relationships across species in the rmc.

Strong relationships among indices were found with F_V/F_M and to a more moderate extent in ϕ_{PSII}. The strongest relationships with F_V/F_M among species tended to be leaf and canopy level PRI over CCI. *P. glandulosa* was found to have the stronger relationships with F_V/F_M and PRI at leaf ($R^2 = 0.83$, $p < 0.01$) and canopy ($R^2 = 0.78$, $p < 0.05$) levels than CCI (leaf $R^2 = 0.58$, $p < 0.05$; Fig 3.7, Table 3.3). This pattern was repeated in *J. ashei* which had stronger relationships between PRI and F_V/F_M at leaf ($R^2 = 0.87$, $p < 0.0001$) and canopy ($R^2 = 0.85$, $p < 0.001$) levels over CCI (leaf $R^2 = 0.66$, $p < 0.004$; canopy $R^2 = 0.74$, $p < 0.006$; Fig 3.7, Table 3.4). *Q. fusiformis* had more moderate values that carried the same pattern with both PRI measurements (leaf & canopy $R^2 = 0.51$, $p < 0.05$) being greater than CCI (leaf $R^2 = 0.42$, $p < 0.04$; Fig 3.7, Table 3.2).

Relationships between F_V/F_M and vegetation indices were moderate to moderately strong in *J. ashei* and *P. glandulosa* respectively for the rmc. Relationships

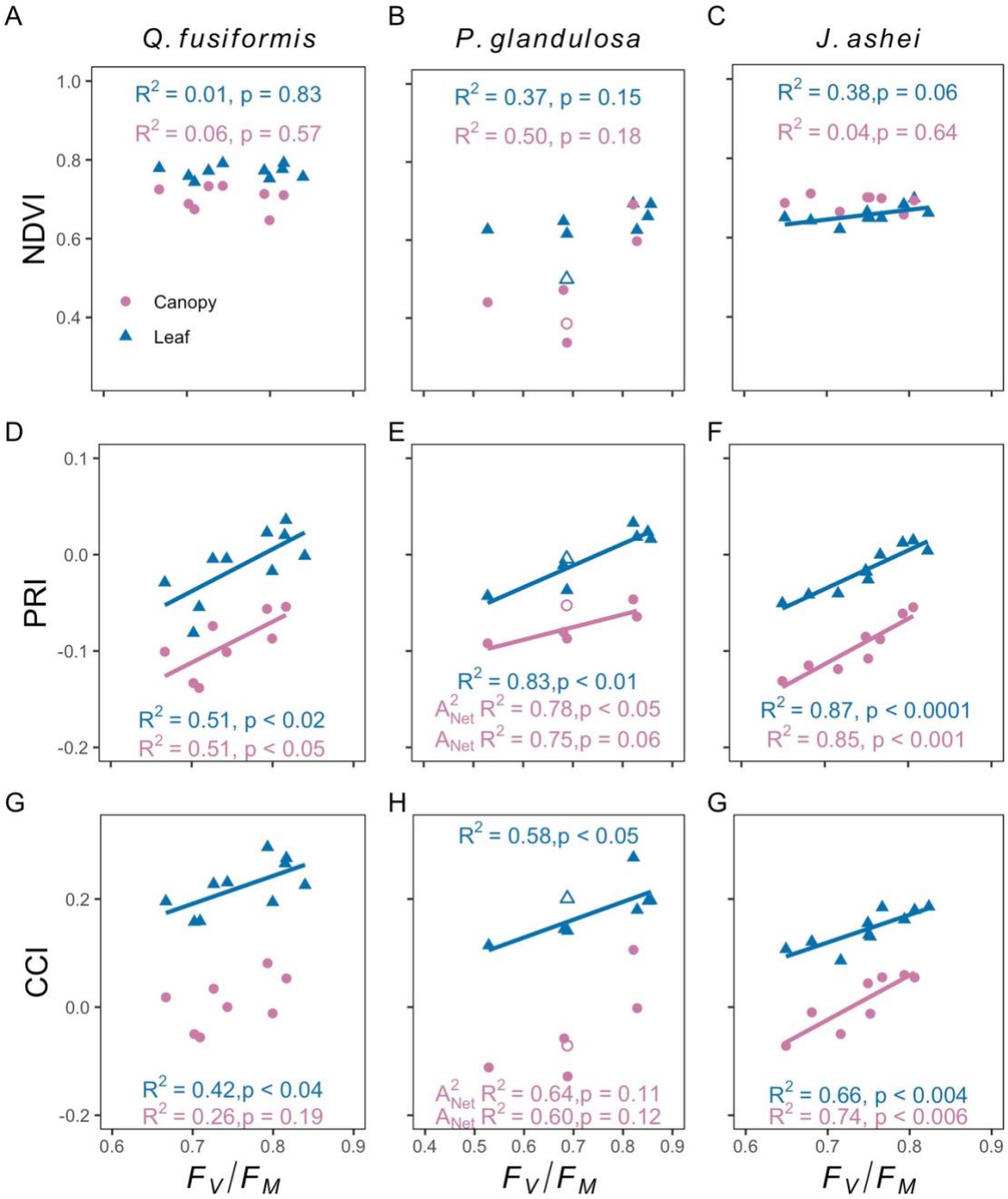

Figure 3.7 Linear relationships between leaf (blue triangles) and canopy (red circles) level NDVI, PRI, and CCI with *FV/FM*. Open symbols for *P. glandulosa* indicate immature leaves in March which were excluded from the final analyses. Original linear relationships at the canopy level shown in E and H and not the relationships with the quadratic transformed *FV/FM* values.

were generally highest with PRI and secondly with CCI. Relationships at both leaf and canopy scales were comparable or slightly weaker at the leaf-level scale. Canopy greenness indices were more weakly associated ($R^2_{rmc} < 0.43$, $p < 0.01$) with F_V/F_M relative to CCI ($R^2_{rmc} = 0.54$, $p < 0.001$) or PRI ($R^2_{rmc} = 0.63$, $p < 0.001$) in *P. glandulosa* (Table A-2). It should be noted that canopy CCI had improved significance in the rmc. Canopy PRI values were more strongly associated with F_V/F_M ($R^2_{rmc} = 0.57$, $p < 0.001$) in *J. ashei* than CCI values ($R^2_{rmc} = 0.38$, $p < 0.001$; Table A-3). Relationships of CCI and PRI to F_V/F_M in *Q. fusiformis* were weak in the rmc (Table A-1).

In both *J. ashei* and *P. glandulosa*, PRI and greenness indices had moderate relationships with $\phi_{PSII,}$ while CCI was non-significant. In *P. glandulosa*, leaf level PRI ($R^2 = 0.77$, $p < 0.01$) and NDVI ($R^2 = 0.56$, $p < 0.05$) was significantly related to ϕ_{PSII}, but relationships were stronger in the other canopy level greenness indices ($R^2 > 0.81$, $p < 0.05$, Table 3.3). *J. ashei* had significant positive correlations between ϕ_{PSII} with leaf-level NDVI ($R^2 = 0.48$, $p <0.05$) and canopy PRI ($R^2 = 0.57$, $p < 0.05$), while canopy SAVI ($R^2 = 0.56$, $p < 0.05$) and EVI2 ($R^2 = 0.55$, $p < 0.05$) had negative relationships. Vegetation indices were not significantly correlated with ϕ_{PSII} in *Q. fusiformis* (Table 3.2).

Relationships between vegetation indices and ϕ_{PSII} were either weakly correlated or not significant in the semi-evergreen *Q. fusiformis* in the rmc (Table A-1). Only canopy PRI recorded a moderate relationship between ϕ_{PSII} in *J. ashei* ($R^2_{rmc} = 0.38$, $p <$

0.001, Table A-3), while all other indices were only weakly correlated or not significant. At the leaf scale, PRI had the strongest relationship with ϕ_{PSII} in *P. glandulosa* (R^2_{rmc} = 0.43, $p < 0.001$), while canopy PRI ($R^2_{rmc} = 0.32$, $p < 0.05$) was generally weaker than SAVI, EVI, and EVI2 ($R^2_{rmc} > 0.49$, $p < 0.001$; Table A-2). The strongest relationship between CCI and ϕ_{PSII} across species was still generally weak and was at the canopy scale for *P. glandulosa* ($R^2_{rmc} = 0.32$, $p < 0.05$; Table A-2).

3.3.4. Discussion

Remote sensing has struggled to capture photosynthetic changes in drylands partially due to use of chlorophyll-based greenness indices in presence of evergreens (Biederman et al. 2017, Smith et al. 2019), and results from this study indicate CCI may improve those capabilities across leaf functional types. Across species at both scales, CCI was found to capture a slow adjusting parameter of photosynthetic phenology, F_V/F_M, while relationships of F_V/F_M to greenness indices were largely constrained to the deciduous *P. glandulosa* at canopy scales (Tables 3.2, 3.3, 3.4, A-2). Tracking F_V/F_M is important due to its slow-adjusting nature in response to seasonal stressors of drought or freezing (Verhoeven et al. 2018) and its ability to exert influence on photosynthetic uptake over the course of the day. Specifically, F_V/F_M has capabilities to constrain photosynthetic uptake under light-limited conditions and light-saturation in more severe instances (Adams et al. 2008, Murchie and Ruban 2020).

Consequently, the ability of CCI to track F_V/F_M across species may improve remote sensing assessments of productivity in drylands over seasonal scales due to the slow-adjusting nature of F_V/F_M and its photosynthetic influence. Similar findings

between F_V/F_M and CCI have been found in boreal forests showing this relationship occurs over a range of stressful conditions from water limitations to freezing events (D'Odorico et al. 2020). As a result, CCI holds promise in tracking general trends in photosynthetic activity across species of varying leaf persistence in drylands based on its relationship with F_V/F_M here.

Tracking photosynthetic activity in drylands may have additionally improved as both scales of CCI captured pigment shifts in Chl:Car across species and FD changes in the deciduous *P. glandulosa* with canopy CCI. Such relationships between pigment and canopy structural changes with CCI across leaf functional types have been similarly reported (Springer et al. 2017). No other vegetation index at the canopy level was capable of capturing both FD changes in the deciduous species and pigment pool changes across species. This highlights the unique capability of CCI to track the photosynthetic phenology of both evergreen and deciduous trees at the canopy level in this water limited system, while PRI and greenness indices had more limited utility capturing both FD and pigment changes across species.

The relationship of CCI to Chl:Car and FD likely drove its ability to capture F_V/F_M across species since all parameters adjust at slow rates in response to environmental stressors. Just as drought and freezing events gradually decrease F_V/F_M from healthy values due to sustained energy dissipation (Verhoeven et al. 2018), these stressors can gradually decrease chlorophyll content and increase carotenoid content (Fernández-Marín 2017). Thus, light-harvesting capacities for photosynthesis in chlorophyll are gradually shifted towards energy dissipating capabilities in carotenoids

(Esteban et al. 2015) by decreasing Chl:Car in response to stress. Such shifts in Chl:Car are captured by leaf CCI and likely drove its strong relationship with F_V/F_M across species as fall temperatures decreased Chl:Car and F_V/F_M. Freezing temperatures can activate leaf senescence and abscission for winter deciduous species (Rosenthal and Camm 1997). The resulting declines in F_V/F_M from senescence were captured by canopy CCI, and it was aided by its ability to track FD decreases in *P. glandulosa* as leaves abscised.

Consequently, CCI showed a strong capability to capture a slow-adjusting photosynthetic parameter (F_V/F_M) across species by capturing the slowly adjusting Chl:Car across species and FD in the deciduous species. The ability of CCI to capture Chl:Car and FD has led to improved capabilities capturing photosynthetic uptake across leaf functional types and scales in boreal systems (Springer et al. 2017, Wong et al. 2020), which is partially supported here in its relationship to Chl:Car, FD, and F_V/F_M for the dryland species. The similar results to past studies provide further evidence that CCI may improve the ability to capture productivity changes in dryland systems varying in leaf functional types such as the species here. These landscapes are heterogenous matrices of grass, soil, deciduous, and evergreen species, so studies at greater spatiotemporal scales are needed in drylands to test the relationship between CCI with ecosystem productivity.

While CCI did have these strong relationships with the parameters above, it was only partially supportive of our expectations as both levels of PRI had stronger relationships across species with F_V/F_M and Chl:Car but not FD. The stronger

relationships with PRI over CCI with photosynthetic parameters have been reported in Wong et al. (2019), Fréchette et al. (2020), but not other studies where CCI has been stronger or had mixed results with PRI (Springer et al. 2017, Wong et al. 2020). Comparisons of PRI and CCI are few as CCI is a recently developed index (Gamon et al. 2016), so the strength of CCI relationships and sources of variation in CCI are not well known compared to other indices. PRI is known to be greatly affected at the canopy level from soil background influence in low LAI vegetation and from changes in solar angle (Barton and North 2001). At seasonal scales, PRI has been mostly tied to Chl:Car, a smaller degree to the xanthophyll cycle, and "deep cold" (i.e. below 4 °C) that causes albedo changes across wavelengths (Wong and Gamon 2015). NDVI is also known to suffer from background soil interference under low LAI and from atmospheric effects which led to the creation of SAVI and EVI (Huete 1988, Liu and Huete 1995). Considering bands from both PRI and NDVI are used to calculate CCI, it appears paramount we understand how the aforementioned sources of variation can affect CCI values. Doing so may clarify how results here and in other studies show PRI having stronger relationships with certain photosynthetic parameters. It should be noted that CCI still has the potential capacity for stronger relationships with photosynthetic changes in these systems in larger spatiotemporal studies due to its capability to capture both canopy FD changes and Chl:Car changes (Springer et al. 2017) unlike PRI here. Additionally, past studies have shown PRI does not track seasonal or interannual photosynthetic changes in these dryland systems better than greenness indices (EVI) due to the sparse vegetation (Smith et al. 2018).

Differences in strengths of relationships between leaf and canopy levels among all indices were influenced by the differing signals at each level and different duration of measurement campaigns at the leaf and canopy level. At the leaf-level, seasonal reflectance signals were driven by shifting pools of chlorophyll and carotenoids (Sims and Gamon 2002, Stylinski et al. 2002, Wong and Gamon 2015). While shifting pigment pools affect canopy reflectance values, the measurements were also influenced by changing FD, soil background interference for NDVI and PRI, and solar angle for PRI (Barton and North 2001, Xue & Su 2017). While canopy measurements had these additional sources of variation, it was also sampled over a smaller period of time starting in September (8 months) that mostly included fall, winter, and spring, while leaf-level measurements started earlier in July (10 months).

Consequently, canopy measurements did not include summer measurements—unlike leaf-reflectance—which was a period of higher variability in "dynamic" parameters that quickly adjust. These dynamic parameters include gas-exchange, midday fluorescence, and Ψ_{MD} parameters. Fluctuating summer values for those dynamic variables were in contrast to their steadier patterns each season for fall, winter, and spring. As a result, across species canopy relationships to those dynamic parameters tended to be more significant and stronger than leaf-level relationships with some exceptions. In contrast, the slower adjusting parameters (F_V/F_M, Chl:Car, and FD) had similarly strong relationships at both scales indicating that these relationships strongly extended through all seasons at both levels. These aforementioned sources of variation at leaf and canopy levels become important when interpreting relationships at the two

scales for dynamic parameters with the vegetation indices but less so for the slower adjusting responses (F_V/F_M, Chl:Car, and FD).

In assessing the capabilities of vegetation indices to capture photosynthetic processes in these dryland systems, we found that midday measurements of dynamically changing variables had weak or non-significant relationships (A_{Net}, NPQ, and Ψ_{PD}), while there were species-specific moderate relationships found with others (E, g_s, Ψ_{MD}, and ϕ_{PSII}). These species-specific relationships (E, g_s, Ψ_{MD}, and ϕ_{PSII}) showed contrasting patterns or had inconsistent physiological explanations across all three species. Consequently, relationships of vegetation indices to dynamically changing variables is inconsistently captured across species in these systems and they might only occur in species-specific situations as was the case for *Q. fusiformis, P. glandulosa,* and *J. ashei*.

In the case of *Q. fusiformis*, any relationships of E, g_s, Ψ_{MD}, and ϕ_{PSII} to canopy greenness indices and leaf-level carotenoid indices were influenced by its drought avoiding nature, semi-evergreen leaves, and differing stomatal behavior than the other two species. *Q. fusiformis* did not experience fluctuating Ψ_{PD} or Ψ_{MD} during dry periods consistent with its strategy as a drought avoider (Fonteyn et al. 1985), which allowed for fairly stable g_s values. However, spring rains caused g_s and Ψ_{MD} to increase, while greenness indices declined with FD through winter until new buds emerged in March. As a result, Ψ_{MD} and g_s showed negative relationships with canopy greenness indices. Additionally, steady g_s values during high VPD can allow for increases in E as open stomata tend to have little regulatory capacity (Jones 1998, Lawson and Morison 2004) which likely allowed transpiration to be higher in the summer and spring here. This

seasonal pattern was similar to that of leaf CCI in tracking Chl:Car and created a significant positive relationship with *E* as a result. Leaf PRI similarly tracked Chl:Car and was able to capture the pattern for ϕ_{PSII} that decreased from summer to fall before stabilizing through winter. Consequently, *Q. fusiformis* had negative canopy greenness relationships with g_s and Ψ_{MD} due to decreasing FD, *E* patterns created by open stomata that were captured by leaf-level CCI, and ϕ_{PSII} was positively captured by leaf-level PRI.

P. glandulosa did have contrasting patterns to the other two species with its relationships between vegetation indices and its dynamic parameters *E*, Ψ_{MD}, ϕ_{PSII}, and g_s. Notably for *P. glandulosa*, g_s had non-significant relationships with all vegetation indices, while both *J. ashei* and *Q. fusiformis* showed negative relationships between g_s and canopy greenness indices. Additionally, *P. glandulosa* showed significant positive relationships to *E* with all canopy measurements and leaf-level carotenoid indices in contrast to the moderate negative relationships with canopy greenness indices with *E* found in *J. ashei* and mostly non-significant relationships with *E* in *Q. fusiformis*. Though *E* was more tightly coupled with g_s in *P. glandulosa* than *Q. fusiformis*, *E* had greater declines than g_s over the season compared to their summer values, which matched general declines in Chl:Car that the leaf-level carotenoid indices tracked. At the canopy-level, greenness indices and FD steadily declined from September for *P. glandulosa* which matched *E* but not the slightly more variable g_s patterns over this period. Consequently, these relationships were significant with *E* but not g_s in this species. Further, Ψ_{MD} generally declined for *P. glandulosa* from July due to dry periods and declined at the end of leaf-life to create a positive relation with leaf-level greenness

indices that also slightly declined over this period. This positive relation with Ψ_{MD} was in contrast to the negative relationships with canopy greenness indices and Ψ_{MD} for *Q. fusiformis*. Finally, ϕ_{PSII} declined from July with large drops from September that matched general FD drops and were therefore picked up by canopy greenness indices, while over the longer period of measurement at the leaf-level, declining ϕ_{PSII} was picked up by both leaf NDVI and PRI. Consequently, all of the relationships between *P. glandulosa* dynamic parameters and vegetation indices were positive, were at times in contrast with the other two species, while occasionally differed in significance between leaf and canopy levels due to the differing sampling duration between them.

Surprisingly, canopy greenness indices in *J. ashei* had significant relationships with g_s, E, and ϕ_{PSII} despite its evergreen leaves, which was due to negative relationships similar to that experienced by *Q. fusiformis* with g_s but in contrast to *P. glandulosa* patterns. Increased water availability for *J. ashei* in the spring increased g_s, E, and ϕ_{PSII} to peaks from their lower values in dry September that had marked the start of canopy sampling. In contrast, canopy greenness indices decreased slightly over this period to cause the negative relationships, which was more pronounced in SAVI, EVI, and EVI2 than NDVI from December to March. Greenness declines may be attributed to several mechanisms. FD showed slight declines that were significantly correlated to declining canopy greenness indices indicating some small levels of leaf loss may have occurred even if not directly observed. Additionally, increasing densities of pollen-discharging male juniper cones have been found to significantly lower greenness index values in above canopy spectral measurements—as much as 30% in EVI—due to decreasing NIR

values (Peng et al. 2013). Three of the junipers were male with noticeable cone production occurring during January and February, which is consistent with the known production patterns of the species (Smeins and Fuhlendorf 1997) and likely contributed to lowered greenness values dropping from December to March. Understory vegetation for these species was noticeably senesced during December to February periods which could have additionally influenced declining greenness values if their signal was captured. Consequently, *J. ashei* showed some contrasting patterns with dynamic variables to the other species with differing mechanisms such as male cone production.

In sum, our ability to consistently capture dynamic photosynthetic parameters across species or similar functional types in this dryland system did not occur. Relationships of vegetation indices with dynamic parameters differed in strength among species, differed in their direction of relationship, and differed in their physiological explanations. Consequently, it indicates that these relationships can be species-specific and application across differing species may yield inconsistent results. As a result, using slow changing vegetation indices to track dynamically changing parameters in arid systems may yield inconsistent relationships—particularly since physiological changes decouple from spectral values at short time intervals in this system (Yan et al. 2019).

An objective of this study was to compare the ability of CCI to track the direct photosynthetic uptake of trees varying in leaf functional types versus other greenness indices in this water limited system, and we found that no vegetation index was able to capture instantaneous A_{Net}. These lack of relationships with A_{Net} should not dissuade evaluation of these indices in tracking photosynthetic phenology in these systems as

poor relationships were likely due to the correlation of slow-changing reflectance values with parameters that change dynamically (Yan et al. 2019) and are captured in instantaneous snapshot measurements. This is especially true considering drylands are known to have highly variable productivity responses to rain and dry periods (Scott et al. 2009) while responses may decouple from greenness indices at shorter time scales (Yan et al. 2019).

It should be noted that although other dynamic parameters (g_s, E, and ϕ_{PSII}) had significant relationships occur, A_{Net} did not and it was due to decoupling in its trend from the other variables. Occasional decoupling here refers to one or several sampling periods where A_{Net} trends had differing changes in magnitude relative to the other parameters or when its trend moved in the opposite direction. Occasional decoupling for A_{Net} in *P. glandulosa* occurred in September and October, which was influential as only five canopy measurements were made. Consequently, it led to weak to non-significant relationships with A_{Net} versus the significant relationships with E for all canopy indices and ϕ_{PSII} for canopy level greenness indices. *Q. fusiformis* additionally experienced occasional decoupling in the spring likely due to leaf turnover. Conversely, *J. ashei* experienced more periods of decoupling of A_{Net} from ϕ_{PSII}, E, and g_s for July and December to February allowing for variable strengths in relationships among all the parameters. This occasional decoupling between A_{Net} and other dynamically changing gas-exchange parameters has been reported before in studies of semi-arid plants including *Prosopis juliflora* involving A_{Max} and g_s (Tezara et al. 1998) and both diurnally and seasonally in *P. glandulosa* (De Soyza et al. 1996). *J. occidentalis* and *J. phoenicea*

have also reported some variability in A_{Net} and g_s trends diurnally and seasonally for each species respectively (Miller et al. 1992, Baquedano and Castillo 2007).

While it is not clear what caused A_{Net} to vary and be the only gas-exchange parameter not to have a significant relationship with a vegetation index, its trend could be influenced by: 1) decoupling from g_s or ϕ_{PSII}, and 2) diurnal changes in maximum A_{Net}. Traditionally, A_{Net} synchronously changes with g_s but that relationship is not always consistently reported (Matthews et al. 2017). It has been found that spatial variability can cause g_s and A_{Net} to show contrasting rates at the same location on a leaf, while the fact that leaves are hydraulically connected to the whole plant may cause further variability in the two rates on individual leaves (Lawson and Morison 2004). The spatial variability may have particularly influenced *Q. fusiformis* and *P. glandulosa* which did not always have the complete leaf within the gas-exchange chamber. Additionally, ϕ_{PSII} can adjust faster than A_{Net} as values do not always completely reflect the quantum yield used in photosynthesis but can additionally reflect light absorbed by the photosystems used for photorespiration (Kalaji et al. 2017). Capturing photosynthetic trends with spectral indices may be further hampered by diurnal shifts in photosynthetic capacity for dryland woody species during periods of water stress that both decreases the maximum values of A_{Net} and shifts peaks of maximum A_{Net} from midday to the morning or to peaks on either side of midday (Hellmuth et al. 1971). Peaks of A_{Net} in the morning have been recorded in *P. glandulosa* in late-summer (Soyza et al. 1996), while *J. occidentalis* has experienced shifting and decreasing peaks to mid-morning hours in late summer (Miller et al. 1992). Consequently, spectral indices may be specifically hindered in tracking

instantaneous measurements of photosynthesis in drylands due to decoupling among dynamic parameters and changing magnitudes and shifting peaks of maximum A_{Net} seasonally.

Comparison of these findings to similar studies is limited as few have assessed relationships between vegetation indices and seasonal leaf-level photosynthetic changes of woody plants in dryland systems. The few dryland studies at the leaf-scale have been restricted to sampling at coarse resolutions of ~2-4 months (Stylinski et al. 2002, Zhang et al. 2017). However, seasonal relationships like these do not adequately reflect the ability of indices to track photosynthetic changes over shorter periods of time (~2 weeks – 1 month) which is more useful towards better understanding and capturing the photosynthetic responses to water stress and availability that are predicted to increase in the future (Dai 2013, Trenberth et al.2013, Allen et al. 2015).

In contrast, most studies involving similar vegetation indices and seasonal leaf-level photosynthetic responses of woody individuals have focused on boreal species (Wong and Gamon 2015, Gamon et al. 2016, Springer et al. 2017, Wong et al. 2019, D'Odorico et al. 2020, Fréchette et al. 2020, Wong et al. 2020) whose patterns of productivity are likely to be less variable than these water-limited systems. These boreal systems are likely to experience less variable trends in productivity during the growing season than drylands due to lower VPD, cooler temperatures, and higher water availability located there which likely allowed for stronger relationships between A_{Net} and vegetation indices that were sampled at higher frequencies of ~2 weeks (Gamon et al. 2016, Springer et al. 2017, Wong et al. 2019, D'Odorico et al. 2020, Wong et al.

2020). Consequently, increased frequency of measurements in dryland systems at higher spatial scales should help elucidate the true strengths of these indices—particularly CCI—in capturing photosynthetic dynamics of dryland systems.

3.4. **Conclusions**

Results indicate that CCI may improve our capabilities to capture the photosynthetic phenology of dryland systems where remote sensing has traditionally struggled (Smith et al. 2019). Canopy CCI was the only index to significantly capture FD changes in the deciduous species and pigment pool shifts in Chl:Car across species varying from deciduous to evergreen. Consequently, CCI was both sensitive to leaf flush and abscission in leaves with short life cycles and seasonal physiological changes in evergreens and deciduous species by tracking shifts of relative pigment pools. The tracking of both slow-adjusting parameters (Chl:Car and FD) responding to seasonal drivers allowed CCI at both scales to capture the slow-adjusting photoinhibition of the maximal quantum yield of PSII (F_V/F_M) across species. Tracking of F_V/F_M with CCI is notable as F_V/F_M slowly responds to seasonal stress, while having capabilities to exert influence on photosynthetic uptake over the day (Adams et al. 2008, Murchie and Ruban 2020). Consequently, the ability to track Chl:Car, FD, and F_V/F_M across plants of varying leaf-persistence indicates that CCI has a high potential to track productivity changes in drylands at greater spatiotemporal scales which are often heterogenous matrices of different plant leaf functional types. Future studies are needed to test this possibility.

Both levels of PRI had stronger relationships with F_V/F_M and Chl:Car across species than CCI, which was in contrast to what was expected. PRI is unlikely to be better track at tracking photosynthetic changes at higher spatial scales than CCI though as it suffers substantially from soil background signals in these systems (Smith et al. 2018). To understand how PRI had stronger relationships with Chl:Car and F_V/F_M than CCI, we need more controlled studies assessing how factors like soil reflectance, solar angle, temperature, drought, etc. can influence the variation in bands of CCI versus PRI. This might explain why PRI occasionally records stronger relationships with photosynthetic parameters (Wong et al. 2019, Fréchette et al. 2020).

Relationships of vegetation indices to instantaneous measurements of dynamic parameters that can adjust quickly can yield moderate species-specific relationships or weak to non-significant relationships in these dryland landscapes. The former case included E, Ψ_{MD}, ϕ_{PSII}, and g_s which were found among the three species to differ in strengths of relationships for each parameter, direction of the relationship, and the physiological mechanisms of the trends. These parameters generally showed contrasting patterns and inconsistent drivers in trends among the indices and across species. The latter case of weak to non-significant relationships included NPQ, Ψ_{PD}, but particularly A_{Net} which this study wanted to evaluate. Finding significant relationships with A_{Net} proved difficult as A_{Net} experienced occasional decoupling in trends from other dynamic parameters at midday which may have limited strong relationships with vegetation indices.

The availability of CCI at leaf scales, its presence in continuous spectral reflectance sensors in near-canopy measurements (Wong et al. 2020), and its availability at the satellite scales offers promising opportunities to study its ability to capture photosynthetic phenology at a variety of spatiotemporal scales. We believe such applications need to be applied to dryland landscapes where vegetation ranging from grasses to evergreen trees may benefit from an index that measures both FD changes and pigment changes across leaf functional types. Such assessments may yield better understanding of how these systems respond to warming and dry temperatures that are projected to increase in the severity at the end of the 21st century (Seager et al. 2007, Strzepek et al. 2010, Dai 2013).

3.5. **References**

Adams, W. W., C. R. Zarter, K. E. Mueh, V. Amiard, and B. Demmig-Adams. 2008. Energy dissipation and photoinhibition: a continuum of photoprotection. In Demmig-Adams, B., W. W. Adams, and A. K. Matoo (Ed.), Photoprotection, photoinhibition, gene regulation, and environment Springer, Dordrecht, Netherlands. 49-64.

Ahlstrom, A., M. R. Raupach, G. Schurgers, B. Smith, A. Arneth, M. Jung, M. Reichstein, J. G. Canadell, P. Friedlingstein, A. K. Jain, E. Kato, B. Poulter, S. Sitch, B. D. Stocker, N. Viovy, Y. P. Wang, A. Wiltshire, S. Zaehle, and N. Zeng. 2015. The dominant role of semi-arid ecosystems in the trend and variability of the land CO2 sink. Science **348**:895–899.

Allen, C. D., D. D. Breshears, and N. G. McDowell. 2015. On underestimation of global vulnerability to tree mortality and forest die-off from hotter drought in the Anthropocene. Ecosphere **6**:1-55.

Bakdash, J. Z., and L. R. Marusich. 2017. Repeated measures correlation. Frontiers in Psychology **8**:1-13.

Baquedano, F. J., and F. J. Castillo. 2007. Drought tolerance in the Mediterranean species *Quercus coccifera*, *Quercus ilex*, *Pinus halepensis*, and *Juniperus phoenicea*. Photosynthetica **45**:229-238.

Barger, N. N., S. R. Archer, J. L. Campbell, C. Huang, J. A. Morton, and A. K. Knapp. 2011. Woody plant proliferation in North American drylands: A synthesis of impacts on ecosystem carbon balance. Journal of Geophysical Research: Biogeosciences **116**:1-17.

Barton, C. V. M., and P. R. J. North. 2001. Remote sensing of canopy light use efficiency using the photochemical reflectance index model and sensitivity analysis. Remote Sensing of Environment **10**:264-273.

Bendevis, M. A., M. K. Owens, J. L. Heilman, and K. J. McInnes. 2010. Carbon exchange and water loss from two evergreen trees in a semiarid woodland. Ecohydrology **3**:107–115.

Biederman, J. A., R. L. Scott, T. W. Bell, D. R. Bowling, S. Dore, J. Garatuza-Payan, T. E. Kolb, P. Krishnan, D. J. Krofcheck, M. E. Litvak, G. E. Maurer, T. P. Meyers, W. C. Oechel, S. A. Papuga, G. E. Ponce-Campos, J. C. Rodriguez, W. K. Smith, R. Vargas, C. J. Watts, E. A. Yepez, and M. L. Goulden. 2017. CO2 exchange

and evapotranspiration across dryland ecosystems of southwestern North America. Global Change Biology **23**:4204–4221.

Čepl, J., J. Stejskal, Z. Lhotákova, D. Holá, J. Korecký, M. Lstibůrek, I. Tomášková, M. Kočová, O. Rothová, M. Palovská, J. Hejtmánek, A. Krejzková, S. Gezan, R. Whetten, and J. lbrechtová. 2018. Heritable variation in needle spectral reflectance of Scots pine (*Pinus sylvestris* L.) peaks in red edge. Remote Sensing of Environment **219**:89-98.

Dai, A. 2013. Increasing drought under global warming in observations and models. Nature Climate Change **3**:52–58.

Da Ros Carvalho, H. 2019. Epiticular waxes and the energy balance of sorghum [*Sorghum bicolor* (L.) *Moench*]. Doctoral dissertation, Texas A&M University.

Demmig-Adams, B., and W. W. Adams. 1996. The role of xanthophyll cycle carotenoids in the protection of photosynthesis. Trends in Plant Science **1**:21-26.

De Soyza, A. G., A. C. Franco, R. A. Virginia, J. F. Reynolds, and W. G. Whitford. 1996. Effects of plant size on photosynthesis and water relations in the desert shrub *Prosopis glandulosa* (Fabaceae). American Journal of Botany **83**:99–105.

D'Odorico, P., A. Besik, C. Y. S. Wong, N. Isabel, and I. Ensminger. 2020. High-throughput drone-based remote sensing reliably tracks phenology in thousands of conifer seedlings. New Phytologist **226**:1667–1681.

Esteban, R., O. Barrutia, U. Artetxe, B. Fernández-Marín, A. Hernández, and J. I. García-Plazaola. 2015. Internal and external factors affecting photosynthetic pigment composition in plants: a meta-analytical approach. New Phytologist **206**:268–280.

Fernández-Marín, B., Hernández, A., Garcia-Plazaola, J. I., Esteban, R., Míguez, F., Artetxe, U., & Gómez-Sagasti, M. T. 2017. Photoprotective strategies of Mediterranean plants in relation to morphological traits and natural environmental pressure: A meta-analytical approach. Frontiers in Plant Science **8**:1-16.

Fonteyn, P. J., T. M. McClean, and R. E. Akridge. 1985. Xylem pressure potentials of three dominant trees of the Edwards Plateau of Texas. The Southwestern Naturalist **30**:141-146.

Fréchette, E., C. Y.-Y. Chang, and I. Ensminger. 2020. Variation in the phenology of photosynthesis among eastern white pine provenances in response to warming. Global Change Biology **26**:5217–5234.

Gałecki, A., and T. Burzykowski. 2013. Linear mixed-effects models using R. Springer New York, New York, NY.

Gamon, J. A., K. F. Huemmrich, C. Y. S. Wong, I. Ensminger, S. Garrity, D. Y. Hollinger, A. Noormets, and J. Peñuelas. 2016. A remotely sensed pigment index reveals photosynthetic phenology in evergreen conifers. Proceedings of the National Academy of Sciences **113**:13087–13092.

Gamon, J. A., J. Peñuelas, and C. B. Field. 1992. A narrow-waveband spectral index that tracks diurnal changes in photosynthetic efficiency. Remote Sensing of Environment **41**:35–44.

Goetz, A.F.H. 2012. Making accurate field spectral reflectance measurements. ASD Inc. a PANalytical Company; Boulder, CO. 1-16.

Hellmuth, E. O. 1971. Eco-physiological studies on plants in arid and semi-arid regions in Western Australia: III. Comparative studies on photosynthesis, respiration and water relations of ten arid zone and two semi-arid zone plants under winter and late summer climatic conditions. Journal of Ecology **59**:225–259.

Huete, A. R. 1988. A soil-adjusted vegetation index (SAVI). Remote Sensing of Environment **25**:295–309.

Jones, H. G. 1998. Stomatal control of photosynthesis and transpiration. Journal of Experimental Botany **49**:387–398.

Kalaji, H. M., G. Schansker, M. Brestic, F. Bussotti, A. Calatayud, L. Ferroni, V. Goltsev, L. Guidi, A. Jajoo, P. Li, P. Losciale, V. K. Mishra, A. N. Misra, S. G. Nebauer, S. Pancaldi, C. Penella, M. Pollastrini, K. Suresh, E. Tambussi, M. Yanniccari, M. Zivcak, M. D. Cetner, I. A. Samborska, A. Stirbet, K. Olsovska, K. Kunderlikova, H. Shelonzek, S. Rusinowski, and W. Bąba. 2017. Frequently asked questions about chlorophyll fluorescence, the sequel. Photosynthesis Research **132**:13–66.

Lawson, T and J.I.L. Morison. 2004. Stomatal function and physiology. In A.R. Hemsley, and I. Poole (Eds.), The Evolution of Plant Physiology. Academic Press, 217-238.

Lehmann, J., A. Große-Stoltenberg, M. Römer, and J. Oldeland. 2015. Field spectroscopy in the VNIR-SWIR region to discriminate between Mediterranean native plants and exotic-invasive shrubs based on leaf tannin content. Remote Sensing **7**:1225–1241.

Liu, H. Q., and A. Huete. 1995. A feedback based modification of the NDVI to minimize canopy background and atmospheric noise. IEEE Transactions on Geoscience and Remote Sensing **33**:457–465.

Matthews, J. S. A., S. R. M. Vialet-Chabrand, and T. Lawson. 2017. Diurnal variation in gas exchange: The balance between carbon fixation and water loss. Plant Physiology **174:**614–623.

Maxwell, K., and G. N. Johnson. 2000. Chlorophyll fluorescence—a practical guide. Journal of Experimental Botany **51**:659–668.

Miller, P. M., L. E. E. Leman, and J. M. M. Ler. 1992. The seasonal course of physiological processes in *Juniperus occidentalis*. Forest Ecology and Management **48**:185-215.

Monteith, J. L. 1972. Solar Radiation and Productivity in tropical ecosystems. Journal of Applied Ecology **9**:747–766.

Murchie, E. H., and T. Lawson. 2013. Chlorophyll fluorescence analysis: a guide to good practice and understanding some new applications. Journal of Experimental Botany **64**:3983–3998.

Murchie, E. H., and A. V. Ruban. 2020. Dynamic non-photochemical quenching in plants: From molecular mechanism to productivity. The Plant Journal **101**:885–896.

Peng, D., Z. Jiang, A.R. Huete, G.E. Ponce-Campos, U. Nguyen, and J.C. Luvall. 2013. Response of spectral reflectance and vegetation indices on varying juniper cone densities. Remote Sensing **5**:5330-5345.

Pinheiro, J. C. and Bates, D. M. 2000. Mixed-effects models in S and S-PLUS, Springer, New York.

Pinheiro J, Bates D, DebRoy S, Sarkar D, R Core Team. 2020. *nlme: Linear and Nonlinear Mixed Effects Models*. R package version 3.1-148, https://CRAN.R-project.org/package=nlme.

Pfitzner K, R. Bartolo, G. Carr, A. Esparon, and A. Bollhöfer. 2011. Standards for reflectance spectral measurement of temporal vegetation plots. Supervising Scientist Report 195, Supervising Scientist, Darwin NT.

Poulter, B., D. Frank, P. Ciais, R. B. Myneni, N. Andela, J. Bi, G. Broquet, J. G. Canadell, F. Chevallier, Y. Y. Liu, S. W. Running, S. Sitch, and G. R. van der

Werf. 2014. Contribution of semi-arid ecosystems to interannual variability of the global carbon cycle. Nature **509**:600–603.

Reynolds, J. F., D. M. S. Smith, E. F. Lambin, B. L. Turner, M. Mortimore, S. P. J. Batterbury, T. E. Downing, H. Dowlatabadi, R. J. Fernandez, J. E. Herrick, E. Huber-Sannwald, H. Jiang, R. Leemans, T. Lynam, F. T. Maestre, M. Ayarza, and B. Walker. 2007. Global desertification: Building a science for dryland development. Science **316**:847–851.

Roby, M.C., R.L. Scott, and J. P. Moore. 2020. High vapor pressure deficit decreases the productivity and water-use efficiency of rain-induced pulses in semiarid ecosystems. Journal of Geophysical Research-Biogeosciences 1-14.

Rosenthal, S. I., and E.L. Camm. 1997. Photosynthetic decline and pigment loss during autumn foliar senescence in western larch (*Larix occidentalis).* Tree Physiology **17**:767-775.

Rouse, W., and R. H. Haas. 1974. Monitoring vegetation systems in the Great Plains with ERTS. NASA (Goddard Space Flight Center 3rd ERTS-1 Symposium), **1**:309-317.

Running, W., R.R. Nemani, F.A. Heinsh, M. Zhao, M. Reeves, and H. Hashimoto. 2002. A continuous satellite derived measure of global terrestrial primary production. Bioscience **54**:547-560.

Seager, R., M. Ting, I. Held, Y. Kushnir, J. Lu, G. Vecchi, H.-P. Huang, N. Harnik, A. Leetmaa, N.-C. Lau, C. Li, J. Velez, and N. Naik. 2007. Model projections of an imminent transition to a more arid climate in Southwestern North America. Science **316**:1181–1184.

Scott, R. L., G. D. Jenerette, D. L. Potts, and T. E. Huxman. 2009. Effects of seasonal drought on net carbon dioxide exchange from a woody-plant-encroached semiarid grassland. Journal of Geophysical Research: Biogeosciences **114**:1-13.

Serbin, S. P., J. Wu, K. S. Ely, E. L. Kruger, P. A. Townsend, R. Meng, B. T. Wolfe, A. Chlus, Z. Wang, and A. Rogers. 2019. From the Arctic to the tropics: multibiome prediction of leaf mass per area using leaf reflectance. New Phytologist **224:**1557–1568.

Shiklomanov, A. N., M. C. Dietze, T. Viskari, P. A. Townsend, and S. P. Serbin. 2016. Quantifying the influences of spectral resolution on uncertainty in leaf trait estimates through a Bayesian approach to RTM inversion. Remote Sensing of Environment **183**:226–238.

Sims, D. A., and J. A. Gamon. 2002. Relationships between leaf pigment content and spectral reflectance across a wide range of species, leaf structures and developmental stages. Remote Sensing of Environment **81**:337–354.

Singmann, H., M. Hervé, J. Love, and P. Buerkner. 2020. *emmeans: Estimated marginal means AKA least square means*. R package version 1.5, https://cran.r-project.org/web/packages/emmeans/index.html

Smeins, F.E., and S.D. Fuhlendorf. 1997. Ch. 3 Biology, ecology, and ecophysiology of juniper: Biology and ecology of Ashe juniper. Texas Agricultural Experiment Station Technical Report 97-1 (Proceedings of 1997 Juniper Symposium), Taylor CA (ed.) Texas A&M University Research and Extension Center: Sonora, TX; 9–22.

Smith, W. K., J. A. Biederman, R. L. Scott, D. J. P. Moore, M. He, J. S. Kimball, D. Yan, A. Hudson, M. L. Barnes, N. MacBean, A. M. Fox, and M. E. Litvak. 2018. Chlorophyll fluorescence better captures seasonal and interannual gross primary productivity dynamics across dryland ecosystems of southwestern North America. Geophysical Research Letters **45**:748–757.

Smith, W. K., M. P. Dannenberg, D. Yan, S. Herrmann, M. L. Barnes, G. A. Barron-Gafford, J. A. Biederman, S. Ferrenberg, A. M. Fox, A. Hudson, J. F. Knowles, N. MacBean, D. J. P. Moore, P. L. Nagler, S. C. Reed, W. A. Rutherford, R. L. Scott, X. Wang, and J. Yang. 2019. Remote sensing of dryland ecosystem structure and function: Progress, challenges, and opportunities. Remote Sensing of Environment **233**:1-23.

Springer, K. R., R. Wang, and J. A. Gamon. 2017. Parallel seasonal patterns of photosynthesis, fluorescence, and reflectance indices in boreal trees. Remote Sensing **9:**1-18.

Stevens, N., C. E. R. Lehmann, B. P. Murphy, and G. Durigan. 2017. Savanna woody encroachment is widespread across three continents. Global Change Biology **23**:235–244.

Stylinski, C., J. Gamon, and W. Oechel. 2002. Seasonal patterns of reflectance indices, carotenoid pigments and photosynthesis of evergreen chaparral species. Oecologia **131**:366–374.

Tezera, W., M.D. Fernndez, C., Donoso, and A. Herrera. 1998. Seasonal changes in photosynthesis and stomatal conductance of five plant species from a semiarid ecosystem. Photosynthetica **35**:399-410.

Trenberth, K. E., A. Dai, G. van der Schrier, P. D. Jones, J. Barichivich, K. R. Briffa, and J. Sheffield. 2014. Global warming and changes in drought. Nature Climate Change **4**:17–22.

Van Auken, O. W. 2009. Causes and consequences of woody plant encroachment into western North American grasslands. Journal of Environmental Management **90**:2931–2942.

Verhoeven, A. 2014. Sustained energy dissipation in winter evergreens. New Phytologist **201**:57–65.

Verhoeven, A., J. I. García-Plazaola, and B. Fernández-Marín. 2018. Shared mechanisms of photoprotection in photosynthetic organisms tolerant to desiccation or to low temperature. Environmental and Experimental Botany **154**:66–79.

Western Regional Climate Center (WRCC). 2020. Sonora, TX: Total of precipitation (inches). Accessed at https://wrcc.dri.edu/cgi-bin/cliMAIN.pl?tx8449.

Weiss, M., F. Baret, G. J. Smith, I. Jonckheere, and P. Coppin. 2004. Review of methods for in situ leaf area index (LAI) determination: Part II. Estimation of LAI, errors and sampling. Agricultural and Forest Meteorology **121**:37–53.

Wellburn, A.R. 1994. The spectral determinations of chlorophylls *a* and b, as well as total carotenoids, using various solvents with spectrophotometers of different resolutions. Journal of Plant Physiology **144**:307-313.

Wong, C. Y. S., P. D'Odorico, M. A. Arain, and I. Ensminger. 2020. Tracking the phenology of photosynthesis using carotenoid-sensitive and near-infrared reflectance vegetation indices in a temperate evergreen and mixed deciduous forest. New Phytologist **226**:1682–1695.

Wong, C. Y. S., P. D'Odorico, Y. Bhathena, M. A. Arain, and I. Ensminger. 2019. Carotenoid based vegetation indices for accurate monitoring of the phenology of photosynthesis at the leaf-scale in deciduous and evergreen trees. Remote Sensing of Environment **233**:1-14.

Wong, C. Y. S., and J. A. Gamon. 2015. Three causes of variation in the photochemical reflectance index (PRI) in evergreen conifers. New Phytologist **206**:187–195.

Xue, J., and B. Su. 2017. Significant remote sensing vegetation indices: A review of developments and applications. Journal of Sensors 1–17.

Yan, D., R. L. Scott, D. J. P. Moore, J. A. Biederman, and W. K. Smith. 2019. Understanding the relationship between vegetation greenness and productivity across dryland ecosystems through the integration of PhenoCam, satellite, and eddy covariance data. Remote Sensing of Environment **223**:50–62.

Zarco-Tejada, P. J., V. González-Dugo, L. E. Williams, L. Suárez, J. A. J. Berni, D. Goldhamer, and E. Fereres. 2013. A PRI-based water stress index combining structural and chlorophyll effects: Assessment using diurnal narrow-band airborne imagery and the CWSI thermal index. Remote Sensing of Environment **138**:38–50.

Zhang, C., I. Filella, M. Garbulsky, and J. Peñuelas. 2016. Affecting factors and recent improvements of the Photochemical Reflectance Index (PRI) for remotely sensing foliar, canopy and ecosystemic radiation-use efficiencies. Remote Sensing **8**:1-33.

Zhang, C., I. Filella, D. Liu, R. Ogaya, J. Llusià, D. Asensio, and J. Peñuelas. 2017a. Photochemical Reflectance Index (PRI) for detecting responses of diurnal and seasonal photosynthetic activity to experimental drought and warming in a Mediterranean shrubland. Remote Sensing **9**:1-129.

4. CONCLUSIONS

Woody encroachment has substantially shifted the landscape of the Southern Great Plains to greater fractions of woody plants that vary in water status and leaf functional traits (Barger et al. 2011). Parts of the Southern Great Plains are water-limited, and semi-arid areas such as these are important in driving the interannual variation in atmospheric CO_2 levels (Poulter et al. 2014, Ahlstrom et al. 2015). As these woody encroachers change the landscape with shifting accumulation of biomass being stored aboveground, there is interest in understanding how these plants will be photosynthetically impacted by "hotter droughts" and changing climatic conditions projected for the future (Seager et al. 2007, Strzepek et al. 2010, Dai 2013, Trenberth et al. 2013, Allen et al. 2015, Cook et al. 2015). This is especially important considering their varying tolerances to water limitations and mortality patterns that have been exhibited (Moore et al. 2016).

However, both our: 1) understanding of their photosynthetic and energetic responses to stressors, and 2) capabilities to remotely sense photosynthetic changes in these dryland systems have remained limited—the latter due to use of greenness indices on evergreen landscapes. The objectives of this study were to fill both of these gaps. The first was to assess if differential water access and leaf persistence affect seasonal photosynthetic and energy dissipation responses of three woody species in the Southern Great Plains that co-occur in Central-Texas. The second objective was to explore use of recently developed carotenoid indices such as the Chlorophyll Carotenoid Index (Gamon et al. 2016, Springer et al. 2017) that tracks both canopy FD and pigment pool changes

in its ability to track the photosynthetic changes of three dryland species varying in leaf persistence.

We found that the drought tolerant *Juniperus ashei* is likely to be the most photosynthetically vulnerable to water limitations, which is concerning since it is largely restricted to the driest parts of the landscape such as steep slopes and rooting in shallow soils (Van Auken and Smeins 2008). It experienced severe declines in midday water status (-5.14 MPa), actual quantum yield of PSII (ϕ_{PSII}) at midday at 4% use and 84% dynamic energy dissipation (ϕ^{r}_{NP}), while midday A_{Net} rates were extremely low (0.66 μmol m^{-2} s^{-1}) during the hot dry period in late summer (August/September). It appeared to be the only species employing some sustained energy dissipation leading to mild photoinhibition of the maximal quantum yield of PSII (F_V/F_M) that recovers overnight (dropped from 82 to 75%) during that period. The two drought avoiding species had some reductions in ϕ_{PSII} during the dry period in August with greatest declines in A_{Net} (48% drop from 21 μmol m^{-2} s-1) concurrent with decreasing water status (September low of -3.97 Mpa) for *Prosopis glandulosa*, while *Q. fusiformis* varied little in A_{Net} consistent with its lack of variability in its water status, but minimal changes in F_V/F_M above 0.82 for both species .

Freezing temperatures appeared to severely hamper the winter deciduous *P. glandulosa* where F_V/F_M dropped considerably upon colder temperature arrival (November low of 0.53) with gas-exchange capabilities declining, while F_V/F_M reductions in the two overwintering species were mild over the winter (~0.75 or slightly less). *J. ashei* appeared most susceptible to sustained photoinhibition during coupled dry

and freezing periods. Interestingly, midday ϕ_{PSII} and A_{Net} for *J. ashei* had their highest values over the Nov-March period consistent with Owens et al. (1996) and Bendevis et al. (2010) showing that *J. ashei* may have positively responded to increases in water availability and reductions of midday temperatures and VPD over this period.

CCI at both levels had moderate to strong relationships to slow adjusting parameters of F_V/F_M and Chl:Car across species and FD in the deciduous species with canopy CCI. The ability of CCI to capture canopy FD changes in the deciduous species ($R^2 = 0.81$, $p < 0.01$), Chl:Car in the evergreen (*J. ashei*: leaf $R^2 = 0.42$, $p < 0.06$, canopy $R^2 = 0.44$, $p < 0.07$), semi-evergreen (*Q. fusiformis*: leaf $R^2 = 0.67$, $p < 0.007$, canopy $R^2 = 0.72$, $p < 0.008$) and deciduous species (*P. glandulosa*: leaf $R^2 = 0.59$, $p < 0.07$, canopy $R^2 = 0.88$, $p < 0.02$), and F_V/F_M across species of varying leaf persistence (*Q. fusiformis*: leaf $R^2 = 0.42$, $p < 0.04$; *P. glandulosa*: leaf $R^2 = 0.58$, $p < 0.05$, canopy $R_{rmc}^2 = 0.54$ (0.48), $p < 0.001$; *J. ashei*: leaf $R^2 = 0.66$, $p < 0.004$, canopy $R^2 = 0.74$, $p < 0.006$) holds promise it may be able to track general trends in photosynthesis at larger scales in dryland landscapes. More studies at greater spatiotemporal scales are needed in drylands to ascertain its utility in these systems and the strength of relationships between CCI and photosynthesis.

Additionally, PRI at both levels were found to have stronger relationships with F_V/F_M and Chl:Car than CCI. While findings of stronger PRI have been reported, the reasoning is not well known as sources of variation in CCI have not been well delineated. Consequently, we need further studies on the possible sources of variation in CCI which might help explain its weaker relationships than PRI. Relationships for

vegetation indices to midday dynamic parameters were species-specific as species had contrasting patterns or inconsistent mechanistic explanations. These inconsistent relationships and other weaker relationships with dynamic parameters (particularly A_{Net}) underscores the difficulty of relating instantaneous measurements to spectral indices in these dryland systems. Consequently, future studies would be aided by more continuous measurement systems for spectral reflectance and carbon assimilation.

4.1. **References**

Ahlstrom, A., M. R. Raupach, G. Schurgers, B. Smith, A. Arneth, M. Jung, M. Reichstein, J. G. Canadell, P. Friedlingstein, A. K. Jain, E. Kato, B. Poulter, S. Sitch, B. D. Stocker, N. Viovy, Y. P. Wang, A. Wiltshire, S. Zaehle, and N. Zeng. 2015. The dominant role of semi-arid ecosystems in the trend and variability of the land CO2 sink. Science **348**:895–899.

Allen, C. D., D. D. Breshears, and N. G. McDowell. 2015. On underestimation of global vulnerability to tree mortality and forest die-off from hotter drought in the Anthropocene. Ecosphere **6**:1-55.

Barger, N. N., S. R. Archer, J. L. Campbell, C. Huang, J. A. Morton, and A. K. Knapp. 2011. Woody plant proliferation in North American drylands: A synthesis of impacts on ecosystem carbon balance. Journal of Geophysical Research: Biogeosciences **116**:1-17.

Bendevis, M. A., M. K. Owens, J. L. Heilman, K. J. McInnes. 2010. Carbon exchange and water loss from two evergreen trees in a semiarid woodland. Ecohydrology **3**:107–115.

Cook, B. I., T. R. Ault, and J. E. Smerdon. 2015. Unprecedented 21st century drought risk in the American Southwest and Central Plains. Science Advances **1**:1-7.

Dai, A. 2013. Increasing drought under global warming in observations and models. Nature Climate Change **3**:52–58.

Gamon, J. A., K. F. Huemmrich, C. Y. S. Wong, I. Ensminger, S. Garrity, D. Y. Hollinger, A. Noormets, and J. Peñuelas. 2016. A remotely sensed pigment index reveals photosynthetic phenology in evergreen conifers. Proceedings of the National Academy of Sciences **113**:13087–13092.

Moore, G. W., C. B. Edgar, J. G. Vogel, R. A. Washington-Allen, R. G. March, and R. Zehnder. 2016. Tree mortality from an exceptional drought spanning mesic to semiarid ecoregions. Ecological Applications **26**:602–611.

Owens, M. K. 1996. The role of leaf and canopy-level gas exchange in the replacement of *Quercus virginiana* (Fagaceae) by *Juniperus ashei* (Cupressaceae) in semiarid savannas. American Journal of Botany **83**:617–623.

Poulter, B., D. Frank, P. Ciais, R. B. Myneni, N. Andela, J. Bi, G. Broquet, J. G. Canadell, F. Chevallier, Y. Y. Liu, S. W. Running, S. Sitch, and G. R. van der Werf. 2014. Contribution of semi-arid ecosystems to interannual variability of the global carbon cycle. Nature **509**:600–603.

Seager, R., M. Ting, I. Held, Y. Kushnir, J. Lu, G. Vecchi, H.-P. Huang, N. Harnik, A. Leetmaa, N.-C. Lau, C. Li, J. Velez, and N. Naik. 2007. Model projections of an imminent transition to a more arid climate in Southwestern North America. Science **316**:1181–1184.

Springer, K. R., R. Wang, and J. A. Gamon. 2017. Parallel seasonal patterns of photosynthesis, fluorescence, and reflectance indices in boreal trees. Remote Sensing **9:**1-18.

Strzepek, K., G. Yohe, J. Neumann, and B. Boehlert. 2010. Characterizing changes in drought risk for the United States from climate change. Environmental Research Letters **5**:1-9.

Trenberth, K. E., A. Dai, G. van der Schrier, P. D. Jones, J. Barichivich, K. R. Briffa, and J. Sheffield. 2014. Global warming and changes in drought. Nature Climate Change **4**:17–22.

Van Auken, O.W. and F. Smeins. 2008. Western North American *Juniperus* communities: Patterns and causes of distribution and abundance. In Van Auken, O.W. (Ed.), Western North American *Juniperus* communities: A dynamic vegetation type. Springer, New York. 3 -18.

APPENDIX A

REPEATED MEASURES CORRELATION TABLES

Table A-1. Repeated measures correlation (rmc) coefficients of determination for *Q. fusiformis*.

Vegetation Index	A_{Net}	E	g_s	F_V/F_M	ϕ_{PSII}	NPQ	Chl:Car	FD	Ψ_{PD}	Ψ_{MD}
Leaf NDVI	**0.11*** (0.05)	0.02 (0.06)	0.02 (0.02)	0.00 (0.00)	0.00 (0.00)	0.00 (0.00)	0.03 (0.01)	0.00 (0.05)	0.03 (0.01)	0.02 (0.02)
Canopy NDVI	0.00 (0.02)	0.03 (0.00)	0.05 (0.01)	**0.12*** (0.00)	0.03 (0.03)	0.03 (0.01)	0.01 (0.00)	**0.17*** (0.31)	**0.14*** (0.00)	0.09 (0.00)
Leaf PRI	**0.13*** (0.01)	**0.20**** (0.06)	0.02 (0.00)	**0.27***** (0.24)	**0.18**** (0.07)	0.04 (0.04)	**0.38***** (0.34)	0.01 (0.02)	0.05 (0.02)	0.00 (0.01)
Canopy PRI	0.07 (0.08)	**0.18*** (0.10)	0.01 (0.00)	**0.30***** (0.27)	**0.14*** (0.12)	0.03 (0.05)	**0.55***** (0.51)	0.00 (0.03)	**0.13*** (0.10)	0.01 (0.01)
Leaf CCI	0.07 (0.01)	**0.15**** (0.09)	0.01 (0.00)	**0.17**** (0.18)	**0.12*** (0.08)	0.01 (0.01)	**0.40***** (0.36)	0.00 (0.08)	0.04 (0.03)	0.00 (0.00)
Canopy CCI	0.00 (0.00)	0.08 (0.07)	0.01 (0.01)	0.06 (0.11)	0.04 (0.01)	0.03 (0.03)	**0.30***** (0.25)	0.07 (0.12)	0.01 (0.05)	0.01 (0.04)
Leaf SAVI	0.08 (0.03)	0.01 (0.03)	0.00 (0.01)	0.00 (0.00)	0.00 (0.00)	0.01 (0.00)	0.03 (0.02)	0.00 (0.03)	0.01 (0.00)	0.02 (0.01)
Canopy SAVI	0.00 (0.00)	**0.14*** (0.02)	**0.12*** (0.03)	0.06 (0.01)	0.01 (0.00)	0.10 (0.06)	0.03 (0.00)	**0.17*** (0.18)	0.11 (0.00)	**0.25**** (0.06)
Leaf EVI	0.07 (0.06)	0.00 (0.01)	0.00 (0.01)	0.02 (0.01)	0.03 (0.03)	0.00 (0.00)	0.00 (0.00)	0.02 (0.03)	0.05 (0.02)	0.02 (0.02)
Canopy EVI	0.00 (0.00)	**0.15*** (0.02)	**0.12*** (0.04)	0.07 (0.00)	0.01 (0.01)	0.10 (0.09)	0.03 (0.00)	**0.14*** (0.13)	0.10 (0.00)	**0.26**** (0.09)
Leaf EVI2	0.08 (0.05)	0.01 (0.03)	0.00 (0.00)	0.00 (0.00)	0.00 (0.00)	0.01 (0.00)	0.03 (0.03)	0.01 (0.05)	0.01 (0.00)	0.02 (0.02)
Canopy EVI2	0.00 (0.00)	**0.13*** (0.02)	0.11 (0.03)	0.05 (0.00)	0.00 (0.00)	0.09 (0.07)	0.02 (0.00)	**0.16*** (0.18)	0.09 (0.00)	**0.25**** (0.08)

* P-values less than or equal to 0.05 (*), 0.01 (**), or 0.001 (***) respectively. Shown in bold.
Bootstrapped versions of the repeated measures coefficient of determination are found in parentheses. P-values are not available for the bootstrapped versions.

Table A-2. Repeated measures correlation (rmc) coefficients of determination for *P. glandulosa*

Vegetation Index	A_{Net}	E	g_s	F_V/F_M	ϕ_{PSII}	NPQ	Chl:Car	FD	Ψ_{PD}	Ψ_{MD}
Leaf NDVI	0.01 (0.01)	0.01 (0.01)	0.01 (0.00)	0.12 (0.09)	**0.16*** (0.11)	0.02 (0.04)	**0.16*** (0.16)	0.12 (0.06)	0.00 (0.01)	0.12 (0.15)
Canopy NDVI	0.06 (0.03)	**0.43**** (0.23)	0.01 (0.00)	**0.40**** (0.33)	**0.35**** (0.27)	0.03 (0.02)	**0.76***** (0.76)	**0.79***** (0.62)	0.00 (0.01)	0.09 (0.09)
Leaf PRI	0.19[a] (0.21)	**0.27[a] **** (0.27)	0.02 (0.04)	**0.58***** (0.53)	**0.43***** (0.40)	0.01 (0.01)	**0.69***** (0.71)	**0.54***** (0.41)	0.02 (0.01)	0.08 (0.11)
Canopy PRI	0.13 (0.18)	**0.49***** (0.37)	0.04 (0.04)	**0.63***** (0.65)	**0.37**** (0.38)	0.14 (0.08)	**0.63***** (0.49)	0.12 (0.08)	0.01 (0.00)	0.12 (0.07)
Leaf CCI	0.01 (0.00)	**0.13*** (0.05)	0.00 (0.00)	**0.39***** (0.28)	**0.18*** (0.09)	0.07 (0.04)	**0.42***** (0.33)	**0.37**** (0.27)	0.01 (0.01)	**0.21*** (0.24)
Canopy CCI	0.06 (0.03)	**0.39**** (0.25)	0.01 (0.00)	**0.54***** (0.48)	**0.32**** (0.23)	0.09 (0.09)	**0.74***** (0.73)	**0.65***** (0.53)	0.01 (0.02)	0.16 (0.13)
Leaf SAVI	0.03 (0.02)	0.04[a] (0.02)	0.01 (0.01)	0.01 (0.00)	0.01 (0.00)	0.00 (0.00)	0.07 (0.06)	0.02 (0.01)	0.00 (0.01)	0.10 (0.09)
Canopy SAVI	0.10 (0.03)	**0.38**** (0.16)	0.02 (0.00)	**0.38**** (0.22)	**0.49***** (0.20)	0.00 (0.00)	**0.72***** (0.65)	**0.71***** (0.44)	0.02 (0.00)	0.01 (0.04)
Leaf EVI	0.01 (0.01)	0.04[a] (0.03)	0.04 (0.02)	0.00 (0.00)	0.00 (0.01)	0.01 (0.01)	0.02 (0.03)	0.00 (0.00)	0.00 (0.00)	0.10 (0.10)
Canopy EVI	0.11 (0.03)	**0.43**** (0.21)	0.03 (0.00)	**0.43**** (0.28)	**0.51***** (0.27)	0.00 (0.00)	**0.73***** (0.68)	**0.72***** (0.46)	0.02 (0.00)	0.02 (0.04)
Leaf EVI2	0.03 (0.02)	0.03[a] (0.01)	0.01 (0.00)	0.00 (0.00)	0.00 (0.00)	0.00 (0.00)	0.06 (0.07)	0.02 (0.00)	0.00 (0.00)	0.09 (0.09)
Canopy EVI2	0.10 (0.01)	**0.38**** (0.18)	0.02 (0.00)	**0.38**** (0.22)	**0.49***** (0.20)	0.00 (0.00)	**0.69***** (0.61)	**0.69***** (0.40)	0.03 (0.00)	0.01 (0.03)

* P-values less than or equal to 0.05 (*), 0.01 (**), or 0.001 (***) respectively. Shown in bold.

[a] The physiological variable underwent a natural log transformation to improve linearity.

Bootstrapped versions of the repeated measures coefficient of determination are found in parentheses. P-values are not available for the bootstrapped versions.

Table A-3. Repeated measures correlation (rmc) coefficients of determination for *J. ashei*

Vegetation Index	A_{Net}	E	g_s	F_V/F_M	ϕ_{PSII}	NPQ	Chl:Car	FD	Ψ_{PD}	Ψ_{MD}
Leaf NDVI	**0.10*** (0.03)	**0.15**** (0.06)	0.07 (0.01)	**0.17**** (0.17)	**0.20**** (0.17)	0.03 (0.01)	**0.31***** (0.34)	0.01 (0.00)	0.04 (0.01)	0.04 (0.02)
Canopy NDVI	**0.14*** (0.11)	0.10 (0.09)	**0.24**** (0.17)	0.01 (0.06)	0.06 (0.03)	0.05 (0.10)	0.02 (0.00)	0.07 (0.00)	0.01 (0.03)	0.02 (0.01)
Leaf PRI	0.07 (0.05)	**0.24***** (0.19)	0.07 (0.04)	**0.61***** (0.60)	**0.20**** (0.23)	0.01 (0.02)	**0.56***** (0.60)	0.03 (0.02)	0.01 (0.01)	0.00 (0.00)
Canopy PRI	**0.25**** (0.28)	**0.40***** (0.34)	**0.19**** (0.20)	**0.57***** (0.59)	**0.38***** (0.45)	0.01 (0.01)	**0.59***** (0.61)	0.02 (0.00)	0.10 (0.06)	0.07 (0.05)
Leaf CCI	0.01 (0.01)	0.04 (0.02)	0.00 (0.00)	**0.35***** (0.34)	0.07 (0.06)	0.01 (0.01)	**0.24**** (0.26)	0.01 (0.00)	0.00 (0.01)	0.01 (0.01)
Canopy CCI	0.06 (0.06)	**0.12*** (0.07)	0.01 (0.01)	**0.38***** (0.42)	**0.18**** (0.19)	0.00 (0.01)	**0.31***** (0.33)	0.00 (0.00)	0.00 (0.00)	0.00 (0.00)
Leaf SAVI	0.01 (0.00)	0.02 (0.00)	0.01 (0.00)	0.04 (0.09)	0.02 (0.05)	0.01 (0.00)	0.01 (0.07)	0.00 (0.00)	0.02 (0.00)	0.02 (0.01)
Canopy SAVI	0.10 (0.19)	**0.27**** (0.28)	**0.27**** (0.34)	0.03 (0.00)	**0.13*** (0.14)	0.08 (0.12)	**0.14*** (0.07)	0.09 (0.05)	**0.17*** (0.15)	**0.20**** (0.13)
Leaf EVI	0.02 (0.01)	0.03 (0.01)	0.03 (0.01)	0.05 (0.12)	0.04 (0.07)	0.01 (0.00)	0.03 (0.10)	0.01 (0.00)	0.05 (0.01)	0.04 (0.01)
Canopy EVI	0.06 (0.13)	**0.21**** (0.23)	**0.21**** (0.30)	0.02 (0.00)	0.08 (0.08)	0.07 (0.12)	0.10 (0.03)	0.07 (0.02)	**0.13*** (0.12)	**0.15*** (0.10)
Leaf EVI2	0.00 (0.00)	0.01 (0.00)	0.01 (0.00)	0.03 (0.08)	0.01 (0.04)	0.00 (0.00)	0.01 (0.08)	0.00 (0.00)	0.01 (0.00)	0.02 (0.00)
Canopy EVI2	0.08 (0.19)	**0.26**** (0.26)	**0.24**** (0.34)	0.03 (0.00)	**0.11*** (0.14)	0.07 (0.12)	**0.13*** (0.06)	0.09 (0.04)	**0.16***(0.15)	**0.18**** (0.12)

* P-values less than or equal to 0.05 (*), 0.01 (**), or 0.001 (***) respectively. Shown in bold.
Bootstrapped versions of the repeated measures coefficient of determination are found in parentheses. P-values are not available for the bootstrapped versions.